MONONUCLEAR COPPER(II) COMPLEXES CONTAINING 2,2′-DIPYRIDYLAMINE AND HYDROXYBENZOATE DERIVATIVES AS CATALYST FOR AEROBIC OXIDATION OF HYDROXAMIC ACIDS

BY

WANASSANAN CHAISURIYA

A THESIS SUBMITTED IN PARTIAL FULFILLMENT OF THE REQUIREMENTS FOR THE DEGREE OF

MASTER OF SCIENCE (CHEMISTRY)

DEPARTMENT OF CHEMISTRY

FACULTY OF SCIENCE AND TECHNOLOGY

THAMMASAT UNIVERSITY

ACADEMIC YEAR 2023

MONONUCLEAR COPPER(II) COMPLEXES CONTAINING 2,2′-DIPYRIDYLAMINE AND HYDROXYBENZOATE DERIVATIVES AS CATALYST FOR AEROBIC OXIDATION OF HYDROXAMIC ACIDS

BY

WANASSANAN CHAISURIYA

A THESIS SUBMITTED IN PARTIAL FULFILLMENT OF THE REQUIREMENTS FOR THE DEGREE OF
MASTER OF SCIENCE (CHEMISTRY)
DEPARTMENT OF CHEMISTRY
FACULTY OF SCIENCE AND TECHNOLOGY
THAMMASAT UNIVERSITY
ACADEMIC YEAR 2023

THAMMASAT UNIVERSITY
FACULTY OF SCIENCE AND TECHNOLOGY

THESIS

BY

WANASSANAN CHAISURIYA

ENTITLED

MONONUCLEAR COPPER(II) COMPLEXES
CONTAINING 2,2′–DIPYRIDYLAMINE AND
HYDROXYBENZOATE DERIVATIVES AS CATALYST
FOR AEROBIC OXIDATION OF HYDROXAMIC ACIDS

was approved as partial fulfillment of the requirements for
the degree of Master of Science (Chemistry)

on December 18, 2023

Chairman _____
(Associate Professor Chanatip Samart, Ph.D.)

Member and Advisor _____
(Assistant Professor Nanthawat Wannarit, Ph.D.)

Member and Co–advisor _____
(Assistant Professor Duangduan Chaiyaveij, Ph.D.)

Member _____
(Thapong Teerawatananond, Ph.D.)

Dean _____
(Associate Professor Supet Jirakajohnkool, Ph.D.)

Thesis Title	MONONUCLEAR COPPER(II) COMPLEXES CONTAINING 2,2′-DIPYRIDYLAMINE AND HYDROXYBENZOATE DERIVATIVES AS CATALYST FOR AEROBIC OXIDATION OF HYDROXAMIC ACIDS
Author	Wanassanan Chaisuriya
Degree	Master of Science (Chemistry)
Department/Faculty/University	Department of Chemistry Faculty of Science and Technology Thammasat University
Thesis Advisor	Assistant Professor Nanthawat Wannarit, Ph.D.
Thesis Co-Advisor	Assistant Professor Duangduan Chaiyaveij, Ph.D.
Academic Year	2023

ABSTRACT

This research concerns the design, synthesis, characterization and catalytic properties of new mononuclear Cu(II) complexes containing 2,2′-dipyridylamine (dpyam) and hydroxybenzoate derivatives (x-OHbenz when x = 2-, 3-, and 4-hydroxy-benzoate). The mononuclear Cu(II) complexes have been classified into two series namely, a series **I** was designed with a general formula of [Cu(dpyam)(x-OHbenz)$_2$], [Cu(dpyam)(3-OHbenz)(HCO_2)] (**1**) and [Cu(dpyam)(4-OHbenz)$_2$]·H_2O (**2**) and a series **II** with a general formula of [Cu(dpyam)(x-OHbenz)Cl], when x = 2-OHbenz (**3**) and 3-OHbenz (**4**). All complexes were characterized by using FT-IR, UV-vis, solid-state diffuse reflectance spectroscopy, CHN elemental analysis, TGA and PXRD. The molecular structures of all complexes were determined by using single-crystal X-ray diffraction technique. The structures of Cu(II) complexes in a series **I** present different geometries, a distorted square-pyramidal with [CuN_2O_3] chromophore for complex **1** and a distorted square-planar with a [CuN_2O_2] chromophore for complex **2**. Meanwhile, the Cu(II) complexes **3** and **4** in a series **II** are isostructural as a distorted square-pyramidal geometry with [CuN_2O_2Cl] chromophore. The crystal structures of

these new mononuclear Cu(II) complexes were stabilized by various types of intermolecular interactions such as hydrogen bonding, π–π and C–H$\cdots\pi$, and these supramolecular interactions have been confirmed by Hirshfeld surface analysis (d_{norm}) and two-dimensional fingerprint plots. Unfortunately, complex **1** could not be reproduced sufficiently for further catalysis studies. Consequently, the catalytic properties of complexes **2-4** have been investigated because they are insoluble in THF solution and stable at temperatures up to 250 °C. Therefore, these complexes have been used as the heterogeneous catalyst in the aerobic oxidation reaction of hydroxamic acids to produce nitroso compounds. The progress of reactions was followed up by using the ^{1}H-NMR technique. Interestingly, the result showed that complex **3** presents the most efficiency for catalyzing the reaction, giving the % yield of cycloadduct and ene-product up to 98%, and it could be reused at least five cycles with the TOF value of 15.29 h^{-1}. In addition, the reaction mechanism was also proposed in this research.

Keywords: mononuclear Cu(II) complex, 2,2′-dipyridylamine, hydroxybenzoate derivatives, crystal structure, heterogeneous catalyst, hydroxamic acid

ACKNOWLEDGEMENTS

First and foremost, I would like to thank my thesis advisor, Assistant Professor Dr. Nanthawat Wannarit for advising me of my thesis and perspectives about inside and outside the university's life. Although the thesis was frequently challenging to the point that I grew discouraged and desperate, I always received his advice, which is why I thank you, my advisor. Be calm, be kind, and give me a chance to start over with every problem. In addition, I am also thankful for my thesis co-advisor, Assistant Professor Dr. Duangduan Chaiyaveij for her suggestions and support on the part of the catalytic study. I am grateful to Associate Professor Dr. Kittipong Chainok for the single-crystal X-ray diffraction data and powder X-ray diffraction data of all new mononuclear Cu(II) complexes. I would also like to thank Associate Professor Dr. Chanatip Samart, thank you for serving as a chairman and sacrificing time to review and give suggestions for revising the thesis to improve it. I appreciate Dr. Thapong Teerawattananon for serving to be an external thesis committee and giving advice and guidance on the thesis and the TGA measurement. Indispensable, I would like to thank Gp.Capt. Pimpa Rungnopakunsi from the Royal Thai Air Force Nursing College for bioactivity study and encouragement until this thesis is complete. Apart from this, I would like to thank the Thammasat University Research Unit in Multifunctional Crystalline Materials and Applications (TU-MCMA) for supporting research funding to attend international academic conferences for poster presentations both inside and abroad. The support from this research unit provided me with the opportunity to show off academic abilities and gain many experiences.

I am grateful to my family for their love and support at this trying moment. I was able to succeed in the thesis with their encouragement and motivation. I want to take this opportunity to express my deepest gratitude to Squadron Leader Dr. La-Ongdao Wannarit for giving me the opportunity to improve my English skills and for always supporting me a lot of food during working on the thesis. Most importantly, I would like to thank the NW research group members (Phakamat Promwit, Thawanrat Saelim, Kulwadee Ponanunrirk, Chanikarn Kummuang, Sirinan Thanma, and Chompunuch Bunfrueang) and TU-MCMA members (Chatphorn Theppitak, Suwadee Jiajaroen, Songwuit Chanthee, Kenika Khotchasanthong, Kunlanit Jeanjan, Kanthida

Kummoon, Patcharapon Jiaranaiwiwat, and Jannarong Ngoensri) for supporting me and sharing with me many opportunities—more than just reading a textbook in classrooms and labs. The thesis was successful with their cooperation. Thank you for all that has filled my life in the three years of my Master's degree at Thammasat University.

Wanassanan Chaisuriya

TABLE OF CONTENTS

TABLE OF CONTENTS (CONT.)

TABLE OF CONTENTS (CONT.)

LIST OF TABLES

LIST OF TABLES (CONT.)

LIST OF FIGURES

LIST OF FIGURES (CONT.)

LIST OF FIGURES (CONT.)

LIST OF FIGURES (CONT.)

LIST OF FIGURES (CONT.)

LIST OF FIGURES (CONT.)

LIST OF FIGURES (CONT.)

LIST OF SCHEMES

LIST OF ABBREVIATIONS

Symbols/Abbreviations	Terms
a, b, c	Lengths along the crystallographic axes
α, β, γ	Angles between the axes
CAN	Acetonitrile
Ace	Acetone
Å	Angstrom
C	Concentration
^{o}C	Degree Celsius
Benz	Benzoate
calcd.	Calculated
*C*g	Aromatic centroid
D	Dimensional
DCM	Dichloromethane
DMF	Dimethylformamide
DI water	Deionized water
DMA	Dimethylamine
DMSO	Dimethyl sulfoxide
Dpyam	2,2′-Dipyridylamine
Et_2O	Diethyl ether
EtOAc	Ethyl acetate
EtOH	Ethanol
FT-IR	Fourier transform infrared
G	gram
Hex	Hexane
I	Insoluble
kK	Kilokaiser, 1 kK = 1000 cm^{-1}
MeOH	Methanol
mL	Milliliter

LIST OF ABBREVIATIONS (CONT.)

Symbols/Abbreviations	Terms
mM	Millimolar
Mmol	Millimole
Nm	Nanometer
NMR	Nuclear magnetic resonance
4-NH_2benz	4-aminobenzoate
4-NO_2benz	4-nitrobenzoate
2-OHbenz	2-Hydroxybenzoate
3-OHbenz	3-Hydroxybenzoate
4-OHbenz	4-Hydroxybenzoate
P	Partially soluble
Ppm	Part per million
PXRD	Powder X-ray diffraction
S	Soluble
SCXRD	Single-crystal X-ray diffraction
TGA	Thermal gravimetric analysis
THF	Tetrahydrofuran
TLC	Thin-layer chromatography
Tol	Toluene
UV	Ultraviolet
Vis	Visible

CHAPTER 1
INTRODUCTION

1.1 Introduction

Mononuclear copper(II) complexes have received a great attention in several fields due to their versatile properties, including antitumor, antioxidant, antibacterial, DNA interaction, DNA cleavage [1, 2], anticancer [3], biological [4], industrial catalytic oxidation processes [5], magnetism [6, 7] and catalysis [8]. In the scope of our research activities, we started to search for new mononuclear copper(II) complexes containing mixed *N*- and *O*-donor ligands such as 2,2′-dipyridylamine (dpyam) and hydroxybenzoate derivatives and to study their catalytic properties in some reaction for example, olefin epoxidation [12], aerobic oxidation of alcohols [13, 14], ring-opening reactions [15] and the photocatalytic oxidation of benzyl alcohol [16]. Generally, a Cu(II) ion has the [Ar] $3d^9$ electron configuration with an unpaired electron that can induce magnetic properties. The copper(II) complexes also exhibit a variety of coordination environments with coordination numbers ranging from 4 to 6 [9]. With this in mind, we have designed new mononuclear copper(II) complexes constructed from mixed 2,2′-dipyridylamine (dpyam) derivative as *N*-donor ligands and hydroxy-benzoate derivatives (OHbenz) derivative as *O*-donor ligands. The dpyam ligand contains two aromatic pyridine rings that can by chelating coordination mode and together with a secondary amine (-NH-) group that could support the crystal stability through supramolecular interactions such as hydrogen bonding and π–π stacking interactions, respectively [10]. On the other hand, OHbenz derivatives are interesting because of their carboxylate functional group, which can exhibit a variety of coordination modes, resulting in different structural arrangements [11]. Likewise, the presence of a hydroxy group on the phenyl ring supports crystal stability by hydrogen-bonding interactions, and the different arrangements of this group (*ortho*-, *meta*-, *para*-positions) can be used to influence the crystal packing.

The aerobic oxidation reaction of hydroxamic acids refers to a reaction in which hydroxamic acids are oxidized to nitroso compounds in the presence of

molecular oxygen (O_2) to provide heteroatom Diels-Alder adducts. Cycloadducts are valuable synthetic intermediates for natural product synthesis and have been used to synthesize novel oxazine derivatives, possessing new biological properties [43]. In recent years, copper-catalyzed aerobics has gained significant attention due to its potential for green and sustainable oxidations. It uses atmospheric oxygen as the oxidant, avoiding using environmentally harmful reagents. However, the limitations of using Cu-catalyzed aerobics are that the catalyst is homogeneous, although it provides a high yield, shortest reaction time and good chemoselectivities. Nevertheless, it can be used to catalyze a reaction only one time.

Therefore, this research aims to design and synthesize new mononuclear Cu(II) complexes containing mixed 2,2′-dipyridylamine (dpyam) and hydroxybenzoate (OHbenz) derivatives to provide heterogeneous catalysts, which are designed to be easily synthesized, high-yield, low-cost, and recyclable. To facilitate use in catalyzing the aerobic oxidation of hydroxamic acid to nitroso compound. Meanwhile, the synthesis of heteroatom Diels-Alder adducts also uses lesser toxicity of catalysts, lesser waste and damage to the environment, short reaction time, reduced costs and energy required in various processes, high overall yield and good chemoselectivity.

1.2 Objectives of the research

1.2.1 To design and synthesize new mononuclear Cu(II) complexes containing 2,2′-bipyridylamine (dpyam) and hydroxybenzoate derivatives in two series of [Cu(dpyam)(x-OHbenz)$_2$] and [Cu(dpyam)(x-OHbenz)Cl] which have octahedral and square pyramidal geometry respectively, when x = 2, 3, and 4-hydroxybenzoate, as shown in Figure 1.1.

1.2.2 To characterize new mononuclear Cu(II) complexes using FT-IR, UV-vis, solid state diffuse reflectance spectroscopy, CHN analysis, EPR spectroscopy, TGA and PXRD techniques.

1.2.3 To determine and study the crystal structures of new synthesized mononuclear Cu(II) complexes using the single-crystal X-ray diffraction technique and study intermolecular interaction by using Hirshfeld surface analysis.

1.2.4 To study the catalytic properties by using new mononuclear Cu(II) complexes as a heterogeneous catalyst for the oxidation reaction of hydroxamic acids.

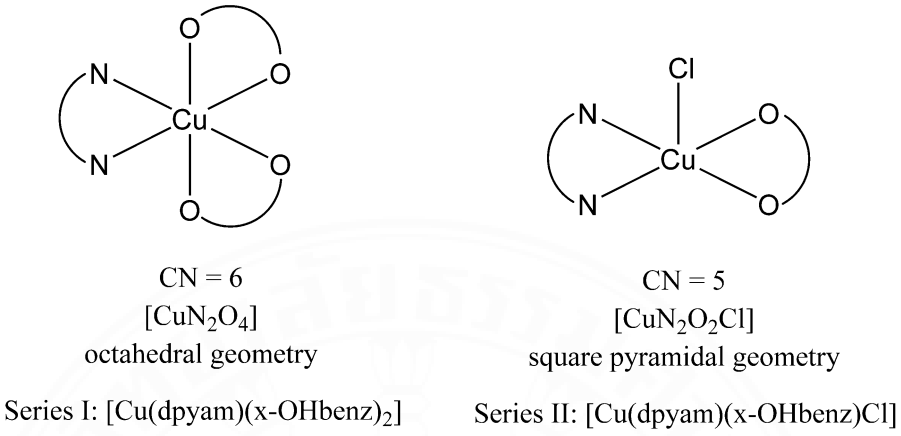

Figure 1.1 Proposed structures of new mononuclear copper(II) complexes

1.3 Scope and limitations of the research

1.3.1 Design and synthesize new mononuclear Cu(II) complexes containing 2,2′-dipyridylamine (dpyam) and hydroxybenzoate derivatives in the series of [Cu(dpyam)(x-OHbenz)$_2$] and [Cu(dpyam)(x-OHbenz)Cl] which have octahedral and square pyramidal geometry respectively, when x = 2, 3, and 4-hydroxybenzoate.

1.3.2 The FT-IR, UV-vis, Solid-state diffuse reflectance spectroscopy, CHN elemental analysis, EPR spectroscopy, TGA and PXRD will be applied to determine functional groups, solubility test, predict geometries, thermal stability, and the purity of synthesized mononuclear Cu(II) complexes, respectively.

1.3.3 The crystal structures of synthesized mononuclear Cu(II) complexes will be determined and studied using single-crystal X-ray diffraction, and intermolecular interaction will be confirmed using Hirshfeld surface analysis.

1.3.4 The catalytic studies of new mononuclear Cu(II) complexes as a heterogeneous catalyst for aerobic oxidation of hydroxamic acids will be investigated.

1.4 Expected results

1.4.1 New mononuclear Cu(II) complexes containing 2,2′-dipyridylamine and hydroxybenzoate derivatives have been synthesized.

1.4.2 New mononuclear Cu(II) complexes have been fully characterized by using FT-IR, UV-vis, solid-state diffuse reflectance spectroscopy, CHN elemental analysis, EPR spectroscopy, TGA and PXRD techniques.

1.4.3 The crystal structure of new mononuclear Cu(II) complexes has been determined and studied using single-crystal X-ray diffraction technique and confirmed intermolecular interaction using Hirshfeld surface analysis.

1.4.4 The heterogeneous catalytic properties of new mononuclear Cu(II) complexes in the aerobic oxidation reaction of hydroxamic acid have been studied.

.

CHAPTER 2
REVIEW OF LITERATURE

This chapter describes the mononuclear copper(II) complexes, ligands, The aerobic oxidation of hydroxamic acids to nitroso compound and literature review are shown in this chapter.

2.1 Mononuclear copper(II) complexes

Mononuclear copper(II) complexes containing a copper(II) ion in a complex act as electron acceptors from donor atoms of ligands by coordinate covalent bonds [17]. Generally, a Cu(II) ion has the [Ar] $3d^9$ electron configuration with an unpaired electron that can induce magnetic properties. The copper(II) complexes also exhibit a variety of coordination environments with coordination numbers ranging from 4 to 6 [9]. A coordination number of four corresponds to tetrahedral and square planar geometries, while a coordination number of five results in trigonal bipyramidal and square pyramidal geometries. For six coordinated leads to an octahedral geometry [9], as shown in Figure 2.1.

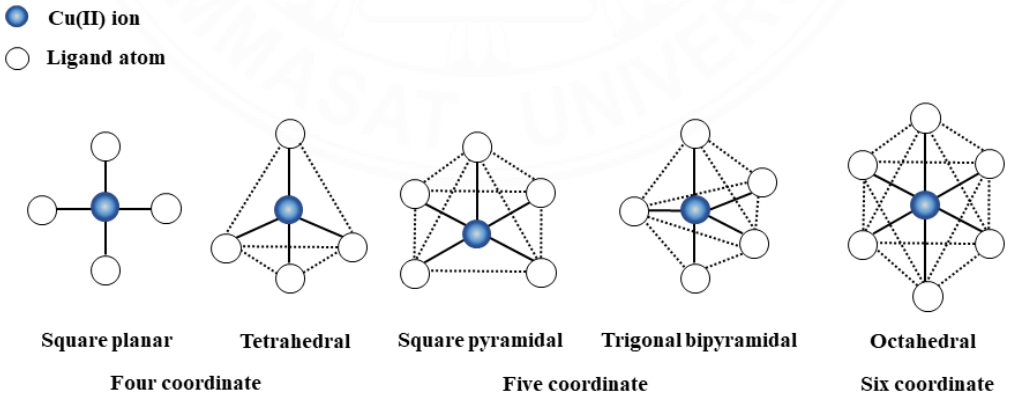

Figure 2.1 The coordination geometries of copper(II) complexes [9]

Copper(II) ion is a popular choice for complex formation due to its ease of control and handling. Additionally, complexes can be characterized using a variety of techniques. UV-visible spectroscopy can verify the presence of the copper(II) ion within the structure because the copper(II) complex is a coloured complex, and the Cu(II) ion absorbs visible light in the 600 to 650 nm range, which can confirm copper(II) ion in the complex in the solution form. In addition, it can provide information about its electronic structure. Solid-state diffuse reactance spectroscopy can analyze the electronic transition and predict the geometries of complexes, and it is often used for solid samples. EPR spectroscopy is used to study the electronic structure of copper(II) complexes, providing information about the unpaired electron and the coordination environment around the copper ion. X-ray diffraction technique can be used to investigate the crystal structure and phase composition of copper(II) complexes in the solid state to confirm phase purity and repeatability. Thermogravimetric analysis is also the technique used to investigate the thermal stability of copper(II) complexes. Therefore, we studied extensively (Figure 2.2).

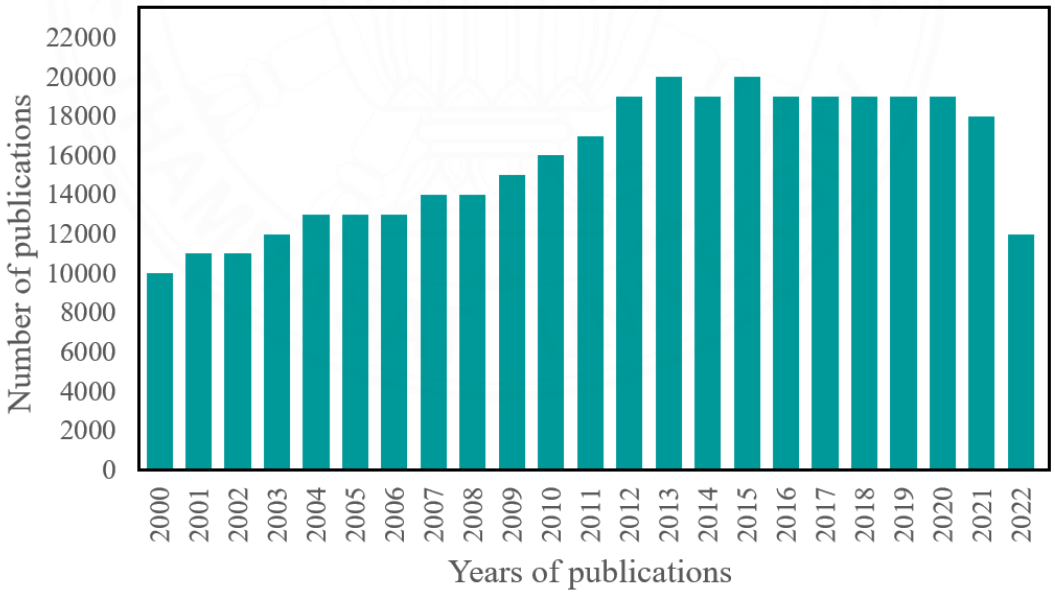

Figure 2.2 The number of publications for copper(II) complexes as catalysts in the Scifinder database, sorted by years 2000-2022 (Retrieved October 25, 2022)

Mononuclear copper(II) complexes have received significant attention in several fields due to antitumor, antioxidant, antibacterial, DNA interaction, DNA cleavage [1, 2, 18], anticancer [3], biological, industrial catalytic oxidation processes and catalysis [4, 8, 19]. Research on copper(II) complexes as catalysts has garnered significant attention from researchers, with a notable and continuous increase in studies from 2000 to 2022, as shown in Figure 2.2. This upward trend exhibits the growing interest and exploration of the catalytic properties of copper(II) complexes over the past two decades.

2.2 Ligand

Ligands are ions or molecules that donate lone pair of electrons to the vacant orbitals of a central metal atom or ion via a coordinate covalent bond to form the complex. For the ligand used in this research, the details are as follows.

2.2.1 2,2′-dipyridylamine

The 2,2′-dipyridylamine (dpyam) ligand contains two aromatic pyridine rings connected by a secondary amine (-NH-) group, as shown in Figure 2.3.

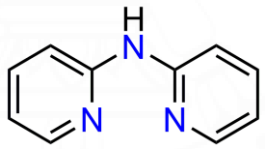

Figure 2.3 Molecular structure of 2,2′-dipyridylamine (dpyam)

For *N*-donor atoms of bipyridine ring act as electron-pair donors to metal centers form complexes and can act as chelating coordination mode form mononuclear units for constructing 1D, 2D and 3D supramolecular frameworks through weak interactions such as hydrogen bonding and π–π stacking interaction among others. The secondary amines can also form hydrogen-bonded networks through the active amine. Characteristics of the dpyam ligands are their ability to adopt three distinct conformations, *cis-cis*, *cis-trans*, and *trans-trans*, as shown in Figure 2.4.

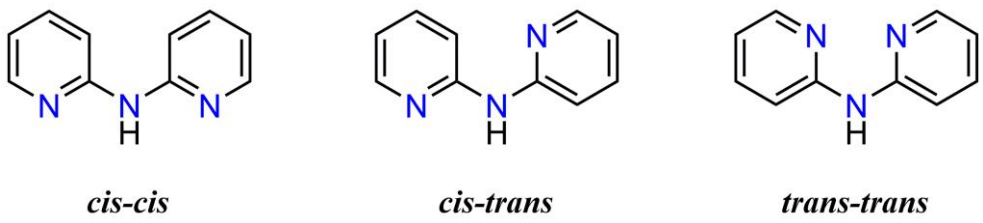

Figure 2.4 Conformations of dpyam ligand [6]

The nitrogen atoms in the pyridine rings can coordinate to bind with metal ions. Due to its chelating properties, the dpyam ligand can form stable complexes with various metal ions, which is significant in coordination chemistry. Furthermore, the dpyam ligand is very versatile, as it can exist in many protonation states, use one of nine different coordination modes as shown in Figure 2.5, and stabilize complexes comprising one, two, or three metal atoms, including mononuclear, dinuclear, and trinuclear complexes.

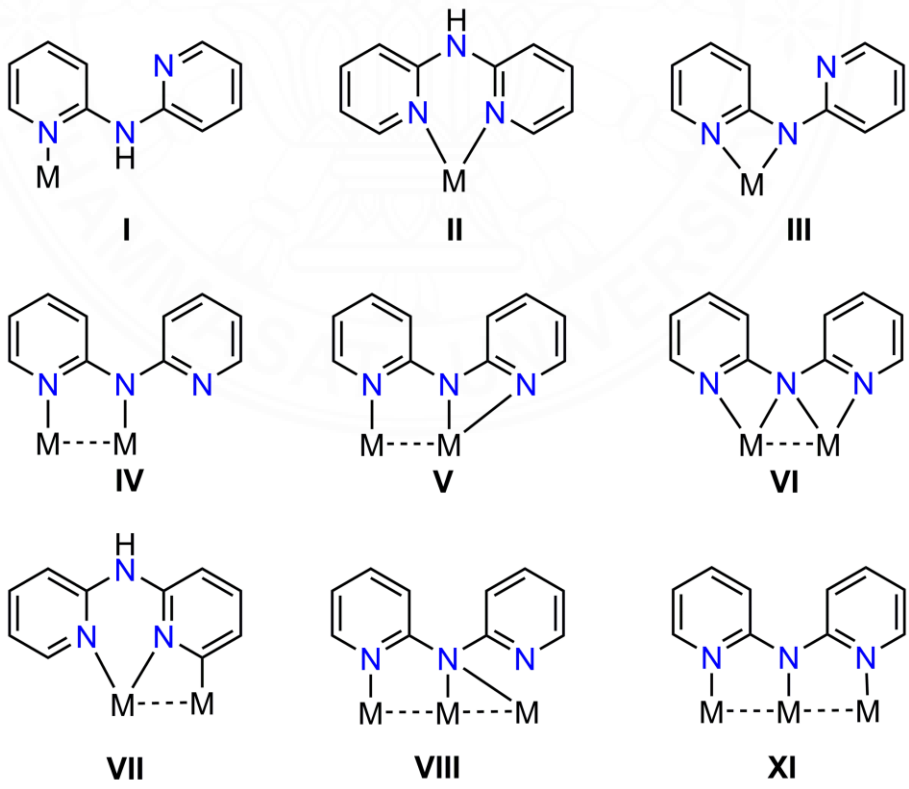

Figure 2.5 Coordination modes of dpyam ligand [6]

Coordination modes **I**, **II**, and **III** are found in mononuclear complexes. Mode **I** dpyam ligand coordinated to metal by monodentate ligand through nitrogen atom of only one pyridine ring. Coordination mode **II** dpyam ligand as a bidentate chelating mode through nitrogen atoms of both pyridine rings connected to metal. Mode **III** dpyam ligand anion as a bidentate chelating mode through nitrogen atoms of only one pyridine ring and deprotonated at primary amine for coordination to metal. In the case of the dinuclear complex, there are four possible coordination modes, modes **IV–VII**. Mode **IV** dpyam ligand as a monodentate mode through nitrogen atoms of only one pyridine ring and deprotonated at primary amine for coordination to each metal. In mode **V**, the dpyam ligand is a monodentate mode through nitrogen atoms of one pyridine ring, for the second bipyridine ring and nitrogen atom of amide group coordination to same metal. Mode **VI**, nitrogen atoms of each pyridine ring coordinated to a different metal center and nitrogen atom of amide coordinated to both metal centers in bridging mode. In coordination mode **VII**, nitrogen atoms of both pyridine rings coordinated to the same metal center and the deprotonated ortho carbon atoms from the pyridine ring coordinated to a separate metal center. Two coordination modes are found in the trinuclear complex. In mode **VIII**, the nitrogen atom of one dpyam is coordinated to the metal center, while the nitrogen atom of the other pyridine ring is uncoordinated. The nitrogen atom of the amide group in this mode bridges two separate metal centers. Coordination mode **IX** is found in a trinuclear complex in which each nitrogen atom of the dpyam ligand is coordinated to different metal centers, forming a linear chain of metal atoms [22].

Cu(II) complexes with the dpyam ligand have been extensively studied in coordination chemistry. The dpyam ligand can coordinate with the Cu(II) ion through nitrogen atoms in the pyridine ring, forming stable complexes. The complexes exhibit diverse properties and have applications in materials science, biological interactions, and catalysis.

2.2.2 Hydroxybenzoate derivatives

Hydroxybenzoate derivatives refer to compounds that are derived from hydroxybenzoic acid, which consists of a phenyl ring with a hydroxyl (-OH) group and a carboxyl (-COOH) group attached to it. When the carboxylic group is deprotonated, it is called a hydroxybenzoate derivative. The carboxylate group in benzoate derivatives contains *O*-donor atoms that can coordinate to the first-row transition metals such as chromium [23], manganese [24, 25], iron [26], cobalt [27], nickel [28], copper [7, 29] and zinc [28, 30] *etc*. The carboxylate group in benzoate can exhibit a variety of coordination modes, resulting in different structural arrangements [11], as shown in Figure 2.6. Likewise, a phenyl ring can provide π–π stacking interactions supporting crystal stability [10].

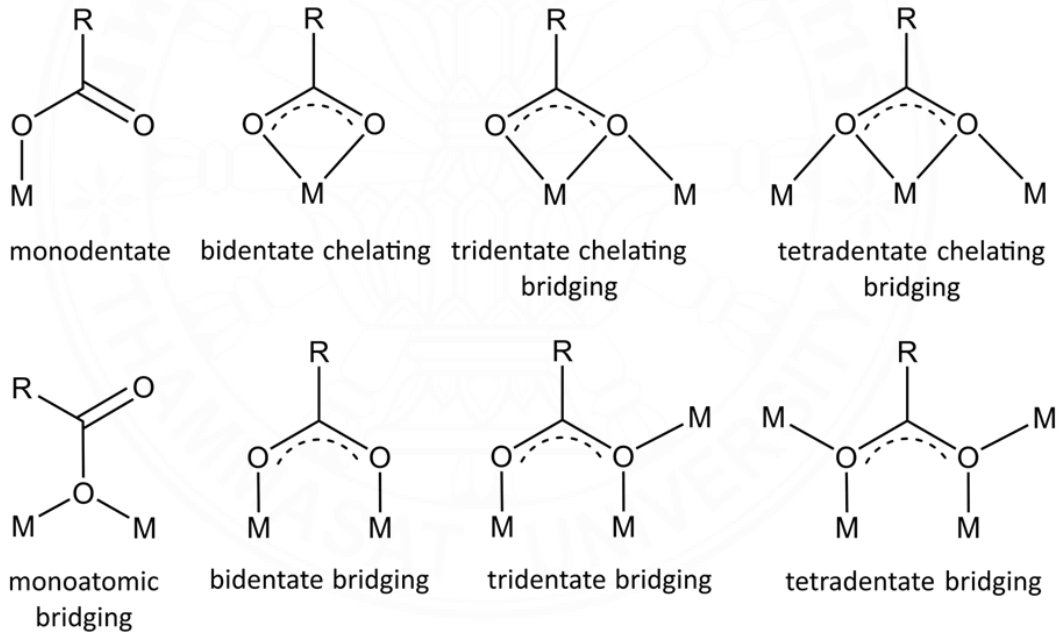

Figure 2.6 Types of carboxylate coordination modes [35]

The presence of a hydroxyl group on phenyl ring in *ortho*-, *meta*-, and *para*-positions that is, 2-hydroxybenzoate, 3-hydroxybenzoate, and 4-hydroxy- benzoate, as shown in Figure 2.7. The hydroxy group supports crystal stability by hydrogen bonding interactions, and the different arrangements of this group can be used to influence the crystal packing.

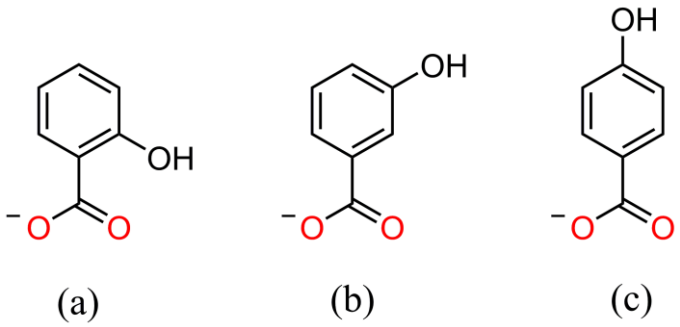

Figure 2.7 The molecular structure of benzoate derivatives of (a) 2-hydroxybenzate, (b) 3-hydroxybenzoate and (c) 4-hydroxybenzoate ligand

Cu(II) complex with carboxylate ligands can have diverse coordination geometries and structures based on the arrangement of the ligands around the Cu(II) ion. The complexes have been studied for magnetic [32, 33], optical properties [34], materials science, bioinorganic chemistry and catalytic. Therefore, we started to search for new mononuclear copper(II) complexes containing mixed *N*- and *O*-donor ligands, such as 2,2′-dipyridylamine (dpyam) and hydroxybenzoate derivatives and to study their catalytic properties in some reaction for example, olefin epoxidation [12], aerobic oxidation of alcohols [13, 14], ring-opening reactions [15] and the photocatalytic oxidation of benzyl alcohol [16].

2.3 The aerobic oxidation reaction of hydroxamic acids to nitroso compound

The aerobic oxidation reaction of hydroxamic acids refers to a reaction in which hydroxamic acids are oxidized to nitroso compounds in the presence of molecular oxygen (O_2), which converts the hydroxylamine group (-NHOH) into a nitroso group (-N=O), as shown in Scheme 2.1.

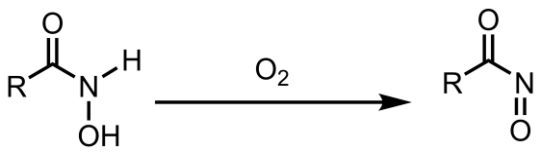

Scheme 2.1 The aerobic oxidation reaction of hydroxamic acids to nitroso compound

Nitroso compounds are intermediates in various chemical reactions, particularly in organic synthesis. They can be prepared in various methods such as direct nitrosation, nitroso-determination, reduction of nitro compound, the oxidation of nitrile oxides [77], cycloreversion of 9,10-dimethylanthracene cycloadducts [76], photochemical cleavage of 1,2,4-oxadiazole-4-oxides [74] and diazo compound rearrangement [75]. By far, the most common method for preparing nitroso compounds is through the oxidation of hydroxamic acid. Common synthesis of nitroso compound, as shown in Scheme 2.2.

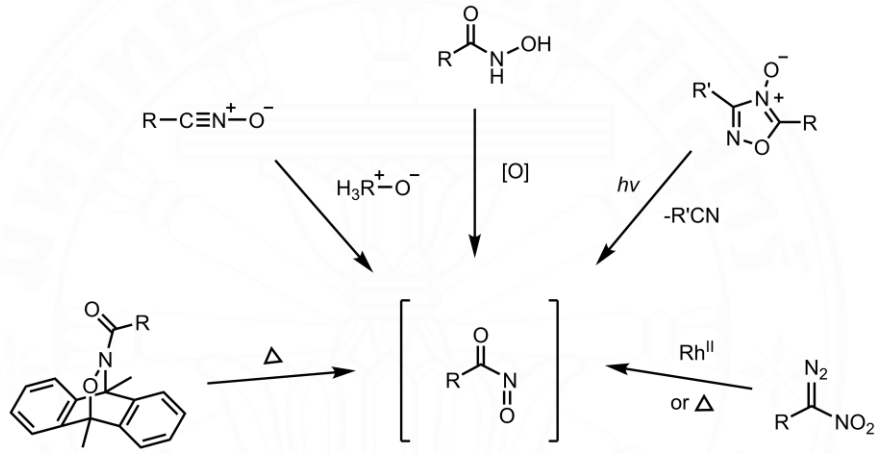

Scheme 2.2 Common synthetic routes to nitroso compound

The oxidation of the hydroxamic acids has been achieved under various oxidation conditions, including Swern oxidation [78], lead(IV), and silver oxides [80], Dess-Martin periodinane (DMP) [81], transition metal-catalyzed oxidation in the presence of peroxide [82-88], and most recently, copper-catalyzed aerobic oxidation [43]. The Swern oxidation reagent is a widely used method for oxidation because it gives a high yield. However, the limitations of this reaction are that the reaction requires low temperatures (-78 °C to 0 °C) for optimal results. In addition, the reaction uses oxalyl chloride ($C_2O_2Cl_2$) and dimethyl sulfoxide (DMSO), which are chemicals that can pose safety hazards to both researchers and the environment and are sensitive to moisture, and the presence of even small amounts of water can lead to side reactions and reduced yields. The reaction can lead to the formation of byproducts, such as carbon

monoxide (CO) and phosgene ($COCl_2$). In the aerobic oxidation reaction of hydroxamic acid oxidations, silver oxide or lead dioxide were found to be excellent [80]. Silver is relatively expensive, and reaction times with silver oxide can be longer compared to more aggressive oxidants. The advantages of lead dioxide are that it is a strong oxidizing agent and can undergo rapid oxidation reactions. However, the disadvantages of lead compounds are that they are toxic, which is dangerous and toxic to the environment. There is a cost for waste disposal. For this reason, this is a restriction on the use of silver oxide or lead dioxide. Dess-Martin periodinane (DMP) [81] is a hypervalent reagent. It operates under mild conditions and provides high selection, high efficiency, and the absence of toxic byproducts. DMP is a stable, crystalline reagent that is easy to handle. However, the limitation of DMP is that it is relatively expensive, and excess reagents are required for complete oxidation in some cases. Peroxides are not the best reagents because they depend on the catalyst for the reaction. Including having to consider catalytic activity with the cost and toxicity of the metal. Therefore, copper-catalyzed aerobics has gained significant attention in recent years due to its being a readily available metal. Relatively cheap, less toxic, and high catalytic properties. It is environmentally friendly and, in the reaction, uses atmospheric oxygen as the oxidant, avoiding using environmentally harmful reagents. For this reason, there are many people interested in developing Cu catalysts.

Nitroso compounds are intermediates in various chemical reactions, particularly in organic synthesis. Nitroso compounds are formed in situ by the oxidation of hydroxamic acid and react with a diene via a Hetero-Diels-Alder (HAD) reaction, resulting in a cycloadduct, as shown in Scheme 2.3. Cycloadducts and ene-products act as intermediates in organic synthesis used in natural products, pharmaceuticals, biological activities, and bioactive agents [91].

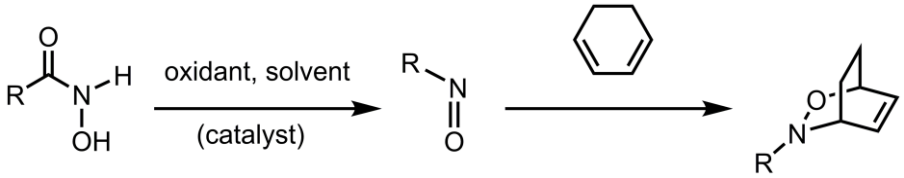

Scheme 2.3 Hetero-Diels-Alder of nitroso compound with 1,3-cyclohexadiene

2.4 Literature reviews for transition metal constructed by 2,2′-dipyridylamine and benzoate derivatives

In 2002, Sujittra Youngme and co-workers [37] synthesized new mononuclear Cu(II) complexes, $[Cu(dpyam)(NO_3)_2]$. The synthesis of the complex was carried out using the slow evaporation method. Initially, a solution of $Cu(NO_3)_2 \cdot 3H_2O$ in acetone was heated to a boiling point and then added to a warm solution of dpyam dissolved in methanol. After that, the solution of $CH_3COONa \cdot 3H_2O$ in water was slowly added and stirred for 5 minutes. The green crystals were obtained with an 82% yield. The asymmetric unit consists of a Cu(II) ion, two chelating dpyam ligands, and two monodentate nitrato ligands. In the structure, the environment Cu(II) ion is surrounded by four nitrogen atoms of pyridine rings from chelating dpyam ligands and two oxygen atoms from two monodentate nitrato ligands, resulting in a distorted octahedral geometry, as shown in Figure 2.8. The crystal structure of this complex is stabilized by the weak C–H···O intermolecular interaction and N–H···O hydrogen bonds.

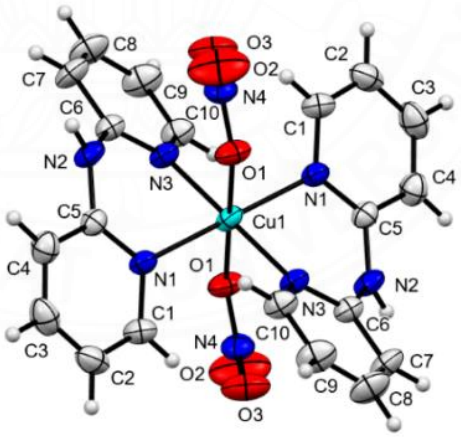

Figure 2.8 View of the molecular structure of $[Cu(dpyam)_2(NO_3)_2]$ with the atomic numbering scheme and displacement ellipsoid drawn at the 50% probability level [37]

In 2007, Nobuo Okabe and co-workers [38] synthesized new ternary Cu(II) complex, [Cu(benz)(dpyam)Cl] by using slow evaporation method. The mixed solution of dpyam dissolved in a methanol-water solution was reacted with benzoic acid, stirred for 5 minutes at room temperature. After that, the solution of $CuCl_2 \cdot 2H_2O$ in water was slowly added and reacted for 15 minutes. After that, this solution was filtrated and allowed to stand and slowly evaporate in the air at room temperature. Finally, the green plate crystals were obtained. This complex crystallizes in the orthorhombic crystal system in the *P*nma space group. The asymmetric unit consists of a Cu(II) ion, one chelating dpyam ligand, one chelating benzoate ligand and one chloride anion, as shown in Figure 2.9. In the structure, the environment Cu(II) ion is surrounded by two nitrogen atoms of the pyridine rings from a chelating dpyam ligand, two oxygen atoms of carboxylate group from a chelating benzoate ligand, and one chloride atom from a monodentate chlorido ligand with a weak Cu–Cl bond (Cu–Cl: 2.502(3) Å). The ligand atoms involved in coordination are almost coplanar, and the Cu atom is positioned 0.2986(1) Å above this plane in the direction of the apical Cl atom. The Cu(II) atom is five-coordinate, forming a square pyramidal CuN_2O_2Cl chromophore with a τ_5 value of 0. The crystal structure is stabilized by N–H···Cl hydrogen bonding interactions and π–π stacking interactions, as shown in Figure 2.10. The distances between the centroids of the aromatic rings are 3.592 (4) Å and 3.468 (4) Å.

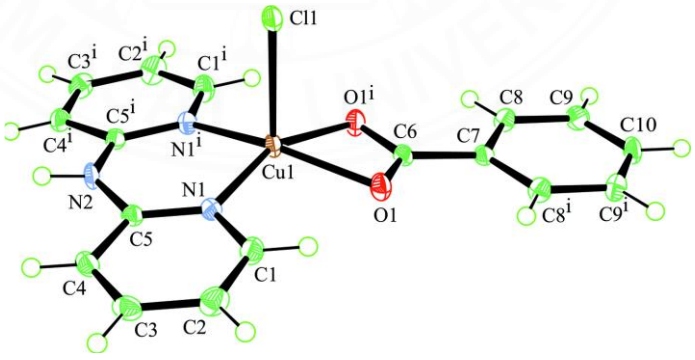

Figure 2.9 View of the molecular structure of [Cu(dpyam)(benz)Cl] with the atomic numbering scheme and displacement ellipsoid drawn at the 50% probability level

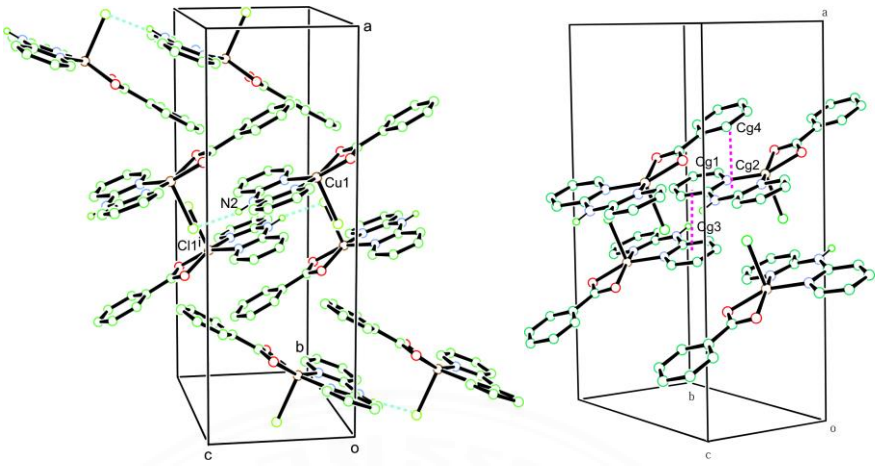

(a) (b)

Figure 2.10 View of crystal packing of [Cu(dpyam)(benz)Cl] complex showing (a) N–H···Cl interactions as green dashed lines and (b) the π–π stacking interactions as purple dashed lines [38]

In 2007, Nobuo Okabe and co-workers [39] synthesized a new ternary Cu(II) complex, [Cu(dpyam)(4-NO_2benz)Cl] by the slow evaporation method. The mixed solution of dpyam dissolved in a methanol-water solution was reacted with 4-nitrobenzoic acid, and stirred for 5 minutes at room temperature. After that, this solution was filtrated, allowed to stand, and slowly evaporated in the air at room temperature. Finally, the green block crystals were obtained. This complex crystallizes in the triclinic crystal system in the *P*1 space group. The asymmetric unit consists of a Cu(II) ion, one chelating dpyam ligand, one chelating 4-nitrobenzoate ligand and one chloride anion, as shown in Figure 2.11(a). In the structure, the environment Cu(II) ion is surrounded by two nitrogen atoms of the pyridine rings from a chelating dpyam ligand, two oxygen atoms of the carboxylate group from a chelating 4-nitrobenzoate ligand, and one chloride atom from a monodentate chlorido ligand with a weak Cu–Cl bond (Cu–Cl: 2.468(3) Å). The ligand atoms involved in coordination are almost coplanar, and the Cu atom is positioned 0.3274(1) Å above this plane in the direction of the apical Cl atom. The Cu(II) atom is five-coordinate, forming a square pyramidal CuN_2O_2Cl chromophore with a τ_5 value of 0.01. The crystal structure is stabilized by N–H···Cl hydrogen bonds and π–π stacking interactions, as shown in Figure 2.11(b).

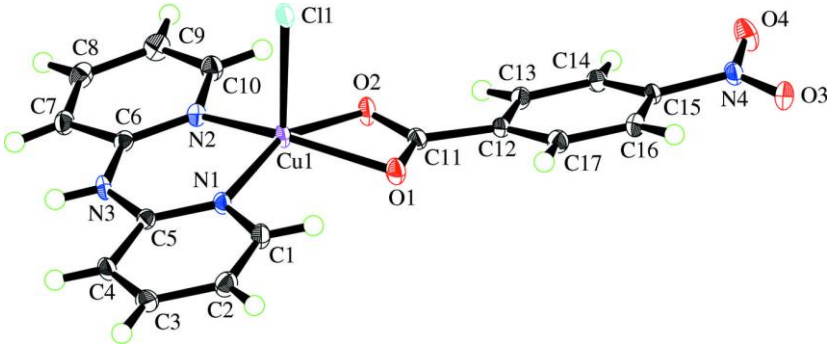

(a)

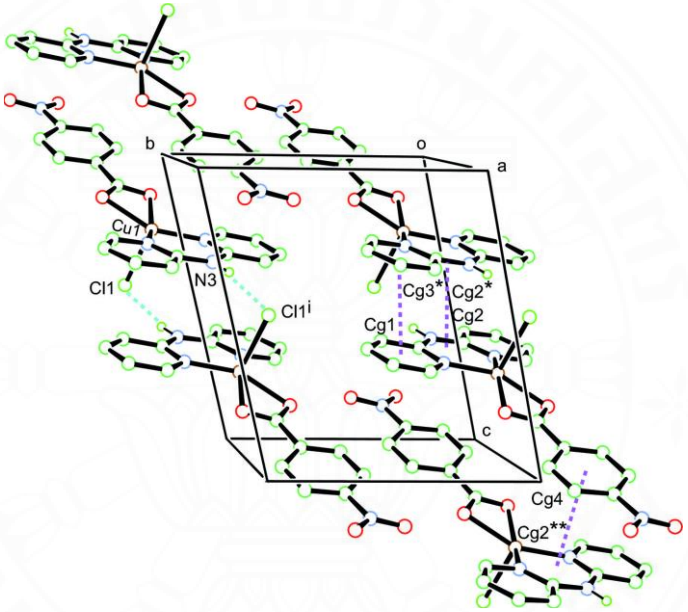

(b)

Figure 2.11 (a) View of the molecular structure of [Cu(dpyam)(4-NO_2benz)Cl], and (b) View of crystal packing of [Cu(dpyam)(4-NO_2benz)Cl] complex showing the N–H···Cl interactions as green dashed lines and the π–π stacking interactions as purple dashed lines [39]

In 2005, Yue Wang and co-workers [40] synthesized a series of ternary transition metal complexes are [Co(dpyam)(4-OHbenz)$_2$] (**1**), [Ni(dpyam)(4-OHbenz)(H_2O)$_2$](NO_3)·H_2O (**2**), [Ni(dpyam)$_2$(4-OHbenz)]$_2$(NO_3)(4-OHbenz)·5H_2O (**3**), [Cu(dpyam)(4-OHbenz)Cl] (**4**) and [Zn(dpyam)(4-OHbenz)$_2$]$_2$·0.5H_2O (**5**) their DNA binding propensity has been evaluated by fluorescence method. The complexes were synthesized by the slow evaporation. In the structure of complex **1**, the Co(II) atom is coordinated to two nitrogen atoms of pyridine rinds from a chelating dpyam ligand and four oxygen atoms of carboxylate group from two 4-OHbenzoate ligands, forming a distorted octahedral geometry with the [CoN_2O_4] chromophore. The crystal structure is stabilized by hydrogen bonding interaction and π–π stacking interaction, as shown in Figure 2.11(a) and 2.11(b). The structure of complex **2** consists of discrete [Ni(dpyam)(4-OHbenz)(H_2O)$_2$]$^+$ cation unit, one nitrate anion and one water molecule. The Ni(II) ion has a slightly distorted octahedron geometry defined by two nitrogen atoms of pyridine rings from a chelating dpyam ligand, two oxygen atoms from two aqua ligands and two oxygen atoms of carboxylate group from one 4-OHbenzoate ligand. The crystal structure is stabilized by N–H···O hydrogen bonds and π–π stacking interactions, as shown in Figure 2.11(c) and 2.1(d). Complex **3** consists of discrete two [Ni(dpyam)$_2$(4-OHbenz)]$^{2+}$ cation units, a nitrate ion, a deprotonated 4-OHbenz anion and five water molecules. The Ni(II) ion has a distorted octahedron geometry defined by four nitrogen atoms of the pyridine rings from two chelating dpyam ligands and two oxygen atoms of the carboxylate group from a 4-OHbenzoate ligand. Hydrogen bonds stabilize the crystal structure. However, no π–π interaction is observed in the packing due to a large coordination sphere, as shown in Figure 2.12(a) and 2.12(b). In the structure complex **4**, the environment Cu(II) ion is surrounded by two nitrogen atoms of the pyridine rings from a chelating dpyam ligand, two oxygen atoms of the carboxylate group from a chelating 4-OHbenzoate ligand and one chloride atom from a monodentate chlorido ligand (Cu–Cl: 2.5876(6) Å). The τ_5 value is 0.03, conforming a distorted square pyramidal geometry with the [CuN_2O_2Cl] chromophore, as shown in Figure 2.12(c) and 2.12(d). Complex **5** contains two crystallographically independent [Zn(dpyam)(4-OHbenz)$_2$] molecules. In each ZnN_2O_2 core unit, the Zn(II) ion is distorted octahedral geometry coordinated by two nitrogen atoms of the pyridine rings from a chelating dpyam ligand, four oxygen atoms of the carboxylate group from two

4-OHbenzoate ligands. The structure is stabilized through networks of N–H···O and O–H···O hydrogen bonds, as well as π–π interactions, as shown in Figure 2.12(e) and 2.12(f).

The complexes indicate competitive inhibition of ethidium binding to DNA, with the relative order: 3 > 2 > 1 > 5 > 4, with the cationic charged Ni(II) complexes **2** and **3** showing the most efficient inhibitory abilities.

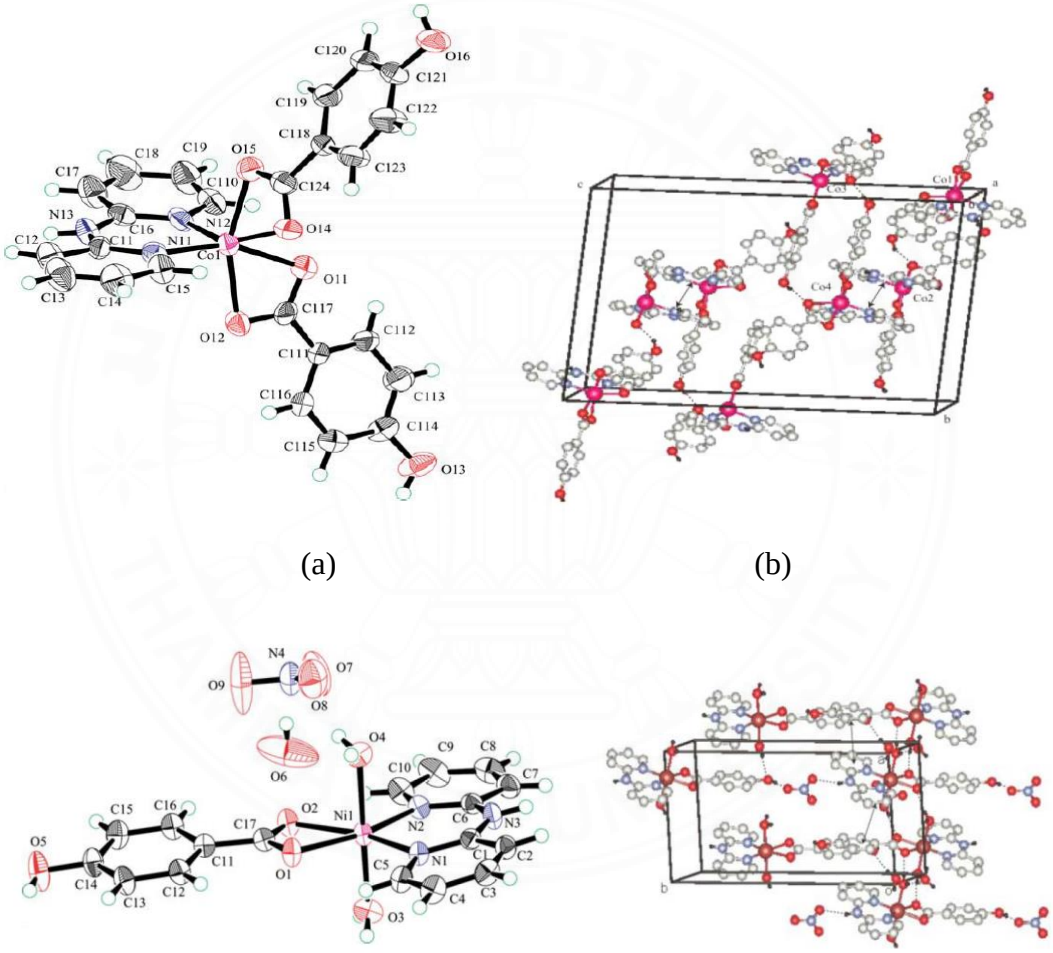

Figure 2.12 (a) The molecular structure of complex **1**, (b) the crystal packing of complex **1** by hydrogen bonding network and the π–π interaction, (c) The molecular structure of complex **2**, and (d) the crystal packing of complex **2** by hydrogen bonding network and the π–π interaction [40]

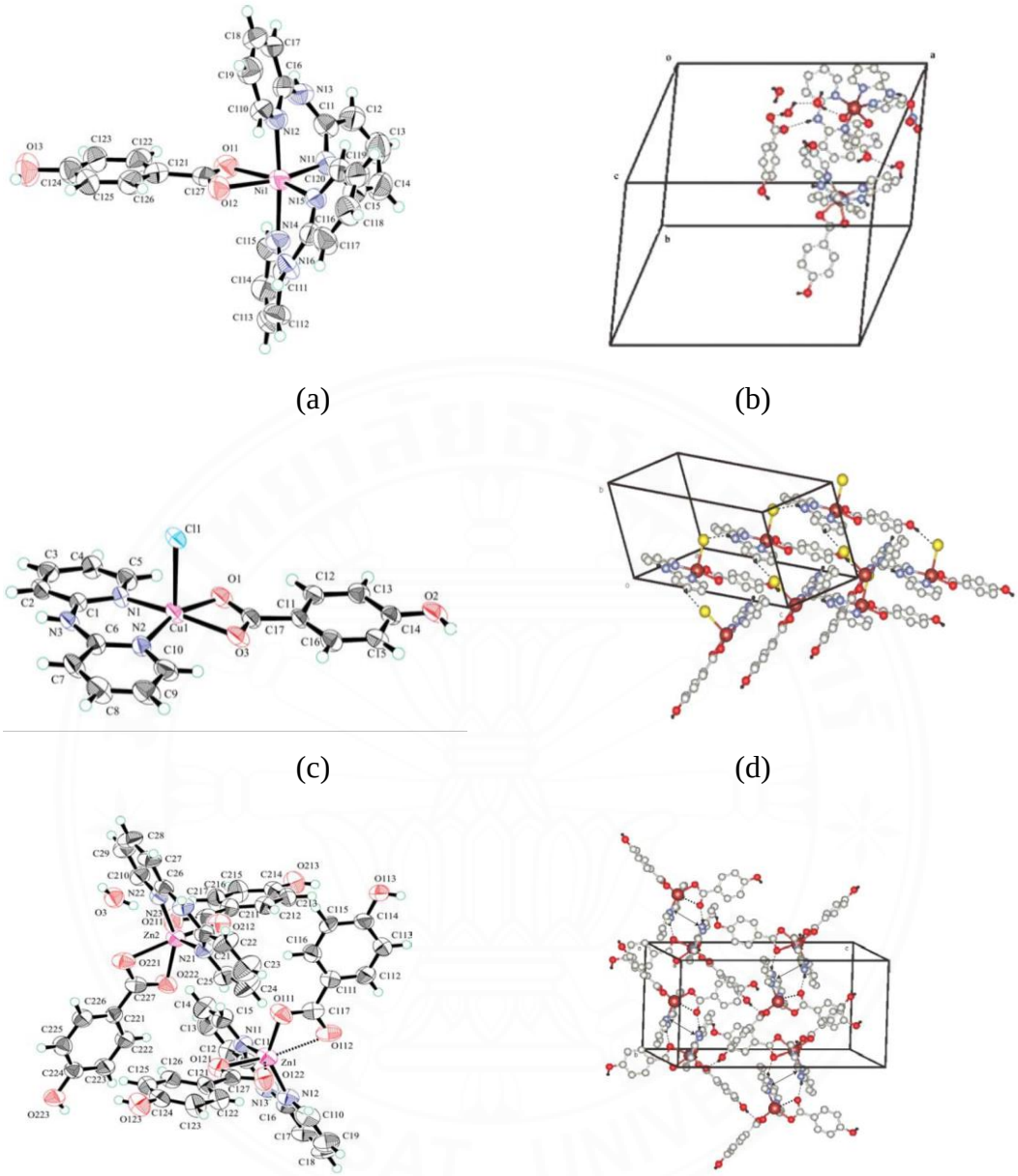

Figure 2.13 (a) The molecular structure of complex **3**, (b) the crystal packing of complex **3** by hydrogen bonding network, (c) The molecular structure of complex **4**, (d) the crystal packing of complex **4** by hydrogen bonding network and the π–π interaction, (e) The molecular structure of complex **5**, and (f) the crystal packing of complex **5** by hydrogen bonding network [40]

In 2009, Yue Wang and co-workers [41] synthesized new ternary transition metal complexes are [Cu(dpyam)(4-NH_2benz)Cl]·H_2O (**1**), [Zn(dpyam)(4-NH_2benz)$_2$]·H_2O (**2**) and their DNA binding propensity has been evaluated by fluorescence and viscosity method. The complexes were synthesized by using the slow evaporation method. Complex **1** was synthesized by using the mixed solution of 4-NH_2benzoic acid in a methanol-water reacted with the solution of dpyam ligand in methanol. Then, the solution of $CuCl_2$·$2H_2O$ in methanol–water was added and reacted for 30 mins. After that, the mixed solution was filtrated and allowed to stand and slowly evaporate in the air at room temperature. Finally, the green plate crystals were obtained. This complex crystallizes in the monoclinic crystal system in the $P2_1/n$ space group. In the structure, the environment Cu(II) ion is surrounded by two nitrogen atoms of the pyridine rings from a chelating dpyam ligand, two oxygen atoms of the carboxylate group from a chelating 4-NH_2benzoate ligand, and one chloride atom from a monodentate chlorido ligand with a weak Cu–Cl bond (Cu–Cl: 2.603(3) Å) , as shown in Figure 2.18(a). The ligand atoms involved in coordination are almost coplanar, and the Cu atom is positioned 0.114(7) Å above this plane in the direction of the apical Cl atom. The Cu(II) atom is five-coordinate, forming a square pyramidal CuN_2O_2Cl chromophore with a τ_5 value of 0.14. The crystal structure is stabilized by hydrogen bonds and π–π stacking interactions, as shown in Figure 2.18(b). Complex **2** was synthesized using the solution of 4-NH_2benzoic acid in a methanol-water and was reacted with dpyam ligand in methanol. Then, the $ZnCl_2$ dissolved in methanol-water solution was added and reacted for 30 mins. After that, this solution was filtrated and allowed to stand and slowly evaporate in the air at room temperature. Finally, the colorless needle crystals were obtained. In the structure of complex **2**, the Zn(II) ion has a distorted octahedral geometry defined by two nitrogen atoms of the pyridine rings from a chelating dpyam ligand and four oxygen atoms of the carboxylate group from two 4-NH_2benzoate ligands, as shown in Figure 2.19(a). The crystal structure is stabilized by hydrogen bonds and π–π stacking interactions, as shown in Figure 2.19(b).

The complexes display competitive inhibition of ethidium binding to DNA, and complex **1** has a DNA binding propensity more than complex **2**.

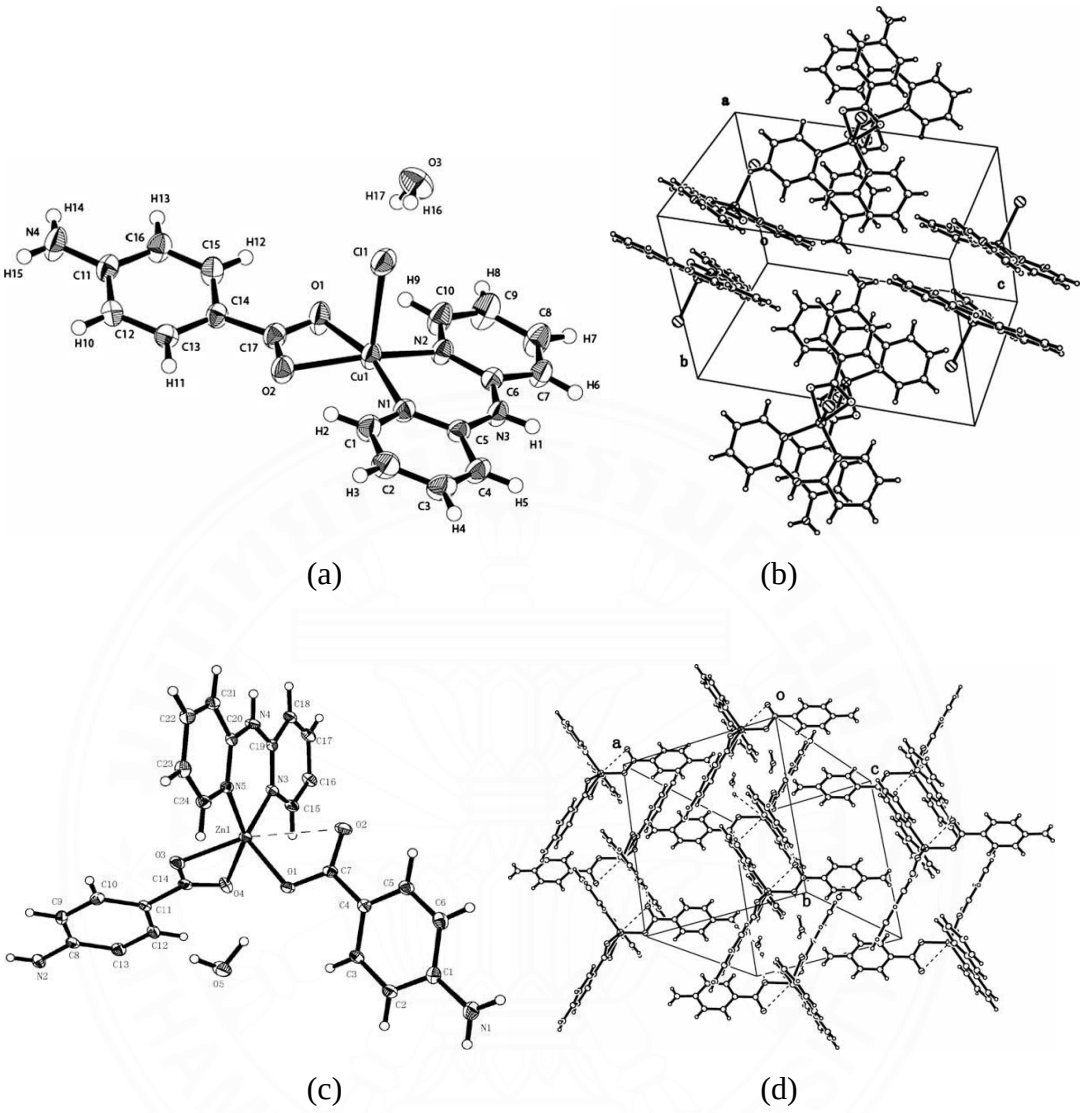

Figure 2.14 (a) The molecular structure of complex **1**, (b) the crystal packing of complex **1** by π–π interaction along *b* direction, (c) The molecular structure of complex **2**, and (d) the crystal packing of complex **2** by π–π interaction along *b* direction [41]

Table 2.1. Summary of literature reviews for mononuclear transition metal(II) constructed by 2,2′-dipyridylamine and benzoate derivatives by slow evaporation

Year	Compound	Crystal system	Space group	Geometry	Application	[Ref.]
2002	$[Cu(dpyam)_2(NO_3)_2]$	Monoclinic	$P2_1/a$	dist. Oct.	-	[37]
2007	[Cu(dpyam)(OHbenz)Cl]	Orthorhombic	*Pnma*	dist. Sq. Py.	-	[38]
2007	$[Cu(dpyam)(4\text{-}NO_2benz)Cl]$	Triclinic	*P*1	dist. Sq. Py.	-	[39]
2005	$[Co(dpyam)(4\text{-}OHbenz)_2]$	Triclinic	*P*1	Oct.	DNA binding	[40]
	$[Ni(dpyam)(4\text{-}OHbenz)\ (H_2O)_2](NO_3)\cdot H_2O$	Monoclinic	$P2_{1/}c$	Oct.		
	$[Ni(dpyam)_2(4\text{-}OHbenz)\ ]_2(NO_3)(4\text{-}OHbenz)\cdot 5H_2O$	Monoclinic	$P2_{1/}c$	Oct.		
	[Cu(dpyam)(4-OHbenz)Cl]	Orthorhombic	$P2_12_12_1$	dist. Sq. Py.		
	$[Zn(dpyam)(4\text{-}OHbenz)_2]_2\cdot 0.5H_2O$	Monoclinic	$P2_1/c$	dist. Oct.		
2009	$[Cu(dpyam)(4\text{-}NH_2benz)Cl]\cdot H_2O$	Monoclinic	$P2_1/n$	dist. Sq. Py.	DNA-binding	[41]
	$[Zn(dpyam)(4\text{-}NH_2benz)_2]\cdot H_2O$	Monoclinic	$P2_1/n$	dist. Oct.	DNA-binding	

Abbreviation: dpyam = 2,2′-dipyridylamine, OHbenz = benzoate, 2-OHbenz = 2-hydroxybenzoate, 3-OHbenz = 3-hydroxybenzoate, 4-OHbenz = 4-hydroxy-benzoate, $4\text{-}NO_2benz$ = 4-nitrobenzoate, $4\text{-}NH_2benz$ = 4-aminobenzoate, dist. Oct. = distorted Octahedral and Sq. Py. = Square Pyramidal

2.5 Literature reviews for mononuclear copper(II) complexes containing mixed *N*- and *O*-donor as catalyze in organic reactions

In 1997, Gopal Das and co-workers [12] synthesized a new mononuclear Cu(II) complex [Cu(L-H){o-(CHO)$C_6H_4O^-$}] by using the slow evaporation method. This complex was synthesized by using $Cu(ClO_4)_2 \cdot H_2O$, 2-(dimethylamino)ethyl-amine (**L**) and salicylaldehyde in 1:1:1 mol ratio in methanol solution, heat at 40 °C for 30 min with 3 equiv of solid KOH resulting dark green solution. After that, the solution was filtrated and allowed to stand and slowly evaporate in the air at 293 K. Finally, the green plate crystals were obtained with 59% yield. This complex crystallizes in the monoclinic crystal system in the C_2/c space group. In the structure, the environment Cu(II) ion is surrounded by one tridentate Schiff base (L) and one bidentate salicylaldehyde ligand, resulting in a distorted square pyramidal geometry with the [CuN_2O_3] chromophore, as shown in Figure 2.20.

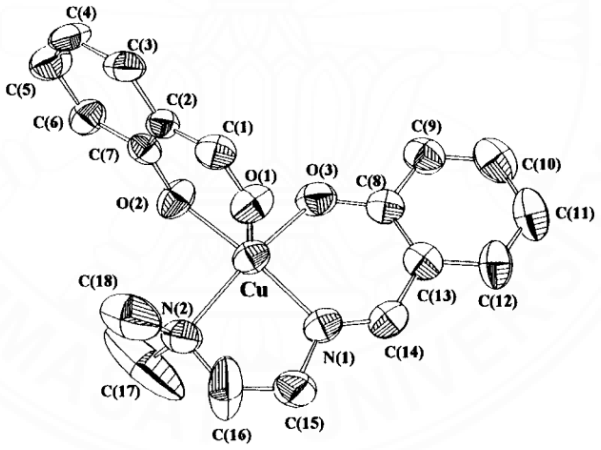

Figure 2.15 The molecular structure of [Cu(L-H){o-(CHO)$C_6H_4O^-$}] complex displacement ellipsoids are drawn at the 50% probability level [12]

The study of catalytic properties for oxidation of olefins to epoxides has been performed by using the following optimized conditions, a substrate (10 mmol) was reacted with 2-methylpropanal (20 mmol) in 15 mL of MeCN solution with 5 mol % of Cu(II) catalyst under an atmosphere of molecular oxygen at ambient pressure and temperature to produce epoxides with 40%yield, as shown in Scheme 2.4.

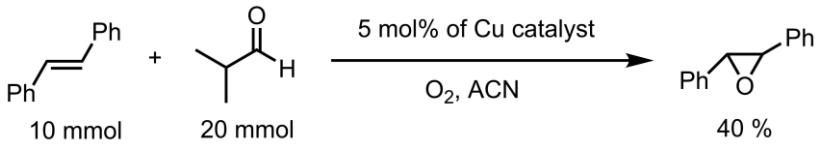

Scheme 2.4 The oxidation of olefins to epoxides with Cu(II) complex as catalyst

In 2007, Alex John and co-workers [15] synthesized a new mononuclear Cu(II) complex, [CuL_2], when L = {2-[1-(2-methylphenylimino)ethyl]phenoxy}by using $Cu(OAc)_2{\cdot}H_2O$ (0.582 g, 2.92 mmol) reacted with 2-[1-(2-methylphenylimino)-ethyl]phenol in 40 mL of methanol solution and stirred at room temperature until a clear solution was obtained. After that, NEt_3 (0.314 g, 3.10 mmol) was added to the mixed solution. The reaction was stirred at reflux for 12 hours and then cooled to room temperature. Finally, the reddish-brown solid was obtained and filtration and vacuum dried with 75 % yield (0.573 g). This complex crystallizes in the monoclinic crystal system in the $P2_1/n$ space group. In the structure, the environment Cu(II) ion is surrounded by two molecules of ligands, resulting in perfectly square planar geometry with the [CuN_2O_2] chromophore, as shown in Figure 2.21.

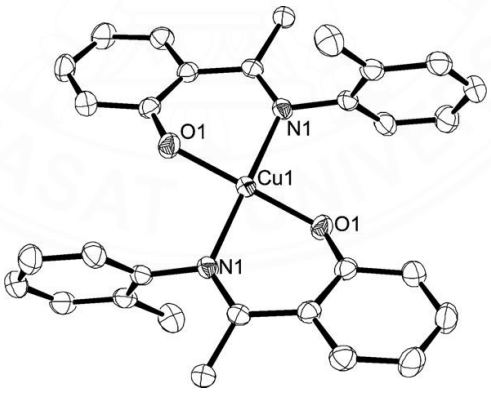

Figure 2.16 The molecular structure of [CuL_2] complex displacement ellipsoids are drawn at the 50% probability level [15]

The study of catalytic properties for ring-opening polymerization of L-lactide has been performed by using the following optimized conditions, L-lactide (1.000 g, 6.94 mmol) with Cu(II) catalyst under solvent-free melt conditions and vacuum at 50 °C for 30 mins. After that, it was heated at 160 °C for 4 hours. Polylactide polymers were obtained with 60% yield, as shown in Scheme 2.5.

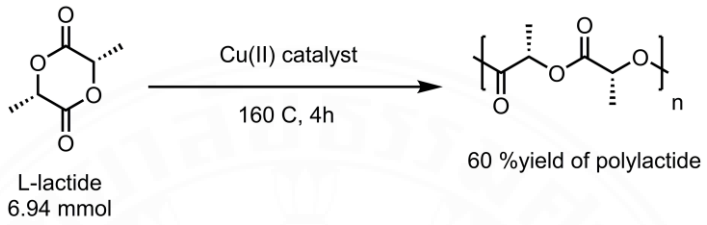

Scheme 2.5 The ring-opening polymerization of L-lactide with Cu(II) complex as catalyst

In 2014, Zahra Alaji and co-workers [14] synthesized a new mononuclear Cu(II) complex by using the solution of 3,5-DTBQ (0.22 g, 1 mmol) reacted with 2-aminobenzylamine (0.122 g, 1 mmol) in 4 ml of MeCN solution and stirred for 30 min at the room temperature in the presence of air resulting in the yellow precipitate. After that, it was filtered and stirred the yellow precipitate in the MeCN solution. Pyridine-2-carbaldehyde (0.096 mL, 1 mmol) was added and stirred. In the next step, $Cu(OAc)_2{\cdot}2H_2O$ (0.199 g, 1 mmol) was added to the reaction mixture, and NEt_3 (2 equiv.) was also added. Finally, a red-brown precipitate was obtained after 4 hours with a yield of 63%. This complex crystallizes in the monoclinic crystal system in the $P1\ 2_1/c$ space group. In the structure, the environment Cu(II) ion is surrounded by three nitrogen atoms of amidate, pyridine, and an iminophenol (N2, N3, N4), with an oxygen atom (O5) of a phenolate ligand, resulting in a distorted square-planar geometry (dihedral angle = 7.9°) with the $[CuN_3O]$ chromophore, as shown in Figure 2.22.

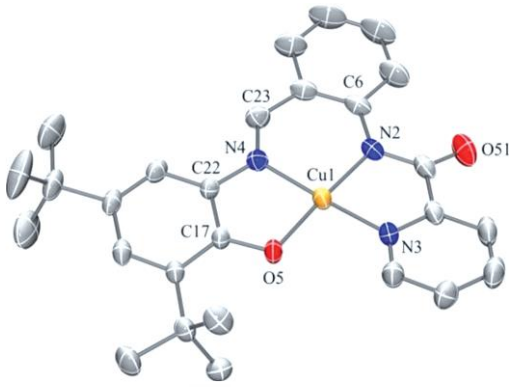

Figure 2.17 The molecular structure of Cu(II) complex displacement ellipsoids are drawn at the 50% probability level [14]

In the study of catalytic properties, the optimized condition of aerobic alcohol oxidation is shown in Scheme 2.6. The results show that the new Cu(II) complex is capable of catalyzing efficient aerobic alcohol oxidation under mild conditions.

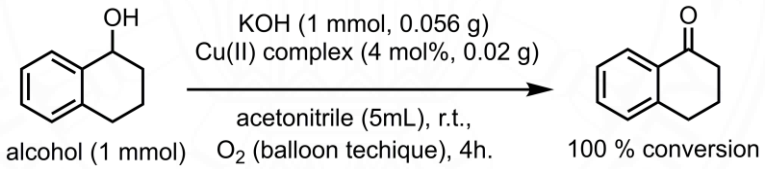

Scheme 2.6 The aerobic alcohol oxidation with Cu(II) complex as catalyst

In 2021, Rashi Ranjan and co-workers [16] synthesized two new mononuclear Cu(II) complexes, [Cu(HL^1)] (**1**) and [Cu(HL^2)] (**2**), when [H_3L^1 = 2-((2-((3,5-dichloro-2-hydroxybenzyl)amino)ethyl)(2-hydroxyethyl)amino)-2-methoxyacetic acid] and [H_3L^2 = 2-((2-((3,5-dichloro-2-hydroxybenzyl)amino)ethyl)(2-hydroxy-ethyl)amino)-2-ethoxyacetic acid] by using the slow evaporation method. Synthesis of complex **1** using the solution of $Cu(OAc)_2 \cdot H_2O$ (0.1 g, 0.5 mmol) in 10 mL of methanol was added to H_2L (0.15 g, 0.5 mmol) and triethylamine (70 µl, 0.5 mmol) in 10 mL of methanol and stirred at room temperature for 4 hours, resulting in a green solution. The mixture was filtered and then slowly evaporated in the air. Finally, after 4 days, dark

green crystals were obtained with a yield of 75%. Complex **2** was obtained following the same procedure as complex **1** by using ethanol instead of methanol. After 3 days, green crystals were obtained with a yield of 72%. Complex **1** crystallizes in a triclinic crystal system in the *P*-1 space group, whereas complex **2** crystallizes in a monoclinic crystal system in the *P*-121/c-1 space group. In the structure of complex **1**, there are two crystallographically independent copper ions. The environment Cu(II) ion is surrounded by three *O*- and two *N*-donor atoms of the ligand, resulting in a square-pyramidal geometry with the [CuN_2O_3] chromophore and τ_5 of 0.20 and 0.21, respectively. While complex **2** has a τ_5 of 0.22.

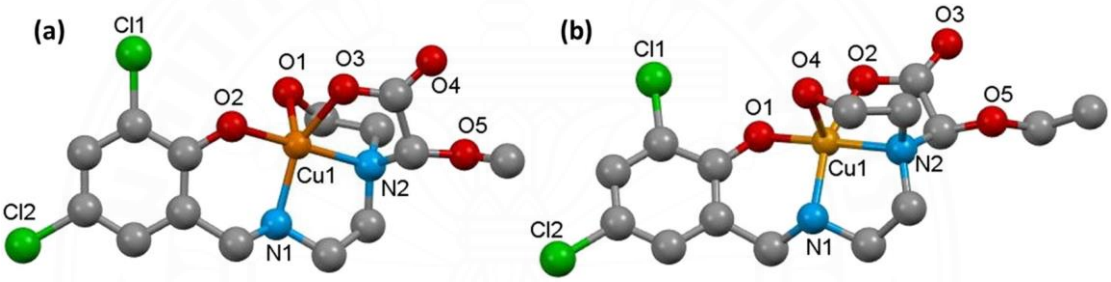

Figure 2.18 The crystal structure of (a) complexes **1** and (b) **2**. Hydrogen atoms are omitted for clarity [16]

In the study of catalytic properties, the optimized condition uses benzyl alcohol (0.96 mmol) with catalyst (1 mol%, 0.0096 mmol) and TEMPO (3 mol%, 0.0288 mmol) in 1 mL of DCM in 25°C stir under O_2 (balloon pressure) for 3 hours and light intensity (12-W LED bulb, 400–800 nm wavelength). The result showed that both complexes had shown their ability to act as an efficient photocatalyst to oxidize primary alcohol into corresponding aldehyde at ambient temperature and in the presence of aerial oxygen and TEMPO. Complex **1** selectively produces only aldehyde with a conversion of 96%, whereas complex **2** up to 92% conversion in 3 hours.

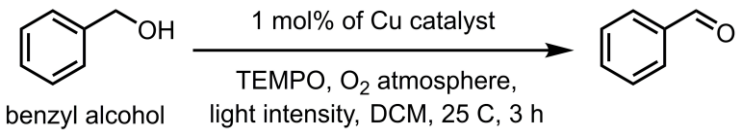

Scheme 2.7 The visible-light-driven alcohol oxidation with Cu(II) complex as catalyst

From the literature review, these studies present that mononuclear copper(II) complexes containing mixed *N*- and *O*-donor ligands can be the catalysts for a variety of organic reactions, such as olefin epoxidation, aerobic oxidation of alcohols, ring-opening reactions and the photocatalytic oxidation of benzyl alcohol. Therefore, we are interested in the design and synthesis of new mononuclear copper(II) complexes containing mixed *N*- and *O*-donor ligands, 2,2′-dipyridylamine (dpyam), and hydroxybenzoate derivatives and studying their catalytic properties.

CHAPTER 3
RESEARCH METHODOLOGY

This chapter describes the methodology for designing the structure and design conditions of new mononuclear Cu(II) complexes. Materials of this research include chemicals, glassware and equipment, synthesis, characterization and the technique for determining crystal structure, including the catalytic properties of new mononuclear Cu(II) complexes.

3.1 Design

The new mononuclear Cu(II) complexes have been designed for two series, namely, series **I** designed with the general formula of [Cu(dpyam)(x-OHbenz)$_2$] and series **II** with the general formula of [Cu(dpyam)(x-benzoate ligand)Cl] (when x = 2-, 3- and 4-OHbenz). The structure of series **I** consists of a Cu(II) ion, a chelating dpyam ligand, and two hydroxybenzoate chelating ligands, forming an octahedral geometry with a CuN_2O_4 chromophore. Meanwhile, the structure of series **II** consists of a Cu(II) ion, a chelating dpyam ligand, a chelating hydroxybenzoate ligand, and a chloride ligand, forming a square pyramidal geometry with $[CuN_2O_2Cl]$ chromophore. For Cu(II) complexes in a series **II,** the geometry aimed to be a five-coordinate to increase the active site and the Cl atom is expected to be the leaving group on Cu(II) center. All mononuclear Cu(II) complexes will be synthesized by using the slow evaporation method. For the synthetic conditions, the influence of the mole ratio of the reactant as Cu(II) salt: dpyam: x-OHbenz and the type of solvents have been studied. The proposed structures of new mononuclear Cu(II) complexes and synthetic conditions are shown in Figures 3.1 and 3.2.

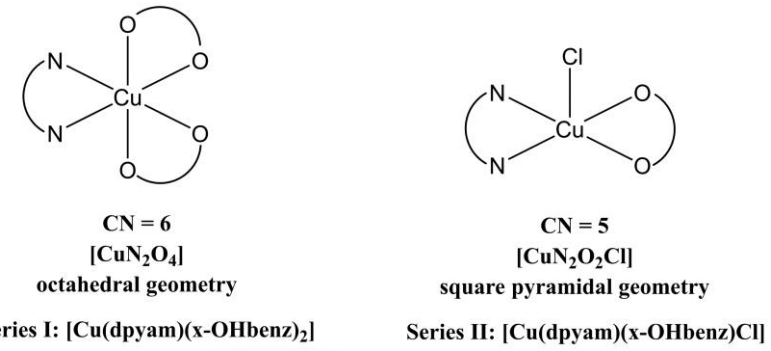

Figure 3.1 Proposed structures of new mononuclear copper(II) complexes

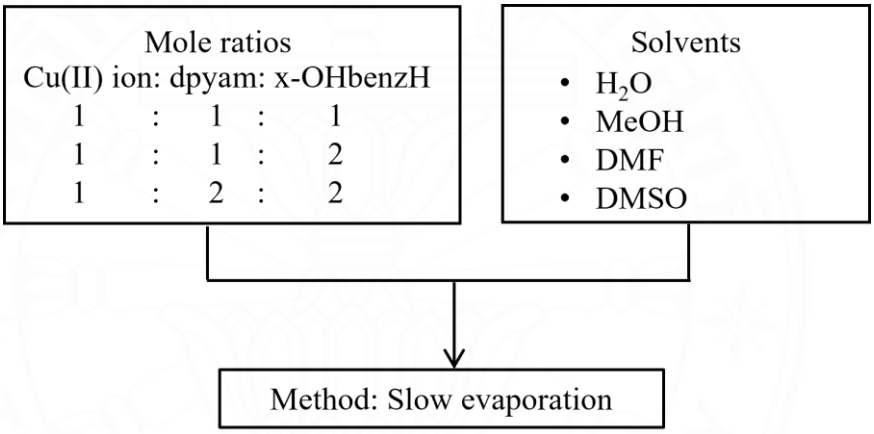

Figure 3.2 Designed synthetic conditions of new mononuclear Cu(II) complexes

3.2 Materials

3.2.1 Chemicals

All chemicals were purchased commercially from chemical sources and used without further purification and are listed in Table 3.1. Additionally, the glassware and experimental apparatus employed in the research are detailed in Table 3.2.

Table 3.1 List of chemicals and solvents used in this work

Chemicals and reagents	Formula	Mw (g/mol)	%Purity	Company
Copper(II) nitrate trihydrate	$Cu(NO_3)_2 \cdot 3H_2O$	241.60	98.5	Carlo Erba group
Copper(II) chloride dihydrate	$CuCl_2 \cdot 2H_2O$	170.48	>99	Carlo Erba group
2,2′-Dipyridylamine	$C_{10}H_9N_3$	171.20	98	Sigma-Aldrich
2-Hydroxybenzoic acid	$C_7H_6O_3$	138.12	99.5	Lobachemie
3-Hydroxybenzoic acid	$C_7H_6O_3$	138.12	99.0	Aldrich
4-Hydroxybenzoic acid	$C_7H_6O_3$	138.12	99.0	Acros Organics
Sodium hydroxide	NaOH	40.00	97.0	Merck KGaA
Methanol	CH_3OH	32.04	99.9	Carlo Erba group
N,*N*-Dimethylformamide	$HCON(CH_3)_2$	73.09	99.8	Carlo Erba group
Acetone	CH_3COCH_3	58.08	99.9	Merck KGaA
Ethanol	CH_3CH_2OH	46.07	99.5	Merck KGaA
Toluene	C_7H_8	92.14	99.8	RCI labscan
Acetonitrile	C_3H_6O	58.08	99.5	RCI labscan
Dichloromethane	CH_2Cl_2	84.93	99.8	RCI labscan
Hydrochloric acid	HCl	36.46	-	Merck KGaA
Hexane	C_6H_{14}	86.18	-	RCI labscan
Tetrahydrofuran	C_4H_8O	72.11	99.8	Fisher chemical
Ethyl acetate	$C_4H_8O_2$	88.11	-	RCI labscan
Ether	C_2H_5O	74.12	-	-
Benzyl chloroformate	$ClCO_2CH_2C_6H_5$	170.59	≥98	Aldrich
Hydroxylamide hydrochloride	$NH_2OH \cdot HCl$	69.49	-	Ajax Finechem
Potassium carbonate	K_2CO_3	138.21	-	KEMAUS
Magnesium Sulfate	$MgSO_4$	120.37	-	ITW Reagents
2-ethyl-2-oxazoline	C_5H_9NO	99.13	>98	TCI
2,3-dimethyl-1,3-butadiene	C_6H_{10}	82.14	>98	TCI

3.2.2 Glassware and equipment

Table 3.2 List of glassware and equipment used in this work

Glassware	Equipment
Beakers	Qualitative Filter Paper
Glass funnels	Hotplate Stirrer
Cylinders	Magnetic Stirrer Bar
Stirring rods	Thermometers
Droppers	Condenser clamp
Round bottom flask	Retort stand with clamp
Condenser	Parafilm

3.3 Experimental outline

The experimental outline of this research consists of five parts, including design, synthesis, characterizations, structural determination, and catalytic properties, which are described in detail in the following content.

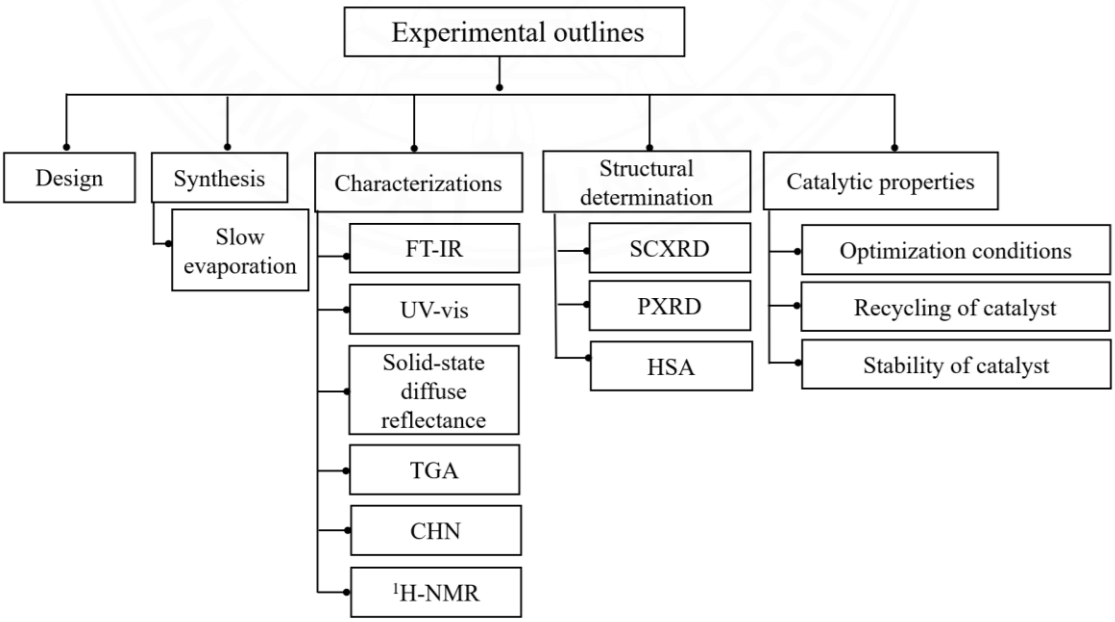

Figure 3.3 The experimental outlines of this research

3.3.1 Synthesis

The slow evaporation method is a conventional and straightforward method to prepare mononuclear complexes for this work. This method dissolves metal salts and organic ligands as reactants in suitable solvents. After that, the solution was filtrated and allowed to stand and slowly evaporate in the air at room temperature to obtain suitable crystals.

Synthesis of [Cu(dpyam)(3-OHbenz)(HCO_2)] (1)

A blue solution of $Cu(NO_3)_2 \cdot 3H_2O$ (0.2416 g, 1 mmol) in distilled water (10 mL) was heated at 65 ºC and stirred. Then, a solution of dpyam (0.1712 g, 1 mmol) in DMF (5 mL) was added, resulting in a clear dark green solution. After that, the mixed solution of 3-OHbenzH (0.2762 g, 2 mmol) and sodium hydroxide (0.08 g, 2 mmol) in distilled water (5 mL) were slowly added, resulting in a dark green solution. Then, the mixed solvent of distilled water 5 ml and DMF 5 ml was added and continuously stirred for 30 minutes. After that, the solution was filtrated and allowed to stand and slowly evaporate in the air at room temperature for 2 days. Finally, green plate crystals were obtained with a yield of 10.09% (based on Cu(II) salt).

Synthesis of [Cu(dpyam)(4-OHbenz)$_2$]·H_2O (2)

A blue solution of $Cu(NO_3)_2 \cdot 3H_2O$ (0.2416 g, 1 mmol) in distilled water (10 mL) was heated at 65 ºC and stirred. Then, a solution of dpyam (0.1712 g, 1 mmol) in methanol (10 mL) was added, resulting in a clear dark green solution. After that, the mixed solution of 4-OHbenzH (0.2762 g, 2 mmol) and sodium hydroxide (0.08 g, 2 mmol) in distilled water (10 mL) was slowly added, resulting in a green precipitate. Then, DMF 2 ml was added and continuously stirred for 30 minutes. After that, the solution was filtrated and allowed to stand and slowly evaporate in the air at room temperature for 2 days. Finally, dark green block crystals were obtained with a yield of 77.89% (188.20 mg based on Cu(II) salt). Elemental analysis calculated for $C_{24}H_{21}CuN_3O_7$: C 54.60, H 4.20, N 7.96%; found: C 54.28, H 4.07, N 8.12%.

Synthesis of [Cu(dpyam)(2-OHbenz)Cl] (3)

A blue solution of $CuCl_2 \cdot 2H_2O$ (0.1705 g, 1 mmol) in distilled water (10 mL) was heated at 65 ºC and stirred. Then, a solution of dpyam (0.1712 g, 1 mmol) in methanol (10 mL) was added, resulting in a clear green solution. After that, the mixed solution of 2-OHbenzH (0.2762 g, 2 mmol) and sodium hydroxide (0.08 g) in distilled water (10 mL) was added, resulting in a green precipitate. Then, DMF (9 mL), 1M HCl (3 ml), and DI water (5 ml) were added and continuously stirred for 30 minutes leading to a clear green solution. After that, the solution was filtrated and allowed to stand and slowly evaporate in the air at room temperature for 2 days. Finally, brown block crystals were obtained with a yield of 73.77% (286.10 mg based on Cu(II) salt). Elemental analysis calculated for $C_{17}H_{14}ClCuN_3O_3$: C 50.01, H 3.70, N 10.29; found: C 50.264, H 3.5800, N 10.341%.

Synthesis of [Cu(dpyam)(3-OHbenz)Cl] (4)

A blue solution of $CuCl_2 \cdot 2H_2O$ (0.1705 g, 1 mmol) in distilled water (10 mL) was heated at 65 ºC and stirred. Next, a solution of dpyam (0.1712 g, 1 mmol) in methanol (10 mL) was added, resulting in a clear green solution. After that, the mixed solution of 3-OHbenzH (0.2762 g, 2 mmol) and sodium hydroxide (0.08 g, 2 mmol) in distilled water (10 mL) was slowly added, leading to a green precipitate solution. Then, DMF (9 mL), 1M HCl (4 ml), and DI water (5 ml) were added and continuously stirred for 30 minutes leading to a clear green solution. After that, the solution was filtrated and allowed to stand and slowly evaporate in the air at room temperature for two days. Finally, green block crystals were obtained with a yield of 59.59% (101.20 mg based on Cu(II) salt). Elemental analysis calculated for $C_{17}H_{14}ClCuN_3O_3$: C 50.01, H 3.70, Cl 8.68, Cu 15.56, N 10.29, O 11.75%; found: C 50.297, H 3.6412, N 10.375%.

3.3.2 Instruments

Microscope

The Olympus BX50 microscope is a widely used tool for examining the external characteristics of crystals, such as their shape, color, and external characteristics of crystals. In addition, using the SCXRD technique helps understand the internal arrangement of atoms in a crystal, which provides deeper information than the external features visible under a microscope.

Fourier transform infrared (FT-IR) spectroscopy

IR spectra were recorded in KBr pellets with a Perkin Elmer infrared spectrometer spectrum GX in the 4000 to 400 cm^{-1} regions. FT-IR can provide crucial insights into the types of chemical bonds, functional groups, and structural characteristics present within a complex.

UV-vis spectroscopy

On a SHIMADZU UV-1900 spectrophotometer, the UV-vis spectra of solution samples were measured over the wavelength range of 400 to 1100 nm. This technique can verify the presence of the Cu(II) ion within the structure because the Cu(II) complex is a coloured complex, and the Cu(II) ion absorbs visible light in the 600 to 650 nm range, which can evaluate the impact of the solvent and is in the form of a solution.

Solid-state diffuse reflectance spectroscopy

The Solid-state diffuse spectra were measured as polycrystalline samples on a SHIMADZU UV-2600 spectrophotometer over the 200-1100 nm wavelength range. This technique is used for measuring the relative charge in the amount of reflected light off a surface to obtain molecular spectroscopic information that can be used to analyze the electronic transition and structure relating to the geometries of complexes in the range of 200 to 1100 nm.

Thermogravimetric analysis (TGA)

Thermogravimetric analysis (TGA) is a technique used to study the thermal stability and decomposition behavior of ligands in complexes. TGA measures the weight change of a sample as it is heated under controlled temperature conditions. Thermal gravimetric analysis curves were recorded at 25-800 °C under an N_2 atmosphere on a Thermogravimetric Analyzer (TGA) instrument SDT Q600 with the the nitrogen flow.

Elemental analysis (CHN analysis)

Elemental analysis is an important technique used to determine the amount of carbon, hydrogen, and nitrogen elements in complexes, which consists of ligands coordinated to the metal center. This technique plays a crucial role in confirming verify the identity and purity of the complex, therefore verifying its identity for various applications.

Nuclear magnetic resonance (NMR)

NMR spectroscopy is an analytical chemistry technique used in quality control to determine an organic compound's quantity, purity, amount of compound and molecular structure. ^{1}H-NMR spectra were recorded in $CDCl_3$ 400 MHz NMR spectrometers. ^{1}H-NMR were reported in units of part per million (ppm).

Single-crystal X-ray diffraction (SCXRD)

Single-crystal X-ray crystallographic data of suitable single crystals were collected with a Bruker APEX II D8 QUEST CMOS PHOTON II diffractometer, using Mo-Kα radiation (λ = 0.71073 Å) at 296 K. Single-crystal X-ray diffraction is a non-destructive analytical technique which provides detailed information about the internal lattice of crystalline substances, including unit cell dimensions, bond lengths, bond angles, and details of site-ordering. Directly related is single-crystal refinement, where the data generated from the X-ray analysis is interpreted and refined to obtain the crystal structure.

Powder X-ray Diffraction (PXRD)

Powder X-ray diffraction patterns were obtained on X-ray diffractometer BRUKER, D2 Phaser and X-ray generation at 30 kV and 10 mA with Cu Kα (λ = 1.54060 Å) radiation in the 2theta range 5-50° at room temperature. This technique analyses the diffraction of radiation by the X-rays is diffracted by

distinguishing the phase of atoms as an essential component in the sample. This technique confirms that polycrystalline and powder are obtained by synthesis. It is the same substance as the crystal obtained from the SCXRD technique.

Hirshfeld Surface Analysis (HS)

Hirshfeld surface analysis was used to study and calculate the intermolecular interactions of molecular crystals to provide data support for the SCXRD technique. In this research, the crystal structures are calculated by the *CrystalExplorer17* program, giving the Hirshfeld surface analysis and 2D fingerprint plots.

3.3.3 Study of catalytic properties

3.3.3.1 Synthesis of *N*-(benzyloxy-carbonyl)hydroxylamine (1a)

A solution of hydroxylamide hydrochloride (2.36 g, 34 mmol) and potassium carbonate (5.17 g, 37.4 mmol) in a mixed solvent of ether and distilled water (30:5 ml). A solution of phenyl chloroformate (5.32 g, 34 mmol) in ether was slowly added dropwise for 30 minutes to a stirred solution at 5 °C. After that, the reaction was stirred at room temperature for 4 hours. The organic layer was separated and dried over $MgSO_4$. The solvent was evaporated. Finally, solid white products were obtained with a yield of 4.3932 g.

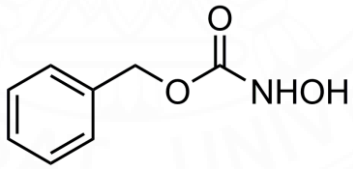

Figure 3.4 The molecular structure of *N*-(benzyloxy-carbonyl)hydroxylamine (**1a**)

3.3.3.2 Optimization of the catalytic conditions

In the first optimization step, we screened for suitable solvents in the reaction using 20 mL of variety solvent, 0.1196 mmol of 2-ethyl-2-oxazoline (**2a**), 10 mol% mononuclear Cu(II) complexes as a catalyst and 0.5982 mmol of *N*-(benzyloxy-carbonyl)hydroxylamine (**1a**) added, followed by 0.5982 mmol of 2,3-dimethyl-1,3-butadiene (**4a**) , as shown in scheme 3.1. The reaction proceeded using a

variety of solvents, non-polar and polar. The solvents used in the reaction are toluene, dichloromethane, hexane, acetonitrile, methanol, and tetrahydrofuran. The resulting solution was stirred at room temperature in the air and was monitored by TLC. The disappearance of the starting material confirmed the completion of the reaction. The solvent was removed by evaporation, resulting in the crude product. (hexane: ethyl acetate, 7:3 v/v as the eluent). After obtaining a suitable solvent for the reaction, we study the amount of catalyst using 1, 5, 10 and 50 mol% of catalyst. Furthermore, in the final step, the effect of the temperatures will be studied at room temperature and the appropriate boiling point of the solvent for the reaction.

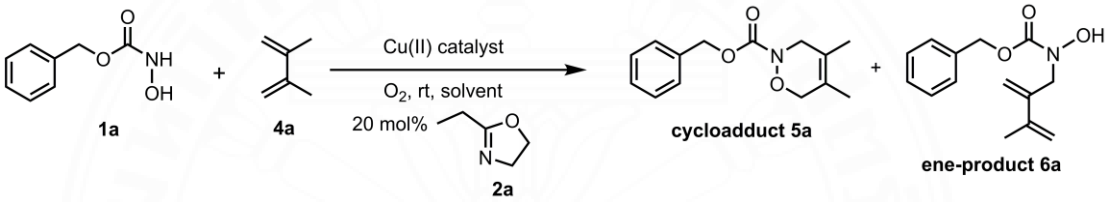

Scheme 3.1 The aerobic oxidation reaction of *N*-(benzyloxy-carbonyl)hydroxylamine (**1a**)

3.3.3.3 Recycling of the catalyst

To study the reuse of the catalyst, after the reaction is complete, filter the catalyst with paper filters and wash the catalyst with hexane: ethyl acetate, 7:3 v/v, to remove any product attached to the catalyst. The catalyst was then rewashed with THF solvent and evaporated. Continue the reaction until the %yield decreases to 80% or the catalyst takes longer to react, which shows that the catalyst was less effective.

3.3.3.4 Stability of the catalyst

After the catalytic study was recycled, the catalyst was filtered and washed with hexane: ethyl acetate, 7:3 v/v, to remove the remaining product from the mononuclear Cu(II) catalyst. The solvent evaporated and left its dried at room temperature again. Afterwards, it will be characterized by FT-IR and PXRD techniques.

CHAPTER 4
RESULTS AND DISCUSSION

This chapter presents the results and discussion about the crystallography, structural description, characterizations of new mononuclear Cu(II) complexes namely [Cu(dpyam)(3-OHbenz)(HCO_2)] (**1**), [Cu(dpyam)(4-OHbenz)$_2$]· H_2O (**2**), [Cu(dpyam)-(2-OHbenz)Cl] (**3**) and [Cu(dpyam)(3-OHbenz)Cl] (**4**). Moreover, the catalytic studies of these complexes were reported.

4.1 Crystallography

To begin studying the crystal structure of new mononuclear Cu(II) complexes, a single crystal with a suitable single crystal size was selected using a microscope. The suitable single crystal of all the complexes has been selected and used for the crystal structure determination using the single-crystal X-ray diffraction technique, which yields unit cell, bond length, bond angle, intermolecular interactions, and other crystal data. The crystal data of all the complexes has been summarized in Table 4.1.

The crystallographic data of all complexes were collected on a Bruker D8 QUEST CMOS X-ray diffractometer using Mo-Kα X-radiation (λ = 0.71073 Å) and a PHOTON II detector with CPAD technology. The structures were refined by *APEX3* and *SAINT* (Bruker, 2016) [49]. The structures were solved by *SHELXT* (Sheldrick, 2015a) [50] and *SHELXL* (Sheldrick, 2015b) [51]. The *OLEX2* software is used to prepare materials for publication and prepare molecular graphics (Dolomanov *et al*., 2009) [52].

Table 4.1 Crystallographic and refinement data for all synthesized complexes

Complexes	**1**	**2**	**3**	**4**
Formula	$C_{18}H_{15}CuN_3O_5$	$C_{24}H_{21}CuN_3O_7$	$C_{17}H_{14}ClCuN_3O_3$	$C_{17}H_{14}ClCuN_3O_3$
Molecular weight	416.87	526.98	407.30	407.30
Temperature/K	296.15	296.15	296.15	296.15
Crystal system	monoclinic	monoclinic	monoclinic	orthorhombic
Space group	$P2_1/c$	$P2_1/n$	Cc	$Pna21$
a(Å)	8.3265(3)	10.6539(3)	10.5106(3)	14.9879(3)
b(Å)	14.9699(5)	17.2008(5)	10.5225(4)	15.2901(3)
c(Å)	13.9523(4)	13.1652(4)	14.8149(5)	7.13780(10)
α(°)	90	90	90	90
β(°)	99.2420(10)	111.2970(10)	90.3420(10)	90
γ(°)	90	90	90	90
Volume/Å^3	1716.53(10)	2247.84(11)	1638.47(10)	1635.74(5)
Z	4	4	4	4
ρ_{calc}g/cm^3	1.613	1.557	1.651	1.654
μ/mm^{-1}	1.309	1.024	1.518	1.521
F(000)	852.0	1084.0	828.0	828.0
Crystal size/mm^3	0.12 × 0.1 × 0.1	0.3 × 0.24 × 0.2	0.02 × 0.02 × 0.02	0.16 × 0.14 × 0.12
Radiation	MoKα (λ = 0.71073)	MoKα (λ = 0.71073)	MoKα (λ = 0.71073)	MoKα (λ = 0.71073)
Reflections collected	18907	81544	10645	37404
Independent reflections	4262 [R_{int} = 0.0748, R_{sigma} = 0.0619]	5578 [R_{int} = 0.0321, R_{sigma} = 0.0119]	4790 [R_{int} = 0.0331, R_{sigma} = 0.0491]	4055 [R_{int} = 0.0437, R_{sigma} = 0.0252]
Data/restraints/ parameters	4262/0/252	5578/0/325	4790/2/227	4055/1/227
Goodness-of-fit on F^2	1.012	1.052	1.028	1.052
Final R indexes [I>=2σ (I)]	R1 = 0.0453, wR2 = 0.0955	R1 = 0.0292, wR2 = 0.0811	R1 = 0.0484, wR2 = 0.1176	R1 = 0.0246, wR2 = 0.0581
Final R indexes [all data]	R1 = 0.0891, wR2 = 0.1143	R1 = 0.0323, wR2 = 0.0830	R1 = 0.0651, wR2 = 0.1306	R1 = 0.0267, wR2 = 0.0591

Computer programs: *APEX3* (Bruker, 2016), *SAINT* (Bruker, 2016), *SHELXT* (Sheldrick, 2015a), *SHELXL* (Sheldrick, 2015b) and *OLEX2* (Dolomanov *et al.*, 2009).

4.2 Crystal structural description

4.2.1 Crytal structure of [Cu(dpyam)(3-OHbenz)(HCO_2)] (1)

The plate green crystals of complex **1** were obtained from the reaction of $Cu(NO_3)_2 \cdot 3H_2O$, dpyam and 3-OHbenz in mixed solvents, H_2O and DMF ratio of 5:2. According to the synthetic condition, the presence of the formate ion can be explained by hydrolysis of DMF [53]. This complex crystallizes in the monoclinic crystal system in the $P2_1/c$ space group. The asymmetric unit consists of a Cu(II) ion, one chelating dpyam ligand, one 3-OHbenz chelating ligand and one formato ligand, as shown in Figure 4.1.

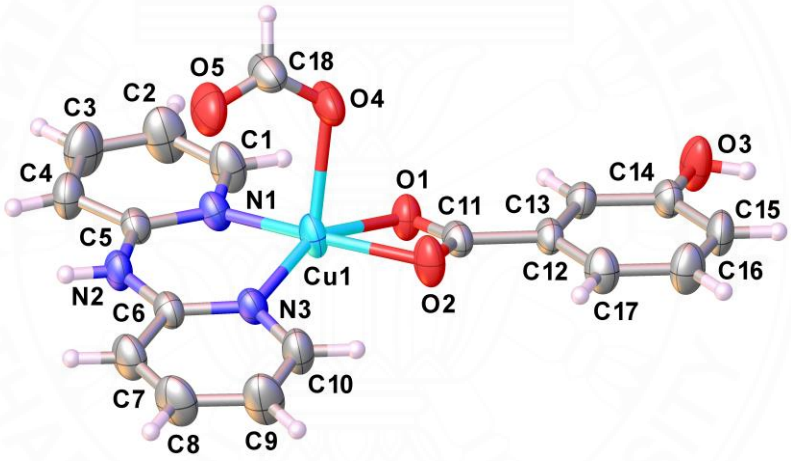

Figure 4.1 The molecular structure of complex **1** with the atom numbering. Displacement ellipsoids are drawn at the 50% probability level

In the structure, the environment Cu(II) ion is surrounded by two nitrogen atoms of the pyridine rings from a chelating dpyam ligand, two oxygen atoms of the carboxylate group from a chelating 3-OHbenz ligand and one oxygen atom of carboxylate group from a monodentate formato ligand, resulting a square pyramidal geometry with the $[CuN_2O_3]$ chromophore. Regarding the bond lengths and angles of complex **1**, there are two sets, [4+1] of the bond lengths, four bond lengths of Cu(1)-N/O donor atoms of dpyam and 3-OHbenz present in a range of 1.936(3) to 2.096(2) Å for the square-base, while the rest highest bond length of Cu(1)-O(4) of formato ligand

is 2.207(2) Å for the apical position, where in general, the bond distance between the Cu(II) atom and the oxygen atom of the formate ligand typically falls within the range of approximately 2.0 to 2.3 angstroms (Å) [54]. The Cu atom lies about 0.265 Å above the basal plane towards the apical oxygen atom of the formato ligand, as shown in Figure 4.2a. In addition, the structural parameter, the t_5 value (t_5 = 0 for an ideal square pyramid and t_5 = 1 for an ideal trigonal bipyramid) [55, 56] calculated from the bond angles around Cu(II) ion is considered, it shows that the *t* value is 0.19, confirming a distorted square pyramidal geometry, as shown in Figure 4.2b.

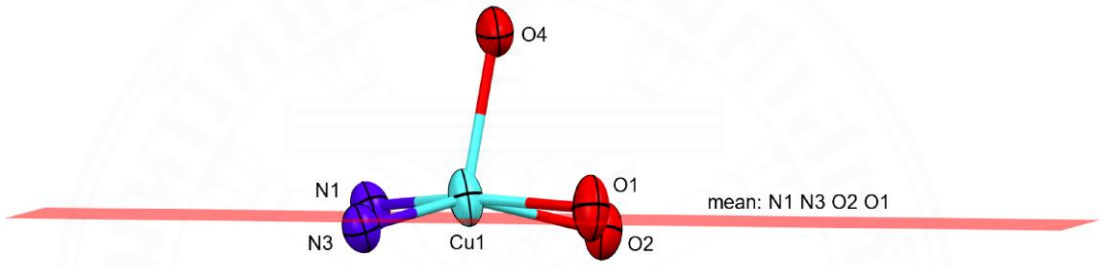

(a)

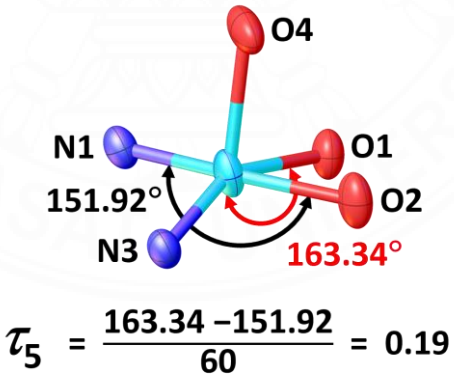

$$\tau_5 = \frac{163.34 - 151.92}{60} = 0.19$$

(b)

Figure 4.2 Views of (a) the Cu(II) atom lies above the basal plane towards the apical oxygen atom of the formato ligand and (b) the τ_5 parameter of Cu(II) center in the complex **1**

The supramolecular interactions of complex **1** are summarized in Table 4.2. The crystal structure of complex **1** is stabilized by intramolecular non-classical hydrogen bonding interactions between C–H of pyridine rings and oxygen atoms of carboxylate group of 3-OHbenz, [C1–H1···O1 and C10–H10···O2]. The crystal structure of complex **1** is further stable by the presence of intermolecular interactions such as hydrogen bonding, π–π stacking and C–H···π interactions, as shown in Figure 4.3 and Figure 4.4. The hydrogen bonding interactions are found through N–H group of dpyam and oxygen atom of carboxylate group of formate [N2–H5···O4^{i}] and the oxygen atom of hydroxide group of 3-OHbenz and oxygen atom of carboxylate group of formate [O3–H14···O5^{ii}]. Also, there is C–H···π interaction between the C–H group of formato ligand and phenyl ring of 3-OHbenz, C18–O18···*C*g7^{iv}. For π–π stacking interaction, it is formed between the one of pyridyl ring of the dpyam and the phenyl ring of the 3-OHbenz with a centroid-to-centroid distance of *C*g7···*C*g5^{i} = 3.978 (2) Å and a slippage of 1.431 Å [slippage = distance between Cg(I) and perpendicular projection of Cg(J) on ring I; *C*g5 and *C*g7 are the centroids of the N1/C1–C5 and C12–C17 rings, respectively]. These hydrogen bonding, π–π stacking and C–H···π intermolecular interactions present in the crystallographic *ac* plane, forming the two-dimensional supramolecular network, as shown in Figure 4.5. Furthermore, the supramolecular interactions are also expanded in crystallographic *b* axis through the non-classical hydrogen bonding interaction between C–H group of dpyam and oxygen atom of hydroxy group of 3-OHbenz [C2–H2···O3^{iii}] leading to three-dimensional supramolecular framework, as shown in Figure. 4.6.

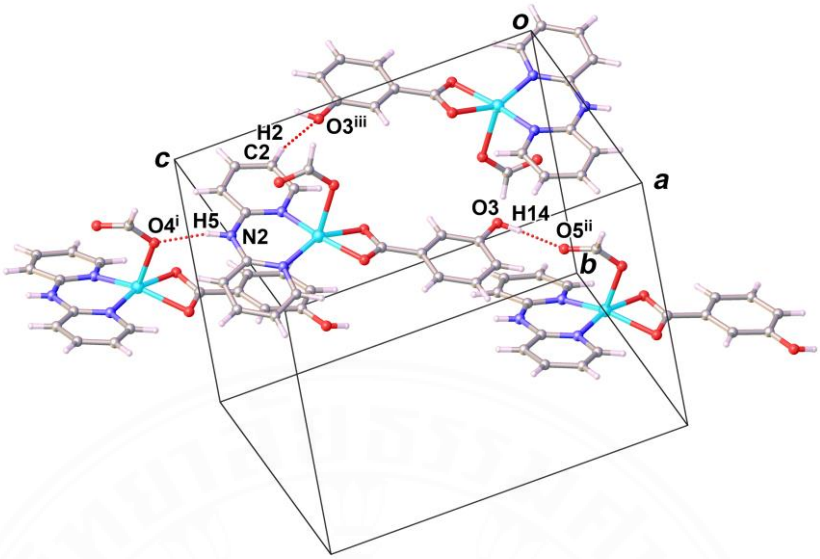

Figure 4.3 View of the hydrogen bonding interactions (dashed lines) in crystal structure of complex **1**. [Symmetry code: (i) = x, 1/2-y, 1/2+z], (ii) = 1+x, 1/2-y, -1/2 +z and (iii) = 1-x, -y, 1-z.]

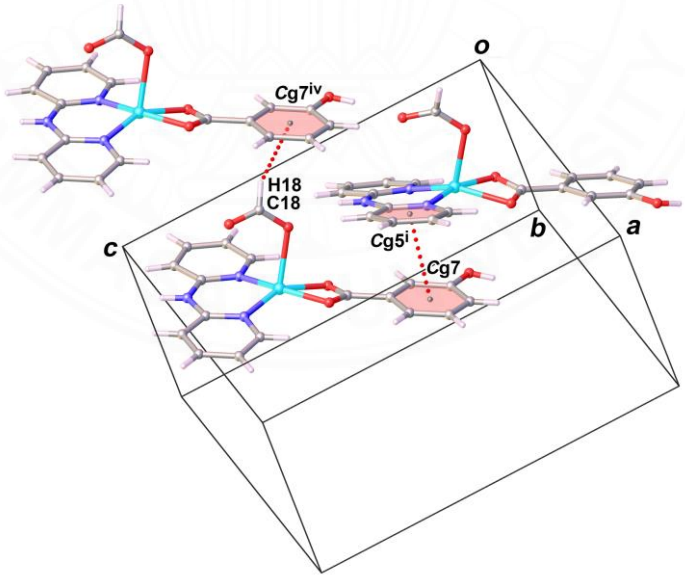

Figure 4.4 View of π–π stacking and C–H$\cdots\pi$ interactions (dashed lines) in the crystal structure of complex **1**. [Symmetry code: (i) = x, 1/2-y, -1/2+z and (iv) = -1+x, y, z; *C*g5 and *C*g7 are the centroids of the N1/C1–C5 and C12–C17 rings, respectively.]

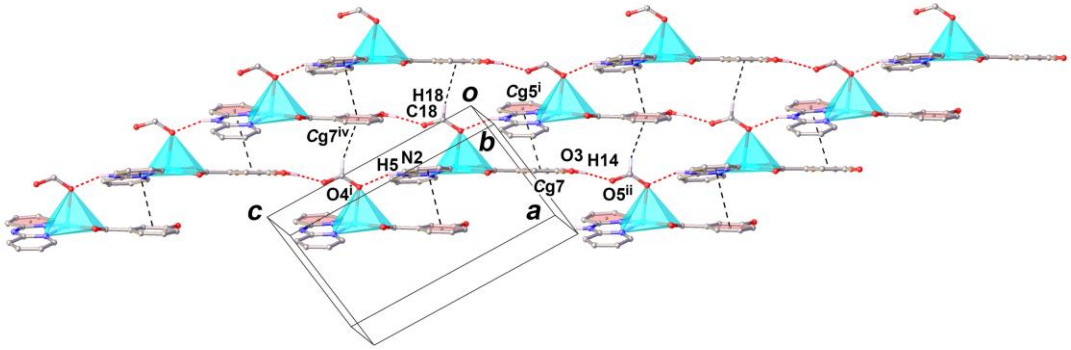

(a)

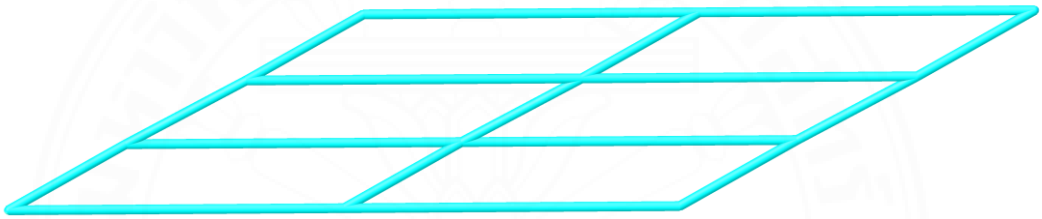

(b)

Figure 4.5 Views of the layered supramolecular network in the crystal structure of complex **1**, showing (a) the crystal packing in the *ac* plane and (b) the schematic skeleton representing the Cu(II) atoms as nodes

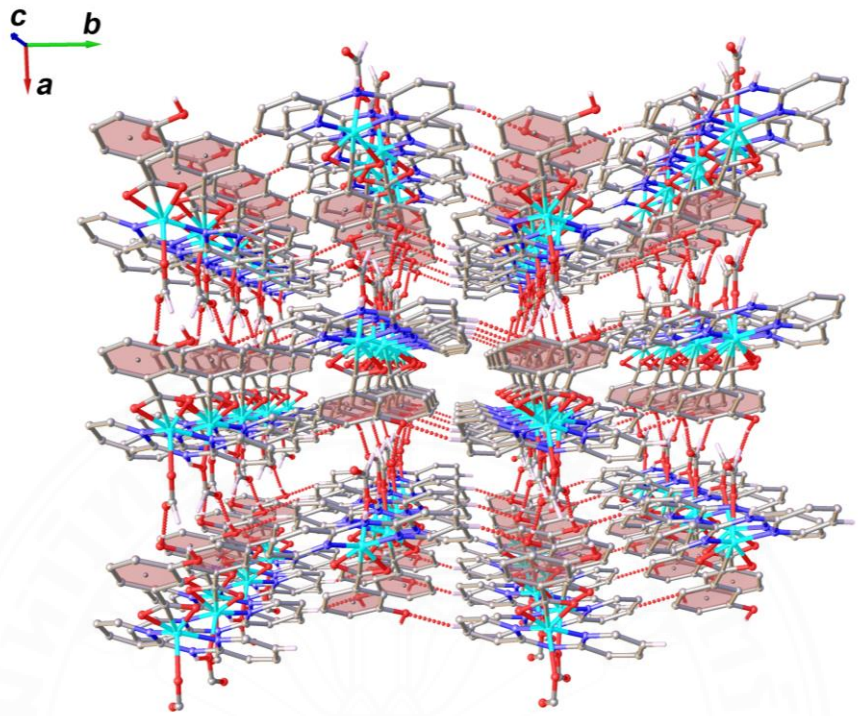

Figure 4.6 A perspective view of three-dimensional supramolecular network of complex **1**

Table 4.2 Selected bond lengths (Å) and bond angles (°) for complex **1**

Bond lengths (Å)			
Cu1–O1	2.096(2)	Cu1–N3	1.963(2)
Cu1–O2	1.984(2)	Cu1–N1	1.936(3)
Cu1–O4	2.207(2)		
Bond angles (°)			
O1–Cu1–O4	89.16(9)	N3–Cu1–O4	114.49(10)
O2–Cu1–O1	64.40(9)	N1–Cu1–O1	99.43(9)
O2–Cu1–O4	90.64(10)	N1–Cu1–O2	163.39(10)
N3–Cu1–O1	151.93(10)	N1–Cu1–O4	92.99(10)
N3–Cu1–O2	98.82(10)	N1–Cu1–N3	94.41(10)

Table 4.3 Hydrogen-bond geometry (Å, °) of complex **1**

D–H···A	d(D–H)	d(H···A)	d(D···A)	∠(D–H···A)
Intramolecular hydrogen bond				
C1–H1···O1	0.93	2.42	3.056(4)	125
C10–H10···O2	0.93	2.38	2.999(4)	124
Intermolecular hydrogen bonds				
N2–H5···O4^{i}	0.86	2.02	2.834(3)	158
O3–H14···O5^{ii}	0.82	1.83	2.645 (4)	170
C2–H2···O3^{iii}	0.93	2.59	3.497 (5)	166
C18–H18···Cg7^{iv}	2.65	2.88	3.634 (3)	139

Symmetry code: (i) x, −y+1/2, z+1/2, (ii) x+1, −y+1/2, z−1/2, (iii) −x+1, −y, −z+1, and (iv) x−1, y, z.

Table 4.4 π–π interaction (Å) of complex **1**

Ring···Ring	**α**	**DC**	**β**	**DZ**
*C*g7···*C*g5^{i}	13.62(16)	3.978(2)	21.1	3.4474(13)

Symmetry codes: (i) = x, 1/2-y, -1/2+z; *C*g rings stand for

*C*g5 = six-membered ring (N1, C1, C2, C3, C4 and C5)

*C*g7 = six-membered ring (C12, C13, C14, C15, C16 and C17)

4.2.2 Crytal structure of [Cu(dpyam)(4-OHbenz)$_2$]·H$_2$O (2)

Complex **2** crystallizes in the monoclinic crystal system in the $P2_1/n$ space group. The asymmetric unit consists of a Cu(II) ion, one chelating dpyam ligand and two monodentate 4-OHbenz ligands with one water lattice solvent, as shown in Figure 4.7.

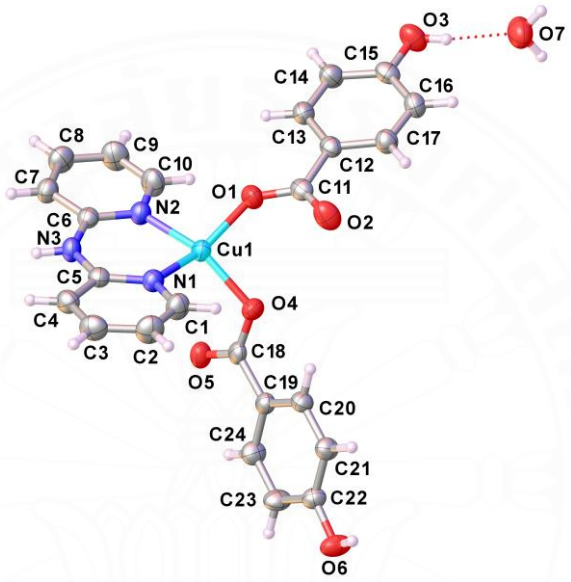

Figure 4.7 The molecular structure of complex **2** with the atom numbering. Displacement ellipsoids are drawn at the 50% probability level.

In the structure, the environment Cu(II) ion is surrounded by two nitrogen atoms of the pyridine ring from a chelating dpyam ligand, two oxygen atoms of the carboxylate group from two monodentate 4-OHbenz ligands resulting in a square planar geometry with the [CuN$_2$O$_2$] chromophore. Regarding the bond lengths and angles of complex **2**, there are four bond lengths by N$_2$O$_2$ donor set of Cu(1)-N/O donor atoms of dpyam and 4-OHbenz present in a range of 1.9231(11) to 1.9926(13) Å. Two nitrogen atoms of the pyridine rings from a chelating dpyam ligand are distance 1.9926(13) and 1.9832 (13) Å, respectively. In comparison, two oxygen atoms of the carboxylate group from two monodentate 4-OHbenz ligands are distance 1.9328(11) and 1.9231(11) Å, respectively. The bond angles of N1–Cu1–N2, O1–Cu1–O2,

N1–Cu1–O1, and N2–Cu1–O4 are 92.99(5)°, 96.21(5)°, 93.38(5)° and 91.67(5)°, respectively, which are closer to the typical value for a distorted square planar angle. The bond angles of N1–Cu1–O4 and N2–Cu1–O1 are 150.08(6)° and 152.03(6)°, respectively, slightly deviating from the ideal bond angle of 180° of square planar. The angle (θ) between the two planes defined by the N1–Cu1–N2 plane on the one hand and O1–Cu1–O4 is 39.71° on the other can be used to express the deviation from square planar toward tetrahedral geometry, as shown in Figure 4.8.

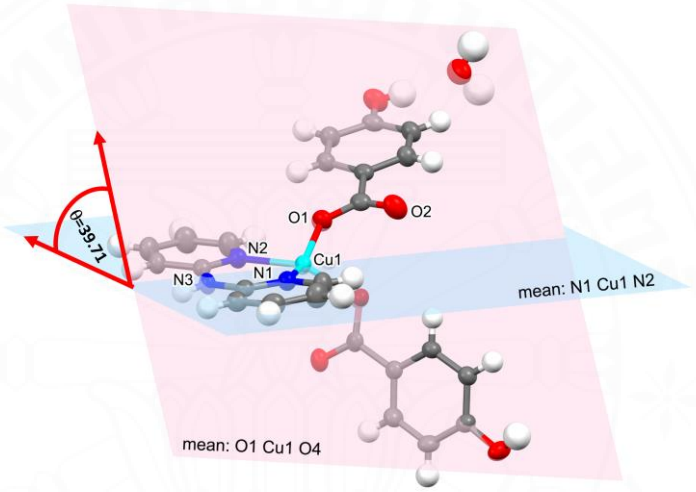

Figure 4.8 View of the bite angle of complex **2**

The supramolecular interactions of complex **2** are summarized in Table 4.6. The crystal structure of complex **2** is stabilized by intramolecular non-classical hydrogen bonding interactions between CH of pyridine rings and oxygen atoms of carboxylate group of 4-OHbenz, [C1–H1···O4 and C10–H10···O1]. The crystal structure of complex **2** is further stable by intermolecular interactions such as hydrogen bonding and π–π stacking, as shown in Figure 4.9 and Figure 4.10. The hydrogen bonding interactions are found through N–H group of the dpyam and oxygen atom of the carboxylate group from 4-OHbenz ligand [N3–H5···O5^{i}; symmetry code (i) =2-x, 1-y, -z], hydrogen atom of the hydroxyl group from 4-OHbenz ligand and oxygen atom of lattice aqua molecule [O3–H6···O7^{ii}; symmetry code (ii) = 2-x, 1-y, -z], hydrogen atom of the hydroxyl group from the 4-OHbenz ligand and oxygen atom

of carboxylate group from 4-OHbenz ligand [O6–H11···O2^{iii}; symmetry code (iii) = -1/2+x, 3/2-y, -1/2+z], hydrogen atom of lattice aqua molecule and oxygen atom of carboxylate group from 4-OHbenz ligand [O7–H18···O2^{iv}; symmetry code (iv) = 1-x, 1-y, 1-z], hydrogen atom of lattice aqua molecule and oxygen atom of carboxylate group from 4-OHbenz ligand [O7–H19···O5^{v}; symmetry code (v) = x, y, 1+z], the CH of pyridine rings and oxygen atoms of the hydroxyl group from the 4-OHbenz ligand [C1–H1···O6^{vi}; symmetry code (vi) = 1/2+x, 3/2-y, 1/2+z] and the C–H of pyridine rings and oxygen atoms of the hydroxyl group from the 4-OHbenz ligand [C8–H8···O3^{vii}; symmetry code (vii) = 1/2+x, 1/2-y, -1/2+z], as shown in Table 4.6. For π–π stacking interaction, it is formed between one of the pyridyl ring of the dpyam ligand and the pyridyl ring of the dpyam ligand of neighboring molecules with a centroid-to-centroid distance of *Cg*3···*Cg*4^{i} = 3.7450(10) Å [symmetry code: (i) = 2-x, 1-y, -z; *Cg*3 and *Cg*4 are the centroids of the N1/C1–C5 and N2/C6–C10 rings, respectively] and it is formed between one of the pyridyl ring of the dpyam ligand and the phenyl ring of the 4-OHbenz ligand with a centroid-to-centroid distance of 3.9545(10) Å [symmetry code: (ii) = 2-x, 1-y, 1-z; *Cg*4···*Cg*5 are the centroids of the N2/C6–C10 rings and C12–C17 rings, respectively]. These hydrogen bonding and π–π stacking interactions form the three-dimensional supramolecular network, as shown in Figure 4.11.

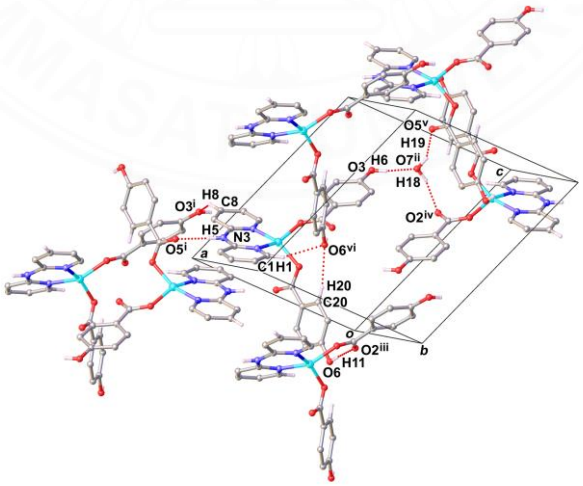

Figure 4.9 View of the hydrogen bonding interactions (dashed lines) in the crystal structure of complex **2**

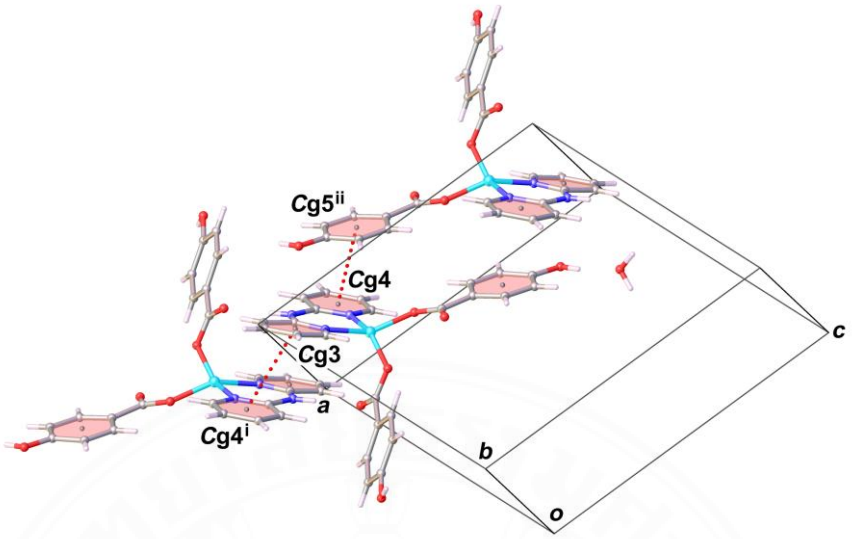

Figure 4.10 View of π–π interactions (dashed lines) in the crystal structure of complex **2** [Symmetry code: (i) = 2-x, 1-y, -z and (ii) = 2-x, 1-y, 1-z; *Cg*3, *Cg*4 and *Cg*5 are the centroids of the N1/C1–C5, N2/C6–C10 and C12–C17 rings, respectively.]

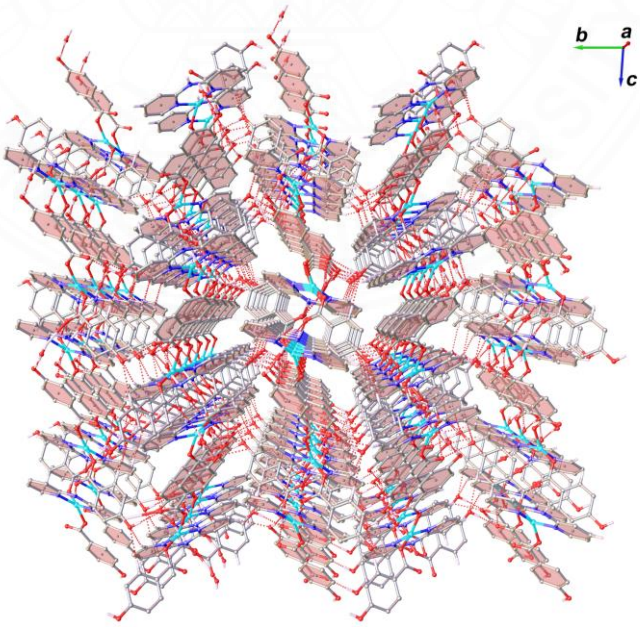

Figure 4.11 A perspective view of three-dimensional supramolecular network of complex **2**

Table 4.5. Hydrogen-bond geometry (Å, °) of complex **2**

Bond lengths (Å)			
Cu1–O1	1.9230(13)	Cu1–N1	1.9923(14)
Cu1–O4	1.9329(12)	Cu1–N2	1.9832(14)
Bond angles (°)			
O1–Cu1–O1	96.22(5)	O4–Cu1–N1	93.38(5)
O1–Cu1–N1	150.08(6)	O4–Cu1–N2	152.04(6)
O1–Cu1–N2	91.67(5)	N2–Cu1–N1	92.98(5)

Table 4.6. Hydrogen bond lengths (Å) and angles (°) of complex **2**

D–H···A	d(D–H)	d(H···A)	d(D···A)	∠(D–H···A)
Intramolecular hydrogen bond				
C1–H1···O4	0.93	2.50	2.963(2)	111
C10–H10···O1	0.93	2.31	2.850(3)	116
Intermolecular hydrogen bonds				
N3–H5···O5^{i}	0.86	1.94	2.803(2)	179
O3–H6···O7^{ii}	0.82	1.85	2.664(2)	172
O6–H11···O2^{iii}	0.82	1.83	2.645(19)	174
O7–H18···O2^{iv}	0.85	2.07	2.900(2)	164
O7–H19···O5^{v}	0.85	2.24	2.998(2)	148
C1–H1···O6^{vi}	0.93	2.53	3.409(3)	158
C8–H8···O3^{vii}	0.93	2.46	3.176(2)	134
C20–H20···O6^{vi}	0.93	2.60	3.513(2)	169

Symmetry code: (i) = 2-x, 1-y, -z, (ii) = 2-x, 1-y, -z, (iii) = -1/2+x, 3/2-y, -1/2+z, (iv) = 1-x, 1-y, 1-z, (v) = x, y, 1+z, (vi) = 1/2+x, 3/2-y, 1/2+z and (vii) = 1/2+x, 1/2-y, -1/2+z.

Table 4.7. π–π interaction (Å) of complex **2**

Ring···Ring	α	DC	β	DZ
*Cg*3···*Cg*4^{i}	6.56(9)	3.7450(10)	24.0	3.4563(7)
*Cg*4···*Cg*5^{ii}	14.87(9)	3.9545(10)	23.9	3.5127(7)

Symmetry codes: (i) = 2-x, 1-y, -z and (ii) = 2-x, 1-y, 1-z; *Cg* rings stand for

*Cg*3 = six-membered ring (N1, C1, C2, C3, C4 and C5)

*Cg*4 = six-membered ring (N2, C6, C7, C8, C9 and C10)

*Cg*5 = six-membered ring (C12, C13, C14, C15, C16 and C17)

4.2.3 Crytal structure of [Cu(dpyam)(2-OHbenz)Cl] (3)

The complex **3** crystallizes in the monoclinic crystal system in the *Cc* space group. The asymmetric unit consists of a Cu(II) ion, one chelating dpyam ligand, one chelating 2-OHbenz ligand and one chlorido ligand, as shown in Figure 4.12.

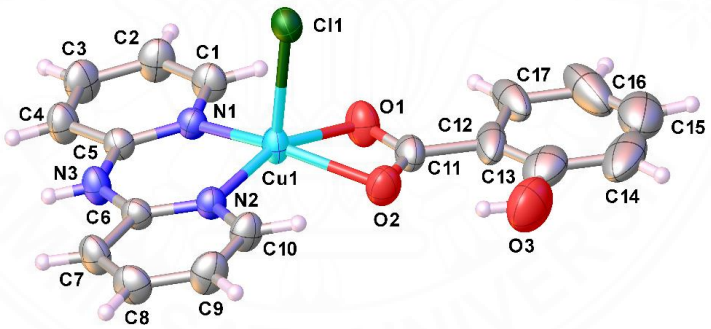

Figure 4.12. The molecular structure of complex **3** with the atom numbering. Displacement ellipsoids are drawn at the 50% probability level

In the structure, the environment Cu(II) ion is surrounded by two nitrogen atoms of the pyridine rings from a chelating dpyam ligand, two oxygen atoms of the carboxylate group from a chelating 2-OHbenz ligand and one chloride atom from a monodentate chlorido ligand, resulting a square pyramidal geometry with the $[CuN_2O_2Cl]$ chromophore. Regarding the bond lengths and angles of complex **3**, there

are [4+1] bond length set, four bond lengths of Cu(1)-N/O donor atoms of dpyam and 2-OHbenz present in a range of 1.956(2) to 2.107(5) Å for the square-based set, while the rest one represents of Cu(II)-Cl atom of chlorido ligand with Cu(1)-Cl(1) of 2.4595(17) Å for the apical position. The Cu–Cl distance is intermediate between the known values from 2.336(2) to 2.733(2) Å [56, 57]. The Cu atom lies about 0.0297 Å above the basal plane towards the apical Cl atom of the chlorido ligand, as shown in Figure 4.13a. In addition, the structural parameter, the τ_5 value (τ_5 = 0 for an ideal square pyramid and τ_5 = 1 for an ideal trigonal bipyramid) [55, 56] calculated from the bond angles around Cu(II) ion is considered, it shows that the τ_5 value is 0.04, confirming a nearly perfect square pyramidal geometry, as shown in Figure 4.13b.

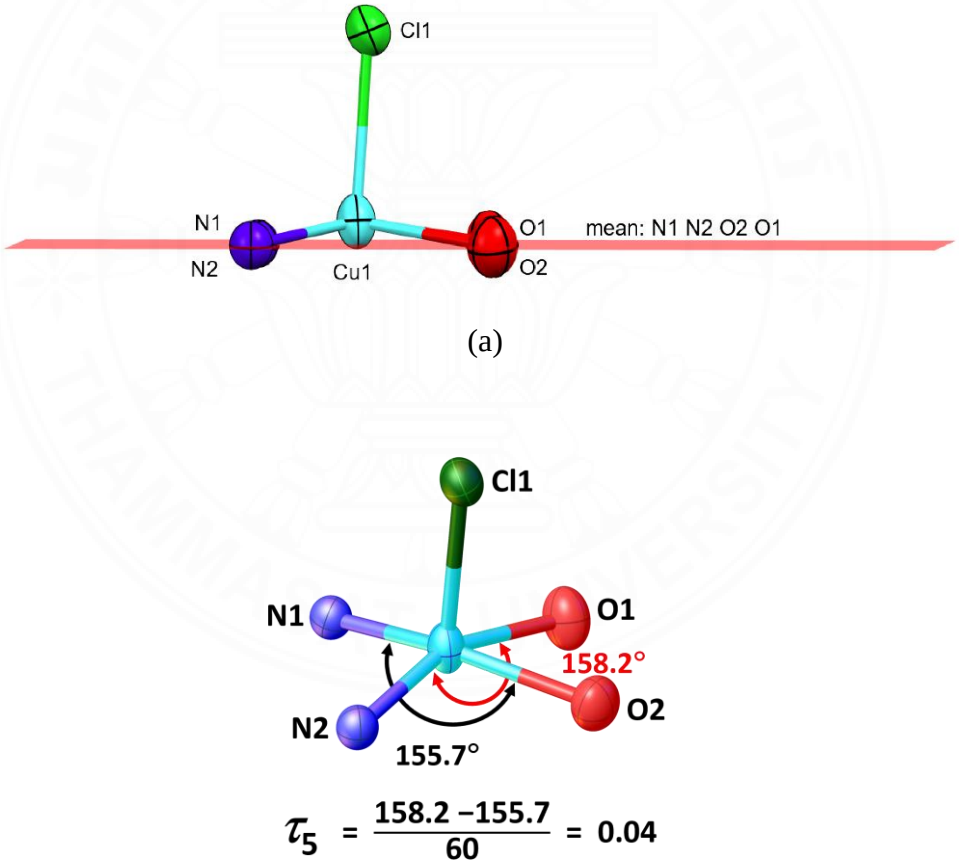

Figure 4.13 Views of (a) the Cu(II) atom lies above the basal plane towards the apical chloride atom of the chlorido ligand and (b) the τ_5 parameter of Cu(II) center in complex **3**

The supramolecular interactions of complex **3** is summarized in Table 4.9 and 4.10. The crystal structure of complex **3** is stabilized by intramolecular non-classical hydrogen bonding interactions between CH of pyridine rings and oxygen atoms of carboxylate group of 2-OHbenz, [C1–H1···O1 and C10–H10···O2] and hydroxyl group of 2-OHbenz and oxygen atoms of carboxylate group [O3–H6···O2]. The crystal structure of complex **3** is further stable by intermolecular interactions such as hydrogen bonding and π–π stacking, as shown in Figure 4.14. The hydrogen bonding interactions are found through N–H group of dpyam and chloride atom of chlorido ligand, the CH group of dpyam ligand and chloride atom of chlorido ligand and the C–H group of dpyam ligand and oxygen atom of carboxylate group from 2-OHbenz ligand [N3–H5···Cl1^{i}, C2–H2···Cl1^{ii} and C8–H8···O1^{iii}; symmetry code (i) = -1/2+x, -1/2+y, z; (ii) = x, 1-y, -1/2+z and (iii) = -1/2+x, 1/2-y, 1/2+z]. Also, there is π–π stacking interaction, and it is formed between the one of pyridyl ring of the dpyam and the phenyl ring of the 2-OHbenz with a centroid-to-centroid distance of *C*g5···*C*g7^{i} = 4.063(5) Å [symmetry code: (i) = -1/2+x, -1/2+y, z; *C*g5 and *C*g7 are the centroids of the N1/C1–C5 and C12-C17 rings, respectively]. These hydrogen bonding and π–π stacking interactions form the three-dimensional supramolecular network, as shown in Figure 4.15.

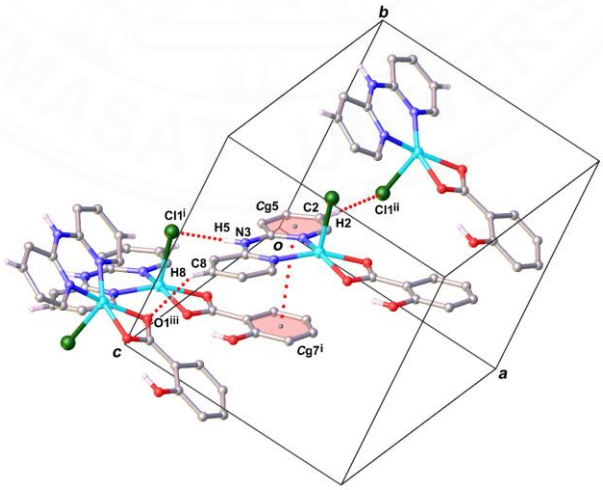

Figure 4.14. View of the hydrogen bonding and π–π interactions (dashed lines) in the crystal structure of complex **3**

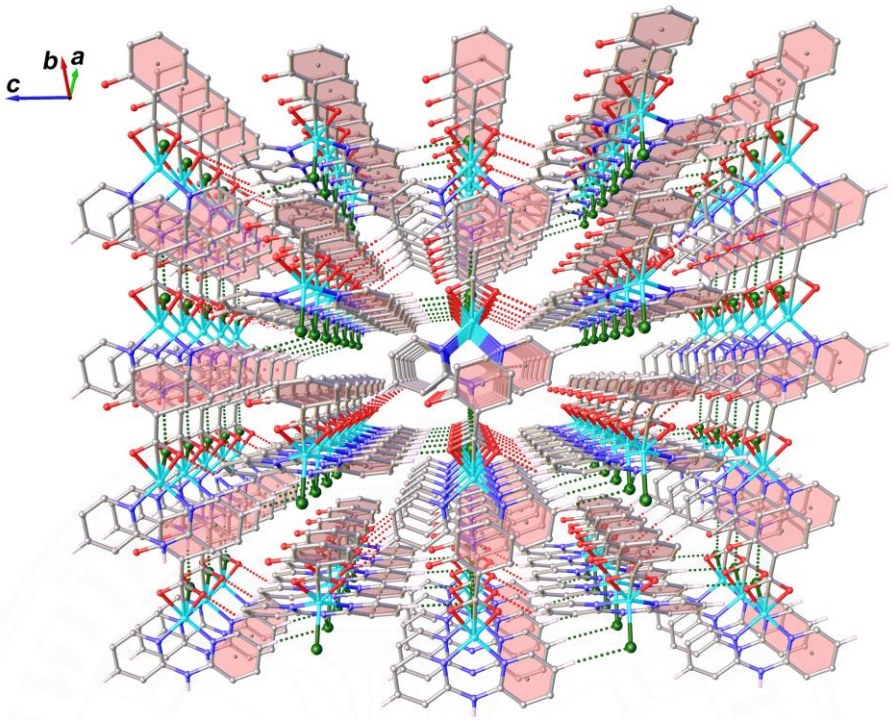

Figure 4.15 A perspective view of three-dimensional supramolecular network of complex **3**

Table 4.8 Selected bond lengths (Å) and bond angles (°) for complex **3**

Bond lengths (Å)			
Cu1–Cl1	2.4595(17)	Cu1–N1	1.963(5)
Cu1–O1	2.032(5)	Cu1–N2	1.962(5)
Cu1–O2	2.107(5)		
Bond angles (°)			
Cl1–Cu1–O1	95.74(16)	Cl1–Cu1–O2	94.71(15)
Cl1–Cu1–N1	102.25(14)	Cl1–Cu1–N2	99.93(15)
O1–Cu1–O2	63.2(2)	O1–Cu1–N1	97.6(2)
O2–Cu1–N1	155.7(2)	O1–Cu1–N2	158.2(2)
N1–Cu1–N2	93.83(19)	O2–Cu1–N2	100.28(19)

Table 4.9 Hydrogen-bond geometry (Å, °) of complex **3**

D–H···A	d(D–H)	d(H···A)	d(D···A)	∠(D–H···A)
Intramolecular hydrogen bond				
O3–H6···O2	0.82	1.94	2.668(10)	148
C1–H1···O1	0.93	2.38	2.991(9)	123
C10–H10···O2	0.93	2.50	3.108(8)	123
Intermolecular hydrogen bonds				
N3–H5···Cl1^{i}	0.86	2.35	3.206(5)	179
C2–H2···Cl1^{ii}	0.93	2.83	3.752(6)	174
C8–H8···O1^{iii}	0.93	2.60	3.423(9)	148

Symmetry code: (i) = -1/2+x, -1/2+y, z; (ii) = x, 1-y, -1/2+z and (iii) = -1/2+x, 1/2y, 1/2+z.

Table 4.10 π–π interaction (Å) of complex **3**

Ring···Ring	**α**	**DC**	**β**	**DZ**
*Cg*5···*Cg*7^{i}	6.6(4)	4.063(5)	30.8	3.451(3)

Symmetry code: (i) = -1/2+x, -1/2+y, z; *Cg* rings stand for

*Cg*5 = six-membered ring (N1, C1, C2, C3, C4 and C5)

*Cg*7 = six-membered ring (C12, C13, C14, C15, C16 and C17)

4.2.4 Crytal structure of [Cu(dpyam)(3-OHbenz)Cl] (4)

The complex **4** crystallizes in the orthorhombic crystal system in the *Pna*2_1 space group. The asymmetric unit consists of a Cu(II) ion, one chelating dpyam ligand, one 3-OHbenz chelating ligand and one chlorido ligand, as shown in Figure 4.16.

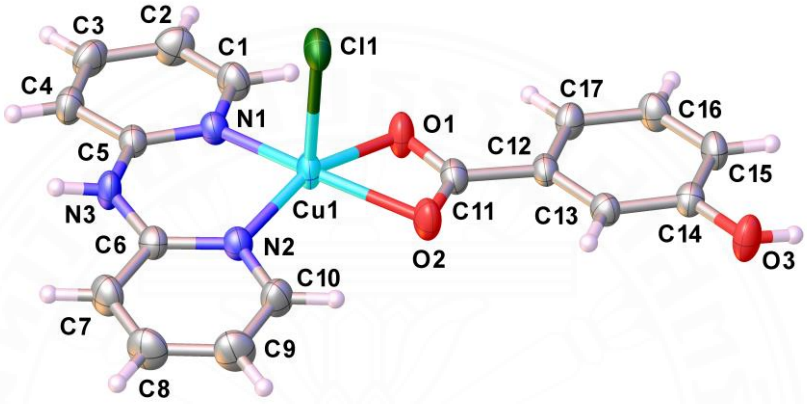

Figure 4.16. The molecular structure of complex **4** with the atom numbering. Displacement ellipsoids are drawn at the 50% probability level.

In the structure, the environment Cu(II) ion is surrounded by two nitrogen atoms of the pyridine rings from a chelating dpyam ligand, two oxygen atoms of the carboxylate group from a chelating 3-OHbenz ligand and one chloride atom from a monodentate chorido ligand, resulting a square pyramidal geometry with the [CuN_2O_2Cl] chromophore. Regarding the bond lengths and angles of complex **4**, there are [4+1] bond length set, four bond lengths of Cu(1)–N/O donor atoms of dpyam and 3-OHbenz present in a range of 1.994(2) to 2.083(2) Å for the square-based set, while the rest one represents of Cu(II)–Cl atom of chlorido ligand with Cu(1)–Cl(1) of 2.5472(8) Å for the apical position. The Cu–Cl distance is intermediate between the known values from 2.336(2) to 2.733(2) Å [56, 57]. The Cu atom lies about 0.2490 Å above the basal plane towards the apical Cl atom of the chlorido ligand, as shown in Figure 4.17a. In addition, the structural parameter, the τ_5 value (τ_5 = 0 for an ideal square pyramid and τ_5 = 1 for an ideal trigonal bipyramid) [55] calculated from the

bond angles around Cu(II) ion is considered, it shows that the τ_5 value is 0.02, confirming a nearly perfect square pyramidal geometry, as shown in Figure 4.17b.

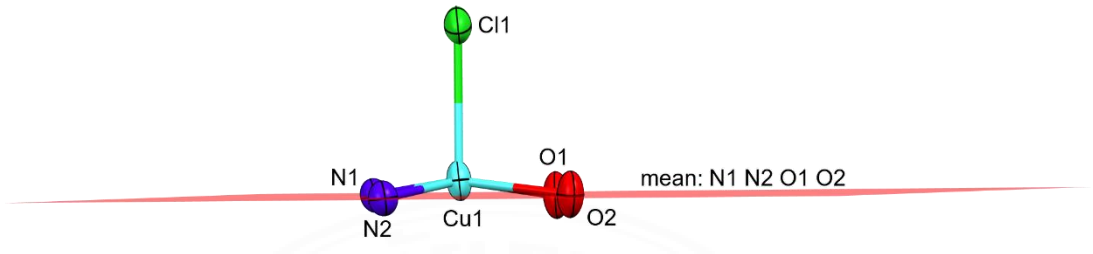

(a)

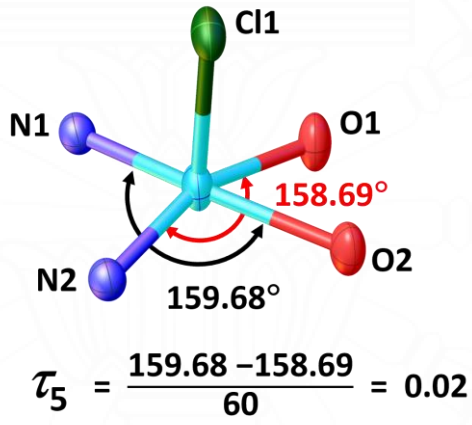

(b)

Figure 4.17 Views of (a) the Cu(II) atom lies above the basal plane towards the apical chloride atom of the chlorido ligand and (b) the τ_5 parameter of Cu(II) center in complex **4**

The supramolecular interaction of complex **4** is summarized in Table 4.12. The crystal structure of complex **4** is stabilized by intramolecular non-classical hydrogen bonding interactions between CH of pyridine rings and oxygen atoms of carboxylate group of 3-OHbenz, [C1–H1···O1 and C10–H10···O2]. The crystal structure is further stable by intermolecular interactions such as hydrogen bonding and π–π stacking, as shown in Figure 4.18. The hydrogen bonding interactions are found

throughout the N–H group of dpyam and chloride atom of chloride ligand, the C–H group of dpyam ligand and chloride atom of chlorido ligand [N3–H5···Cl1^{i} and C4–H4···Cl1^{i}; symmetry code (i) = x, y, 1+z], the oxygen atom of hydroxide group of 3-OHbenz and chloride atom of chlorido ligand and the C–H group of 3-OHbenz ligand and chloride atom of chlorido ligand [O3–H6···Cl1^{ii} and C15–H15···Cl1^{ii}, symmetry code (ii) = 1/2+x, 3/2-y, -1+z]. Also, there is π–π stacking interaction, and it is formed between the one of pyridyl ring of the dpyam and the phenyl ring of the 3-OHbenz with a centroid-to-centroid distance of *C*g5···*C*g7^{i} = 3.8791(16) Å [symmetry code: (i) = x, y, 1+z; *C*g5 and *C*g7 are the centroids of the N1/C5 and C12-C17 rings, respectively]. These hydrogen bonding and π–π stacking interactions are present in the crystallographic *ac* plane, forming the two-dimensional supramolecular network as shown in Figure 4.19. Furthermore, the supramolecular interactions are also expanded in the crystallographic *b* axis through hydrogen bonding interaction between the C–H group of dpyam and the oxygen atom of the hydroxy group of 3-OHbenz [C8–H8···O3^{iii}, Symmetry code (iii) = 1-x, 2-y, 3/2+z], leading to a three-dimensional supramolecular framework, as shown in Figure 4.20.

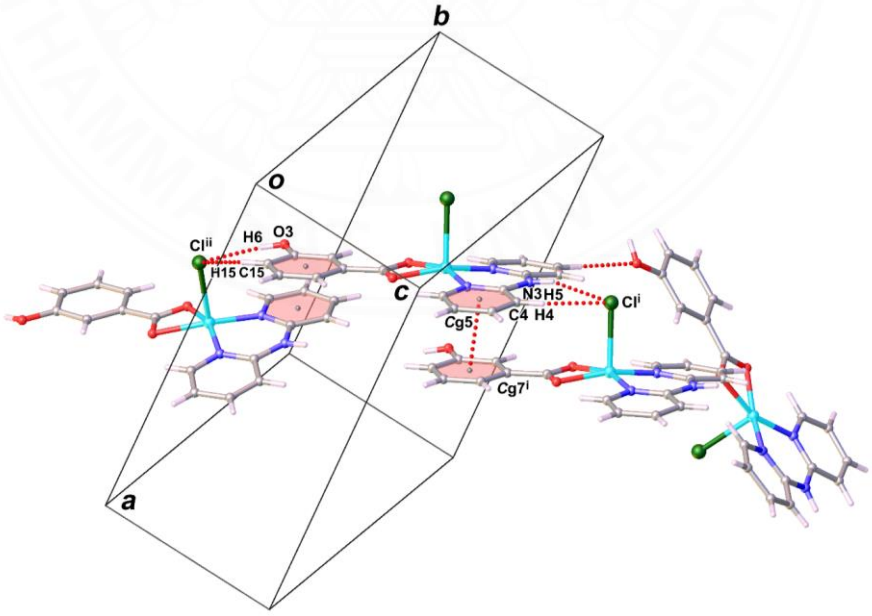

Figure 4.18 View of the hydrogen bonding and π–π interactions (dashed lines) in the crystal structure of complex **4**

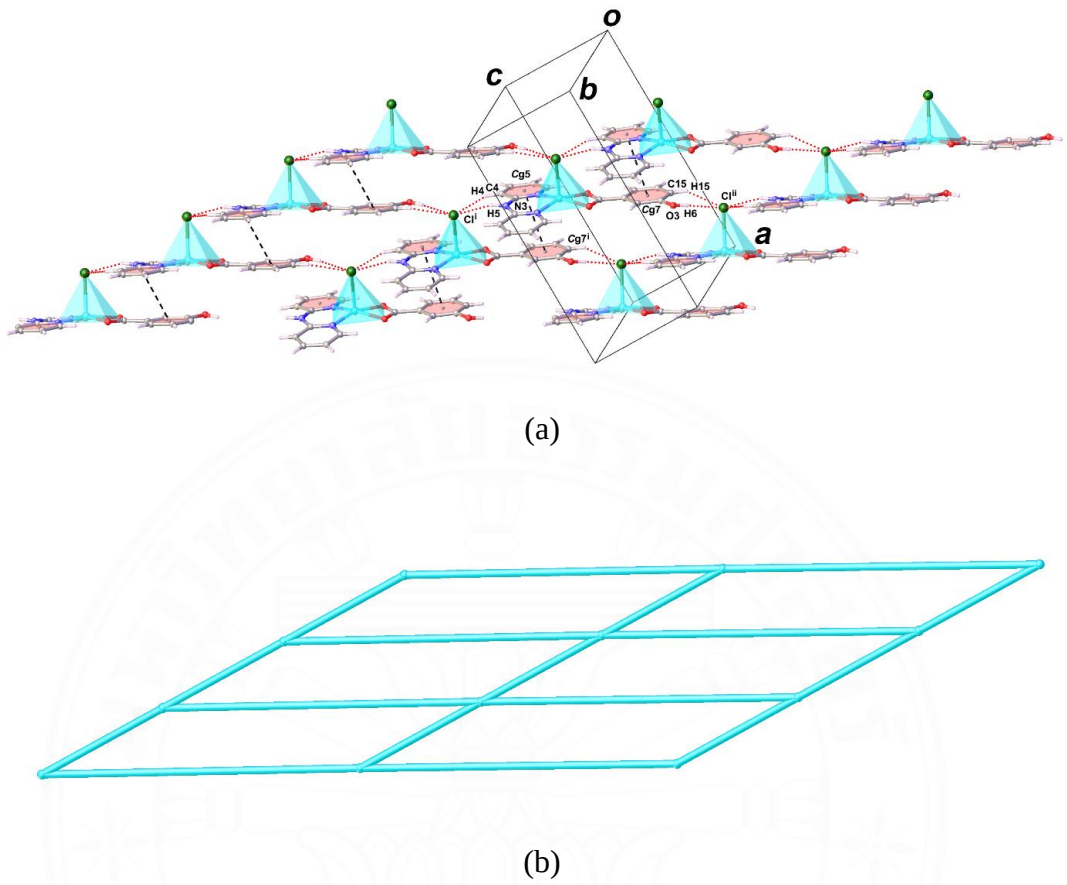

(a)

(b)

Figure 4.19 View of the layered supramolecular network in the crystal structure of complex **4**, showing (a) the crystal packing in *ac* plane and (b) the schematic skeleton representing the Cu(II) atoms as nodes

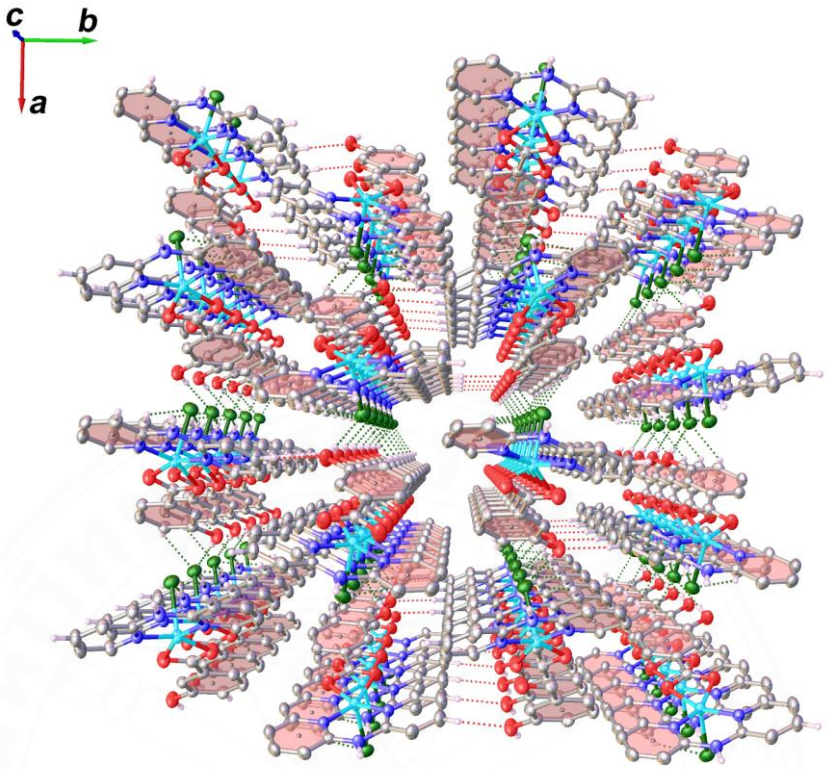

Figure 4.20 A perspective view of three-dimension supramolecular network of complex **4**

Table 4.11. Selected bond lengths (Å) and bond angles (°) for complex **4**

Bond lengths (Å)			
Cu1–Cl1	2.5472(8)	Cu1–N1	1.975(2)
Cu1–O1	1.994(2)	Cu1–N2	1.956(2)
Cu1–O2	2.083(2)		
Bond angles (°)			
Cl1–Cu1–O1	98.64(7)	Cl1–Cu1–O2	95.29(6)
Cl1–Cu1–N1	98.51(7)	Cl1–Cu1–N2	96.26(7)
O1–Cu1–O2	64.40(8)	O1–Cu1–N1	97.35(9)
O2–Cu1–N1	158.67(9)	N1–Cu1–N2	94.02(9)
N1–Cu1–N2	94.02(9)	O2–Cu1–N2	100.58(9)

Table 4.12. Hydrogen-bond geometry (Å, °) of complex **4**

D–H···A	d(D–H)	d(H···A)	d(D···A)	∠(D–H···A)
Intramolecular hydrogen bond				
C1–H1···O1	0.93	2.34	2.959(4)	124
C10–H10···O2	0.93	2.45	3.086(4)	126
Intermolecular hydrogen bonds				
N3–H5···Cl1^{i}	0.86	2.38	3.202(2)	159
O3–H6···Cl1^{ii}	0.82	2.33	3.147(2)	173
C4–H4···Cl1^{i}	0.93	2.82	3.595(3)	142
C8–H8···O3^{iii}	0.93	2.58	3.513(4)	175
C15–H15···Cl1^{ii}	0.93	2.80	3.527(3)	136

Symmetry code: (i) = x, y, 1+z; (ii) = 1/2+x, 3/2-y, -1+z and (iii) = 1-x, 2-y, 3/2+z.

Table 4.13. π–π interaction (Å) of complex **4**

Ring···Ring	α	DC	β	DZ
*Cg*5···*Cg*7^{i}	2.44(13)	3.8791(16)	29.2	3.3065(11)

Symmetry code: (i) = x, y, 1+z; *Cg* rings stand for

*Cg*5 = six-membered ring (N1, C1, SC2, C3, C4 and C5)

*Cg*7 = six-membered ring (C12, C13, C14, C15, C16 and C17)

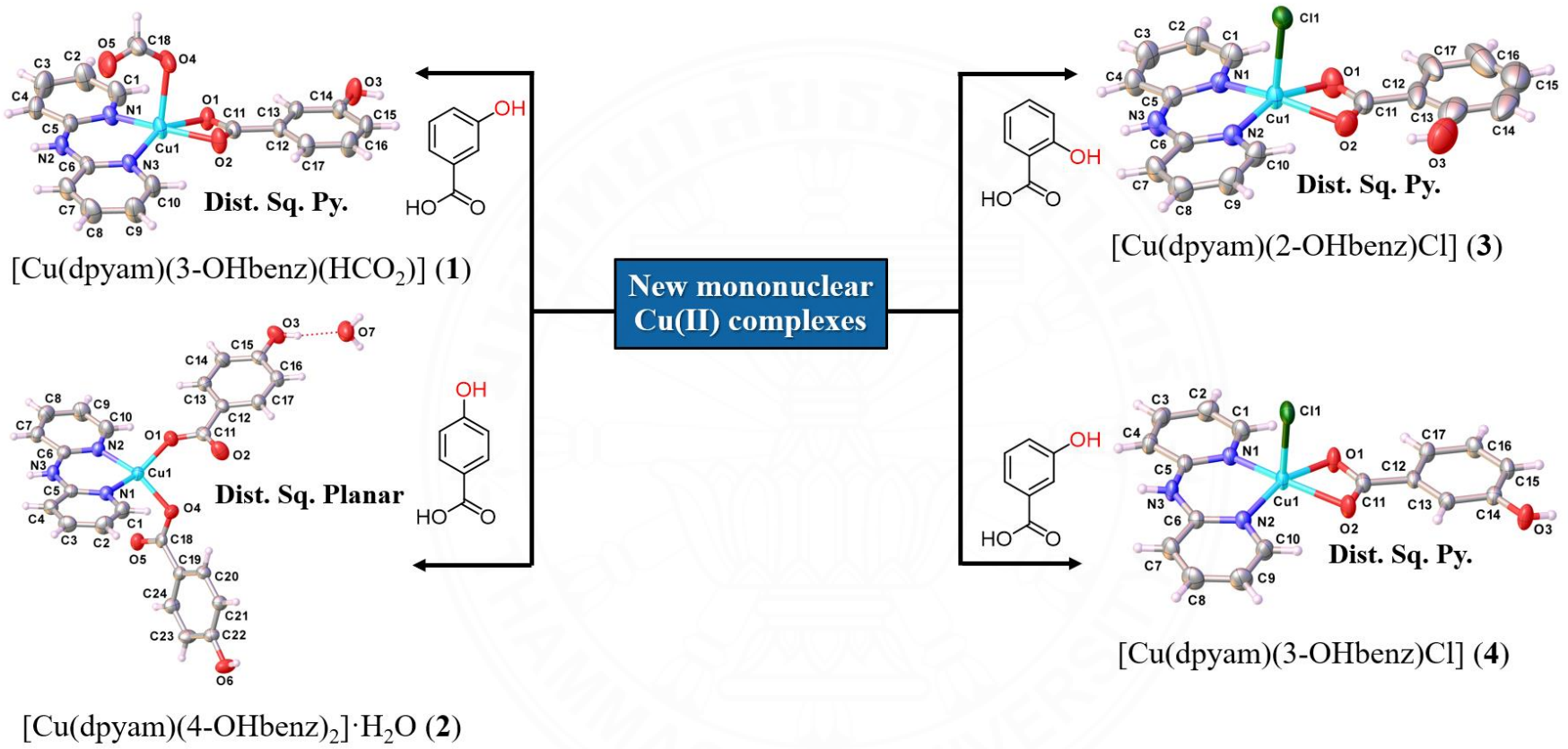

Figure 4.21 Summary of the molecular structure of all new mononuclear copper(II) complexes in this work

4.3 Hirshfeld surface analysis

The Hirshfeld surface analysis was used to quantify the intermolecular interactions of crystal structure to understand the non-covalent interactions on the surface of the molecule and its surroundings that influence molecular packing in crystals. The Hirshfeld surface analysis [70] and 2D-fingerprint plots [71] are generated using the *CrystalExplorer17* program [72], and this program uses the crystallographic information file (.CIF) from single-crystal X-ray diffraction data to study intermolecular interaction of complexes. The Hirshfeld surface mapped over d_{norm} generally presents different surface colours. The colour gradient is used to quantify the interactions taking place between the atoms within the crystal. This gradient varies from blue to red through white. The red surface indicates a distance shorter than the sum of the van der Waals radii, the white surface indicates a distance near the van der Waals radii, and the blue surface indicates a distance longer than the sum of the van der Waals radii.

4.3.1 Hirshfeld surface analysis of [Cu(dpyam)(3-OHbenz)(HCO_2)] (1)

The Hirshfeld surface of complex **1** is shown in Figure 4.22a. The bright-red spots on d_{norm} on the positions of the N–H group of dpyam ligand, oxygen atom of the carboxylate group and hydrogen atom of coordinated formate ligand and the oxygen atom of the hydroxy group of 3-OHbenz, corresponding to strong intermolecular N–H···O, C–H···O and O–H···O hydrogen bonding and also C–H···π interactions found in the crystal of complex **1**. At the same time, the Hirshfeld surface two-dimensional fingerprint plots in Figure 4.22b present the percentage contribution for H···H, O···H/H···O, C···H/H···C and C···C contacts of complex **1**. The H···H intermolecular contacts plot shows the highest percentage contribution of 41.6%, resulting in most of the hydrogen from the organic ligands. The O···H/H···O plot with percentage contributions of 25.0% represents the existence of O···H intermolecular contacts due to O–H···O, N–H···O and C–H···O hydrogen bonding interactions. The plot of C···H/H···C intermolecular contacts with a percentage contribution of 21.1% corresponds to the attractive C–H···π interactions. The plot of C···C contacts with a percentage contributions of 3.8% indicates the π–π interactions in the crystal structure, as shown in

Figure 4.23. So, it confirmed hydrogen bond, C–H···π and π–π interactions that are the dominant stability of the crystal structure and supported crystal packing from X-ray structure of complex **1**.

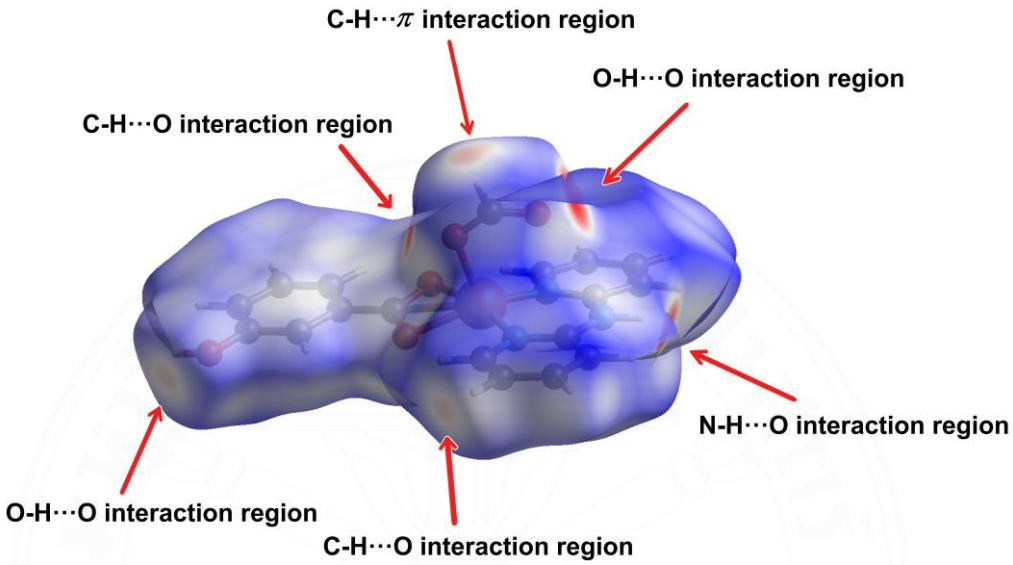

(a)

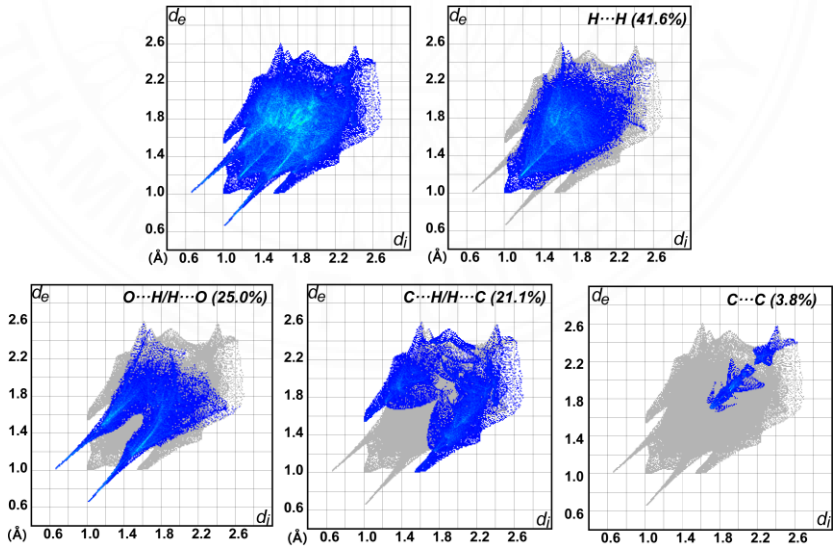

(b)

Figure 4.22 Views of (a) the Hirshfeld surface mapped over d_{norm} and (b) Hirshfeld surface 2D-fingerprint plots for the H···H, O···H/H···O, C···H/H···C and C···C contacts of complex **1**

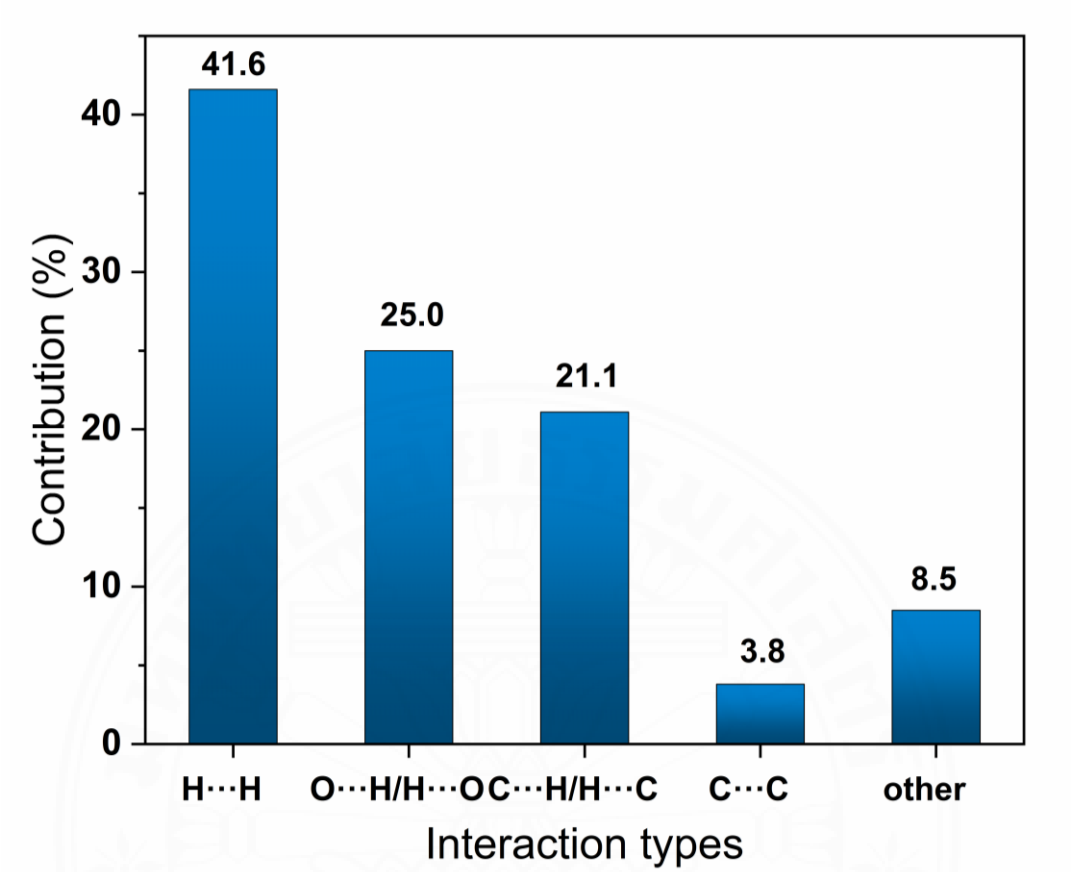

Figure 4.23 Quantitative results of different intermolecular contacts contributing to the Hirshfeld surface of complex **1**

4.3.2 Hirshfeld surface analysis of [Cu(dpyam)(4-OHbenz)$_2$]· H_2O (2)

The Hirshfeld surface of complex **2** is shown in Figure 4.24a. The bright-red spots on d_{norm} on the positions of the N–H group of the dpyam ligand, the oxygen atom of the carboxylate group, the hydrogen atom of the hydroxyl group of 4-OHbenz ligand and the carbon atom of the pyridyl ring of 4-OHbenz, corresponding to strong intermolecular N–H···O, O–H···O, O–H···O and C–H···O hydrogen bonding found in the crystal of complex **2**. At the same time, the Hirshfeld surface two-dimensional fingerprint plots in Figure 4.24b present the percentage contribution for H···H, O···H/H···O, C···H/H···C and C···C contacts of complex **2**. The H···H intermolecular contacts plot shows the highest percentage contribution of 41.6%, resulting in most of the hydrogen from the organic ligands. The O···H/H···O plot with percentage contributions of 23.8% represents the existence of O···H intermolecular

contacts due to O–H···O, N–H···O and C–H···O hydrogen bonding interactions. The plot of C···H/H···C intermolecular contacts with a percentage contribution of 25.3%. The plot of C···C contacts with percentage contributions of 4.7% indicates the π–π interactions in the crystal structure, as shown in Figure 4.25. Therefore, it confirmed hydrogen bond and π–π interactions that are the dominant stability of the crystal structure and supported crystal packing from X-ray structure of complex **2**.

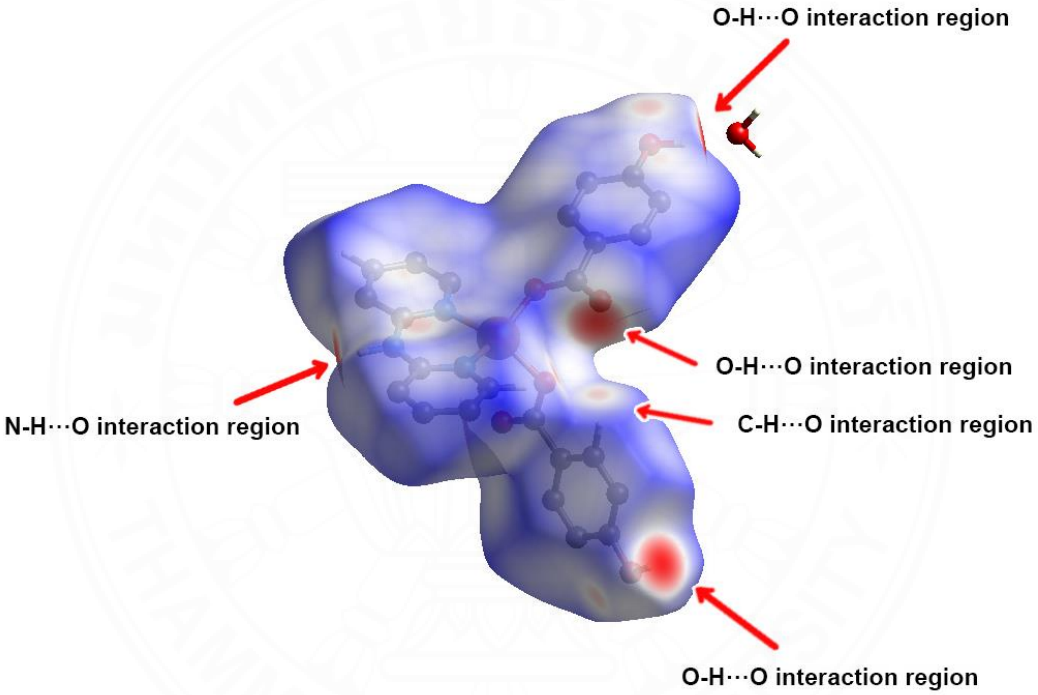

(a)

Figure 4.24 Views of (a) the Hirshfeld surface mapped over d_{norm} and (b) Hirshfeld surface 2D-fingerprint plots for the H···H, C···H/H···C, O···H/H···O and C···C contacts of complex **2**

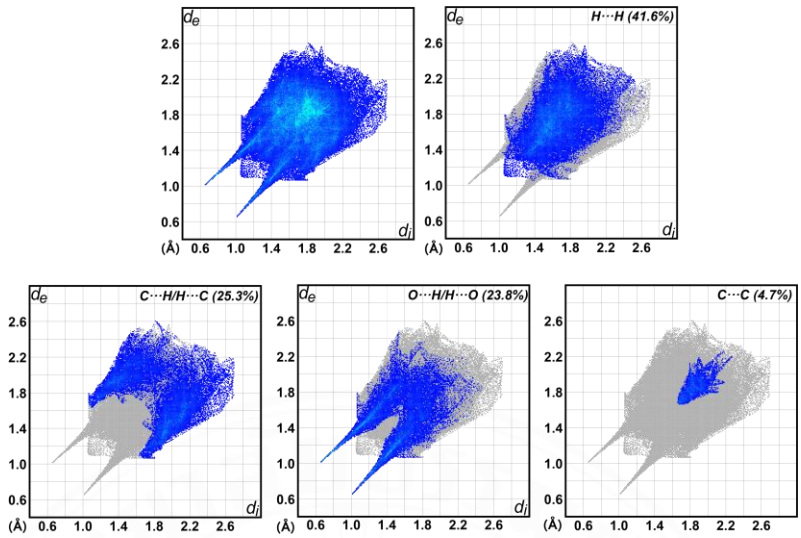

(b)

Figure 4.24 Views of (a) the Hirshfeld surface mapped over d_{norm} and (b) Hirshfeld surface 2D-fingerprint plots for the H···H, C···H/H···C, O···H/H···O and C···C contacts of complex **2** (cont.)

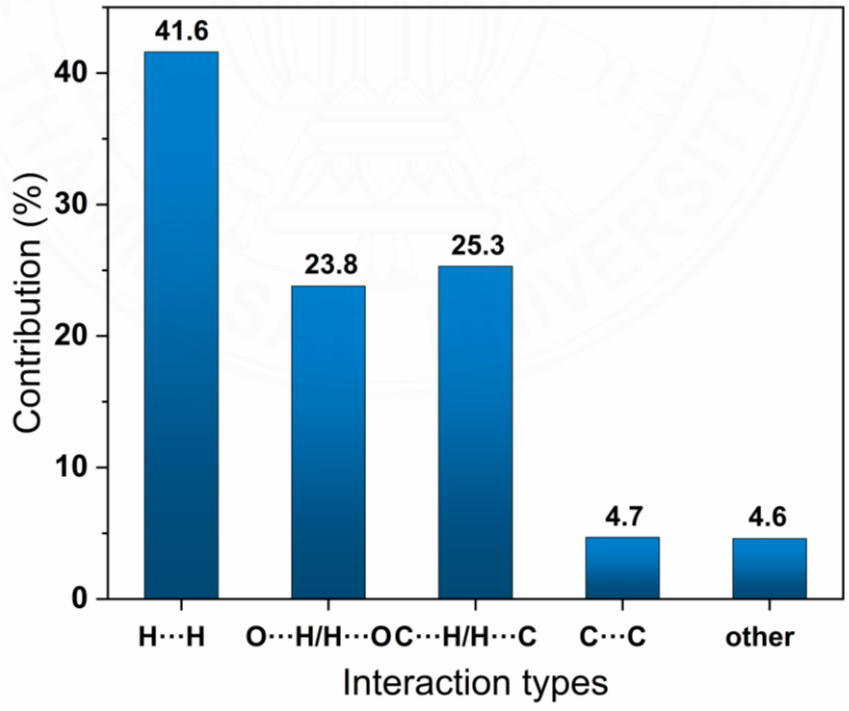

Figure 4.25 Quantitative results of different intermolecular contacts contributing to the Hirshfeld surface of complex **2**

4.3.3 Hirshfeld surface analysis of [Cu(dpyam)(2-OHbenz)Cl] (3)

The Hirshfeld surface of complex **3** is shown in Figure 4.26a. The bright-red spots on d_{norm} on the positions of the N–H group of the dpyam ligand, the CH group of the pyridine ring from the dpyam ligand, the CH group of the pyridine ring from the dpyam ligand to the chlorido ligand corresponding to the strong intermolecular N–H···Cl, C–H···O and C–H···Cl hydrogen bonding in the crystal of these complex. At the same time, the Hirshfeld surface two-dimensional fingerprint plots in Figure 4.26b present the percentage contribution for H···H, C··H/H···C, H··Cl/Cl···H, O···H/H···O and C···C contacts of complex **3**. The H···H intermolecular contacts plot shows the highest percentage contribution of 37.7%, resulting in most of the hydrogen from the organic ligands. The H···Cl intermolecular contact is due to N–H···Cl hydrogen bonding interactions with percentage contributions of 13.2%. The O···H/H···O plot with percentage contributions of 12.3% represents the existence of O···H intermolecular contacts due to O–H···O and C–H···O hydrogen bonding interactions. The plot of C···H/H···C intermolecular contacts with a percentage contribution of 20.2%. The plot of C···C contacts with percentage contributions of 4.3% indicates the π–π interactions in the crystal structure, as shown in Figure 4.27. Thus, it confirmed hydrogen bond and π–π interactions that are the dominant stability of the crystal structure and supported crystal packing from X-ray structure of complex **3**.

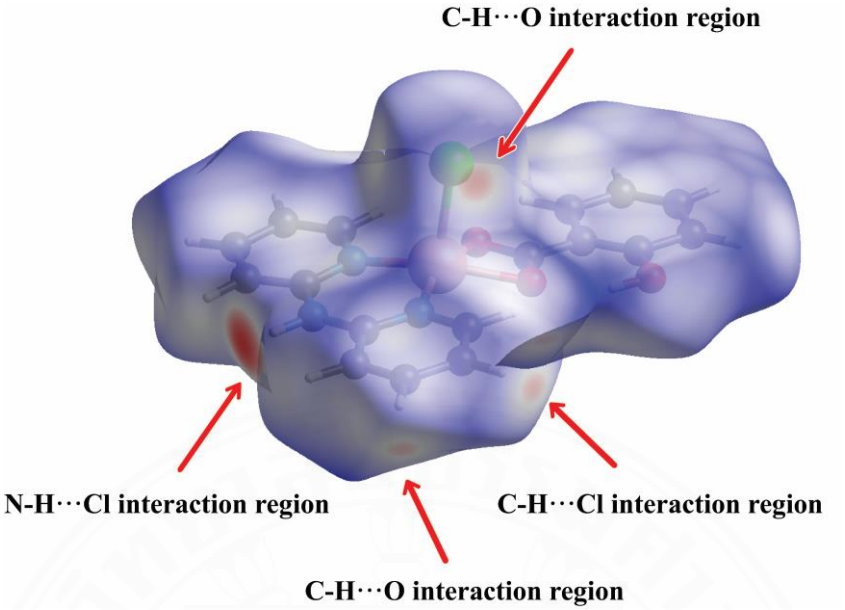

(a)

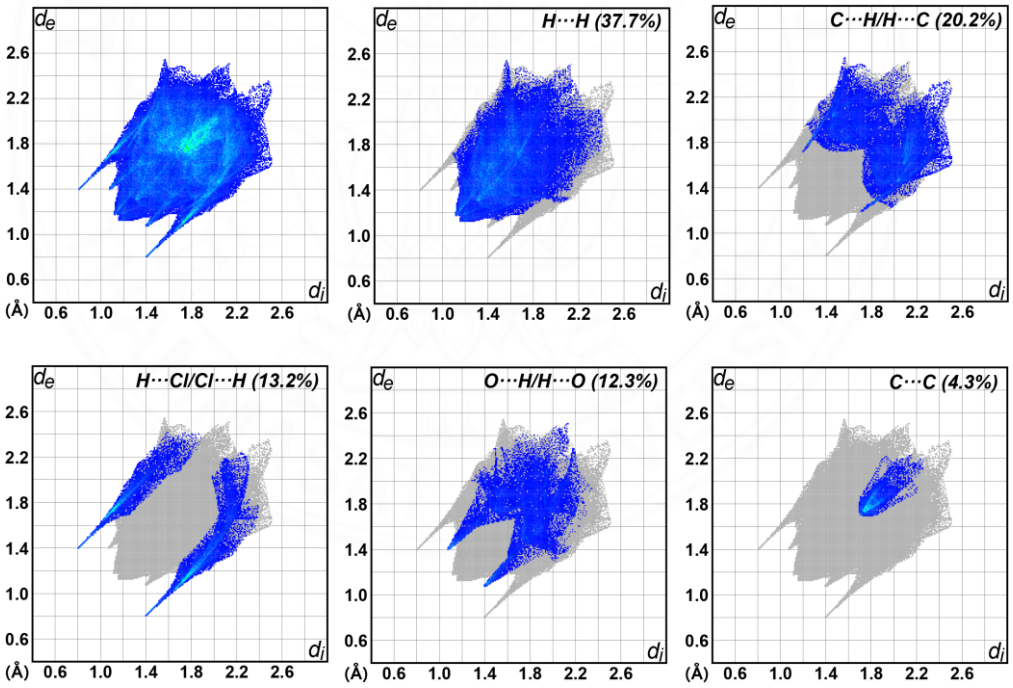

(b)

Figure 4.26 Views of (a) the Hirshfeld surface mapped over d_{norm} and (b) Hirshfeld surface 2D-fingerprint plots for the H···H, C···H/H···C, H···Cl/Cl···H, O···H/H···O and C···C contacts of complex **3**

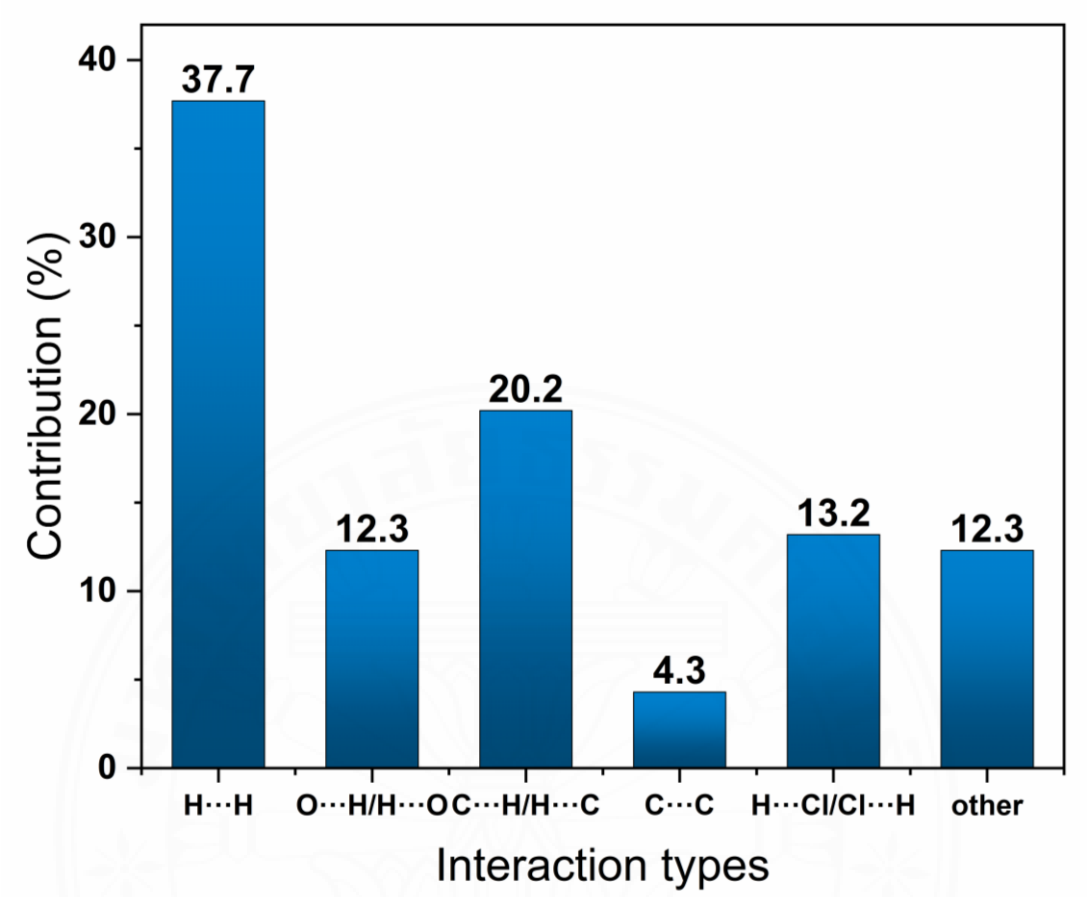

Figure 4.27 Quantitative results of different intermolecular contacts contributing to the Hirshfeld surface of complex **3**

4.3.4 Hirshfeld surface analysis of [Cu(dpyam)(3-OHbenz)Cl] (4)

The Hirshfeld surface of complex **4** is shown in Figure 4.28a. The bright-red spots on d_{norm} on the positions of the N–H group of the dpyam ligand, the CH group of the pyridine ring from the dpyam ligand, the CH group of the pyridine ring from the dpyam ligand to the hydroxyl group from 3-OHbenz ligand and the hydroxyl group of 3-OHbenz to the chloride ligand corresponding to the strong intermolecular N–H···Cl, C–H···O, C–H···O and O–H···Cl hydrogen bonding in the crystal of complex **4**. At the same time, the Hirshfeld surface two-dimensional fingerprint plots in Figure 4.28b present the percentage contribution for H···H, C··H/H···C, H··Cl/Cl···H, O···H/H···O and C···C contacts of complex **4**. The H···H intermolecular contacts plot shows the highest percentage contribution of 37.4%, resulting in most of the hydrogen from the organic ligands. The H···Cl intermolecular contact is due to N–H···Cl hydrogen bonding interactions with percentage contributions of 14.4%. The O···H/H···O plot with percentage contributions of 11.0% represents the existence of O···H intermolecular contacts due to C–H···O hydrogen bonding interactions. The plot of C···H/H···C intermolecular contacts with a percentage contribution of 20.9%. The plot of C···C contacts with percentage contributions of 3.3% indicates the π–π interactions in the crystal structure, as shown in Figure 4.29. Thus, it confirmed hydrogen bond and π–π interactions that are the dominant stability of the crystal structure and supported crystal packing from X-ray structure of complex **4**.

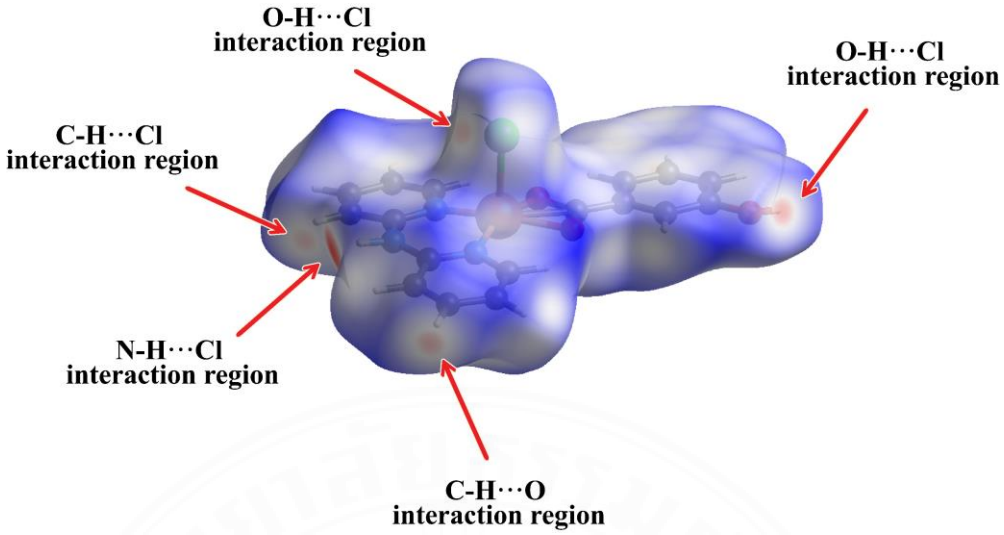

(a)

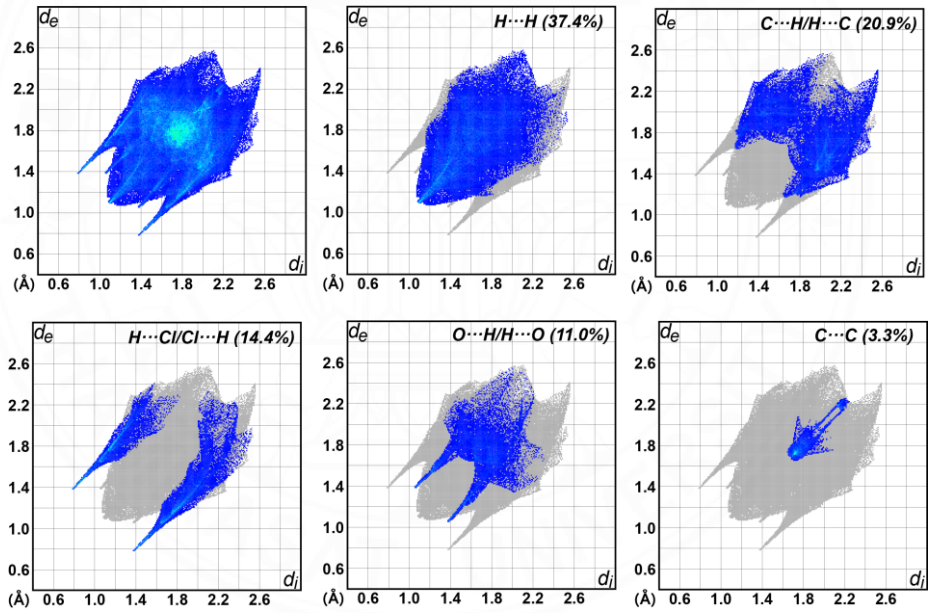

(b)

Figure 4.28 Views of (a) the Hirshfeld surface mapped over d_{norm} and (b) Hirshfeld surface 2D-fingerprint plots for the H···H, C···H/H···C, H···Cl/Cl···H, O···H/H···O and C···C contacts of complex **4**

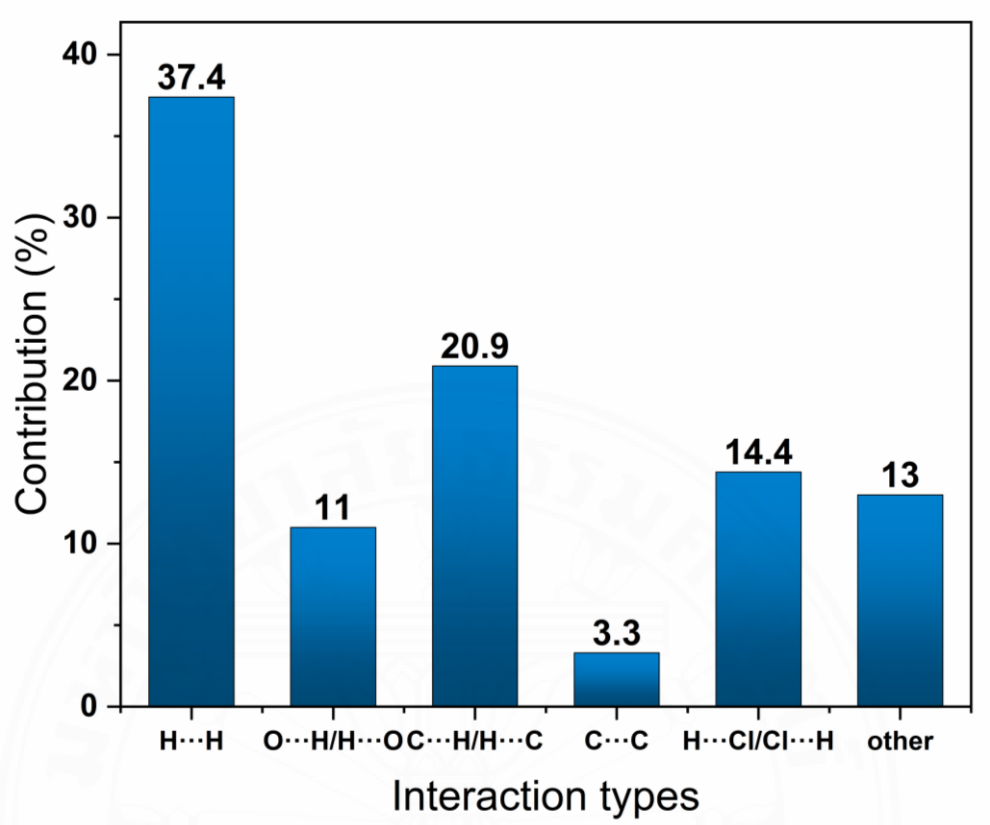

Figure 4.29 Quantitative results of different intermolecular contacts contributing to the Hirshfeld surface of complex **4**

4.4 Structural comparison

In this structural comparison part, the relevant complexes could be categorized into two groups compared to the synthesized complexes. The first group, the closely related complexes to [Cu(dpyam)(3-OHbenz)(HCO_2)] (**1**), [Cu(dpyam)(2-OHbenz)Cl] (**3**) and [Cu(dpyam)(3-OHbenz)Cl] (**4**) are [Cu(dpyam)(4-OHbenz)Cl] [40], [Cu(benz)(dpyam)Cl] [38] and [Cu(4-NO_2-benz)(dpyam)Cl] [39]. The details of the comparison are summarized in Table 4.14. The result showed that the chemical formula consists of Cu(II) ion, dpyam, chloride, and benzoate derivative ligand with substituted groups on benzoate in *para*-positions such as *p*-OH, *p*-NH_2, and *p*-NO_2 groups in mole ratio 1:1:1:1, resulting in square pyramidal geometry with τ_5 value range of 0.00 to 0.14. The distance between Cu and Cl ranges from 2.468(3) to 2.603(3) Å. The most closely related structures compared with complexes **3** and **4** are [Cu(dpyam)(4-OHbenz)Cl] [40]. The substituted groups on the benzoate ligand of complexes **3** and **4** were *ortho*- and *meta*-position, while [Cu(dpyam)(4-OHbenz)Cl] was *para*-position. The geometry of complexes also has nearly perfect square pyramidal geometry with a τ_5 range of 0.02 to 0.04 and [CuN_2O_2Cl] chromophore. The second group, the closely related complexes to [Cu(dpyam)(4-OHbenz)$_2$]·H_2O (**2**) is [Co(dpyam)(4-OHbenz)$_2$], [Ni(dpyam)$_2$(4-OHbenz)]$_2$(NO_3)·(4-OHbenz)·5H_2O and [Zn(dpyam)(4-OHbenz)$_2$]$_2$·0.5H_2O [40]. The details of the comparison are described and summarized in Table 4.15. The result showed that the chemical formula of complexes consists of dpyam and benzoate derivative ligands coordinated to transition metals such as Co(II), Ni(II), and Zn(II) ions in octahedral geometry.

Table 4.14 Summary of relevant mononuclear Cu(II) complexes based on 2,2′-dipyridylamine and benzoate derivatives

Year	Chemical Formula	τ value	Chromophore	Geometry	Cu-X distance (Å)	Mean plane of the basal atoms	Application	Ref.
2005	[Cu(dpyam)(4-OHbenz)Cl]	0.03	CuN_2O_2Cl	Sq. Py.	Cu–Cl: 2.5876(6)	0.230(1)	DNA binding	[40]
2007	[Cu(dpyam)(benz)Cl]	0.00	CuN_2O_2Cl	Sq. Py.	Cu–Cl; 2.502(3)	0.2986(1)	-	[38]
2007	[Cu(dpyam)(4-NO_2benz)Cl]	0.01	CuN_2O_2Cl	Sq. Py.	Cu–Cl; 2.468(3)	0.3274(1)	-	[39]
2009	[Cu(dpyam)(4-NH_2benz)Cl]·H_2O	0.14	CuN_2O_2Cl	Sq. Py.	Cu–Cl; 2.603(3)	0.114(7)	DNA binding	[41]
2023	[Cu(dpyam)(3-OHbenz)(HCO_2)] (**1**)	0.19	CuN_2O_3	Sq. Py.	Cu–O; 2.207(2)	0.2650	Catalytic properties	This work
	[Cu(dpyam)(2-OHbenz)Cl] (**3**)	0.04	CuN_2O_2Cl	Sq. Py.	Cu–Cl: 2.4595(17)	0.0297		
	[Cu(dpyam)(3-OHbenz)Cl] (**4**)	0.02	CuN_2O_2Cl	Sq. Py.	Cu–Cl: 2.5472(8)	0.2490		

Abbreviation: dpyam = 2,2′-dipyridylamine, benz = benzoate, 2-OHbenz = 2-hydroxybenzoate, 3-OHbenz = 3-hydroxybenzoate, 4-OHbenz = 4-hydroxybenzoate, 4-NO_2benz = 4-nitrobenzoate and Sq. Py. = Square Pyramidal

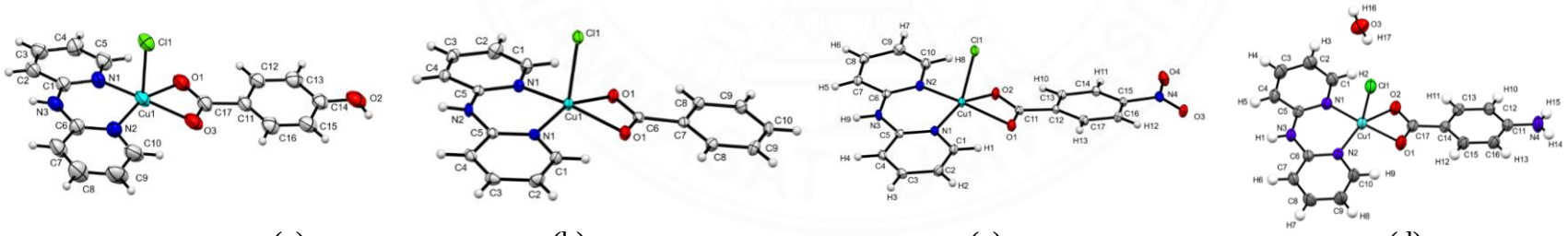

(a) (b) (c) (d)

Figure 4.30 The molecular structure of (a) [Cu(dpyam)(4-OHbenz)Cl], (b) [Cu(OHbenz)(dpyam)Cl], (c) [Cu(4-NO_2benz)(dpyam)Cl] and (d) [Cu(dpyam)(4-NH_2benz)Cl]·H_2O with the atomic numbering-scheme and displacement ellipsoid drawn at the 50% probability level

Table 4.15 Summary of relevant mononuclear transition metal(II) complexes based on 2,2′-dipyridylamine and benzoate derivatives

Year	Chemical Formula	Chromophore	Geometry	Application	Ref.
2005	$[Co(dpyam)(4\text{-}OHbenz)_2]$	CoN_2O_4	Octahedral	DNA binding	[40]
2005	$[Ni(dpyam)_2(4\text{-}OHbenz)]_2(NO_3)\cdot(4\text{-}OHbenz)\cdot 5H_2O$	NiN_4O_2	Octahedral	DNA binding	[40]
2005	$[Zn(dpyam)(4\text{-}OHbenz)_2]_2\cdot 0.5H_2O$	ZnN_2O_4	dist. Octahedral	DNA binding	[40]
2009	$[Zn(dpyam)(4\text{-}NH_2benz)_2]\cdot H_2O$	ZnN_2O_2	dist. Octahedral	DNA binding	[41]
2023	$[Cu(dpyam)(4\text{-}OHbenz)_2]\cdot H_2O$ (**2**)	CuN_2O_2	Sq. Planar	Catalytic properties	This work

Abbreviation: dpyam = 2,2′-dipyridylamine, 4-OHbenz = 4-hydroxybenzoate, dist. Octahedral = distorted octahedral and Sq. Planar = Square Planar

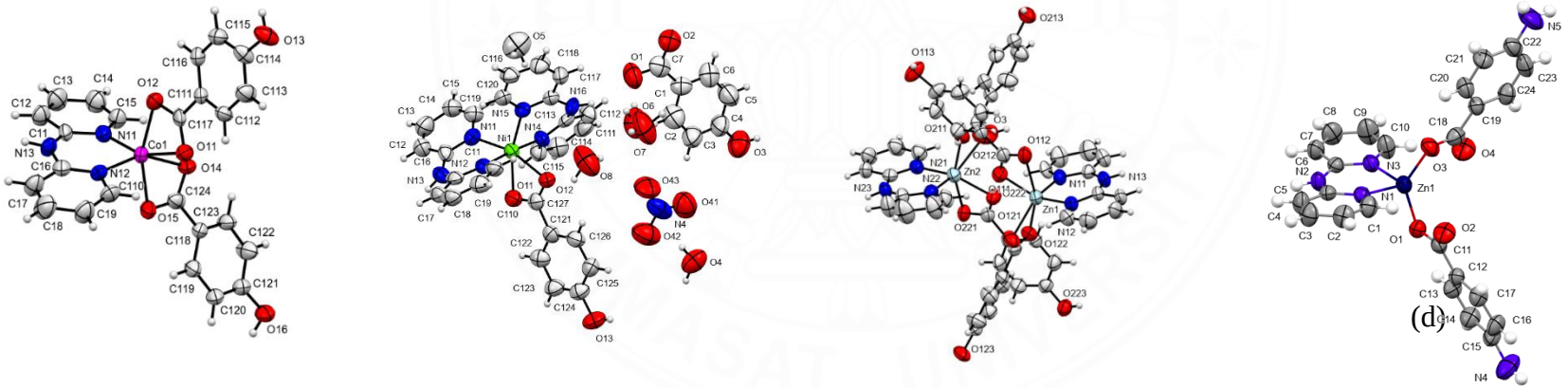

Figure 4.31 The molecular structure of (a) $[Co(dpyam)(4\text{-}OHbenz)_2]$, (b) $[Ni(dpyam)_2(4\text{-}OHbenz)]_2(NO_3)\cdot(4\text{-}OHbenz)\cdot 5H_2O$, (c) $[Zn(dpyam)(4\text{-}OHbenz)_2]_2\cdot 0.5H_2O$ and (d) $[Zn(dpyam)(4\text{-}NH_2benz)_2]\cdot H_2O$ with the atomic numbering-scheme and displacement ellipsoid drawn at the 50% probability level

4.5 Characterizations

4.5.1 The appearance of the crystals

Table 4.16 The appearance of the crystals of all synthesized mononuclear Cu(II) complexes

Chemical formula	Crystals		% Yield (based on Cu(II) salt)
	Shape	Color	
[Cu(dpyam)(3-OHbenz)(HCO_2)] (**1**)	Plate	Green	10.09
[Cu(dpyam)(4-OHbenz)$_2$]·H_2O (**2**)	Block	Dark green	77.89
[Cu(dpyam)(2-OHbenz)Cl] (**3**)	Block	Brown	73.77
[Cu(dpyam)(3-OHbenz)Cl] (**4**)	Block	Green	59.59

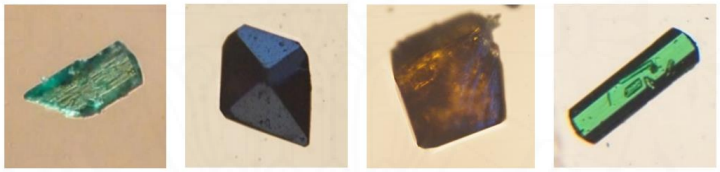

(**1**) (**2**) (**3**) (**4**)

Figure 4.32 The appearance of the crystal of four new mononuclear Cu(II) complexes collected by Olympus BX50 microscope

4.5.2 Infrared spectra

The FT-IR spectrum of complex **1** presents a characteristic broad peak at 3145 cm^{-1}, assigned to the O–H stretching vibration of the hydroxy groups of the 3–OHbenz ligand [10]. The dpyam ligand shows a band at 3204 cm^{-1} due to the N–H stretching of the secondary amine. The strong band in the region 1590 cm^{-1} are assigned to the C=N aromatic stretching of the dpyam ligand [59]. The C=O vibration peak of the chelating 3-OHbenz ligand is present at 1648 cm^{-1}, which was higher than the C=C aromatic vibration peak at 1590 cm^{-1} [60]. The peaks of 826, 768 and 686 cm^{-1} are assigned to the out-of-plane C–H bending of the 3-OHbenz ligand [58]. The

infrared spectrum in the COO^- stretching indicates monodentate metal formate species, consisting of a strong antisymmetric COO^- stretching vibration at 1648 cm^{-1} and a somewhat symmetrical COO^- stretching at 1305 cm^{-1} [61]. These spectral features indicate the coordination and bonding between the metal and the formate ligand in the complex. The characteristic peaks at 532 and 424 cm^{-1} were assigned to Cu–N and Cu–O stretching, respectively [62], as shown in Figure 4.33a. Therefore, it confirms that dpyam, hydroxybenzoate, and formato ligands are coordinated to Cu(II) ion.

The FT-IR spectrum of complex **2** presents a characteristic broad peak at 3027 cm^{-1}, assigned to the O–H stretching vibration of the water molecule and the hydroxy groups of the 4-OHbenz ligand [58]. The dpyam ligand shows a band at 3141 cm^{-1} due to the N–H stretching of the secondary amine. The strong band in the region 1597 cm^{-1} are assigned to the C=N aromatic stretching of the dpyam ligand [59]. The asymmetric and symmetric COO^- peaks of the chelating 4-OHbenz ligand are present at 1597 and 1489 cm^{-1}, respectively [63]. The peaks at 856, 773 and 634 cm^{-1} are assigned to the out-of-plane C–H bending of the 4-OHbenz ligand [58]. The characteristic peaks at 504 and 424 cm^{-1} were assigned to Cu–N and Cu–O stretching, respectively [62], as shown in Figure 4.33b. Therefore, it confirms that dpyam and hydroxybenzoate ligands are coordinated to Cu(II) ion.

The FT-IR spectrum of complex **3** presents a characteristic broad peak at 3194 cm^{-1}, which is assigned to the O–H stretching vibration of the hydroxy groups of 2-OHbenz [58]. The dpyam ligand shows a band at 3299 cm^{-1} due to the N–H stretching of the secondary amine. The strong band in the region 1590 cm^{-1} are assigned to the C=N aromatic stretching of the dpyam ligand [59]. The asymmetric and symmetric COO^- peaks of the chelating 2-OHbenz ligand are present at 1590 and 1481 cm^{-1}, respectively [63]. The peaks at 876, 763 and 670 cm^{-1} are assigned to the out-of-plane C–H bending of the 2-OHbenz ligand [10]. The characteristic peaks at 533 and 418 cm^{-1} were assigned to Cu–N and Cu–O stretching, respectively [62]. The characteristic peak at 309 cm^{-1} can be assigned to terminal Cu–Cl stretching [64], as shown in Figure 4.33c. Therefore, it confirms that dpyam, hydroxybenzoate and chlorido ligands are coordinated to Cu(II) ion.

The FT-IR spectrum of complex **4** displays a characteristic broad peak at 3246 cm^{-1}, which is assigned to the O–H stretching vibration of the hydroxy

groups of 3-OHbenz [58]. The dpyam ligand shows a band at 3246 cm^{-1} due to the N–H stretching of the secondary amine. The strong band in the region 1643 cm^{-1} are assigned to the C=N aromatic stretching of the dpyam ligand [59]. The asymmetric and symmetric COO^- peaks of the chelating 3-OHbenz ligand are present at 1590 and 1482 cm^{-1}, respectively [63]. The peaks at 879, 764 and 681 cm^{-1} are assigned to the out-of-plane C–H bending of the 3-OHbenz ligand [58]. The characteristic peaks at 544 and 423 cm^{-1} were assigned to Cu–N and Cu–O stretching, respectively [62]. The characteristic peak at 310 cm^{-1} can be assigned to terminal Cu–Cl stretching [64]. For this reason, It can be concluded that dpyam, hydroxybenzoate and chlorido ligands are coordinated to Cu(II) ion.

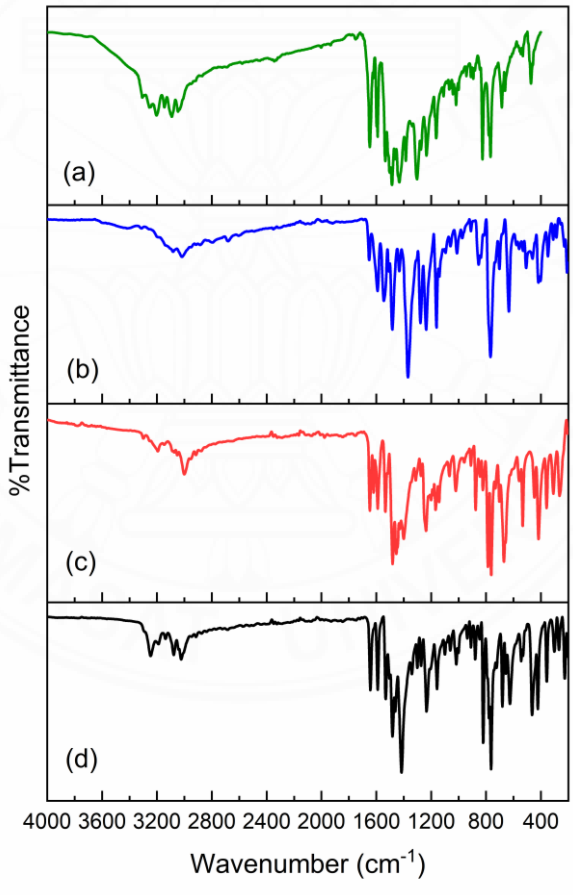

Figure 4.33 The FT-IR spectra of (a) [Cu(dpyam)(3-OHbenz)(HCO_2)] (**1**), (b) [Cu(dpyam)(4-OHbenz)$_2$]·H_2O (**2**), (c) [Cu(dpyam)(2-OHbenz)Cl] (**3**) and (d) [Cu(dpyam)(3-OHbenz)Cl] (**4**)

4.5.3 Solid-state diffuse reflectance spectra

The solid-state diffuse reflectance spectrum of complex **2**, as shown in Figure 4.34, presents a broadening band with λ_{max} in the range of 669 and 842 nm. This feature could be assigned to the electronic *d-d* transitions of $d_{xy} \rightarrow d_{x}^{2} - {}_{y}^{2}$ and $d_{z}^{2} \rightarrow d_{x}^{2} - {}_{y}^{2}$ corresponding to the four-coordinate geometry of copper(II) complexes. Therefore, the solid-state diffuse reflectance spectrum of complex **2** helps support X-ray structure geometry [65, 66].

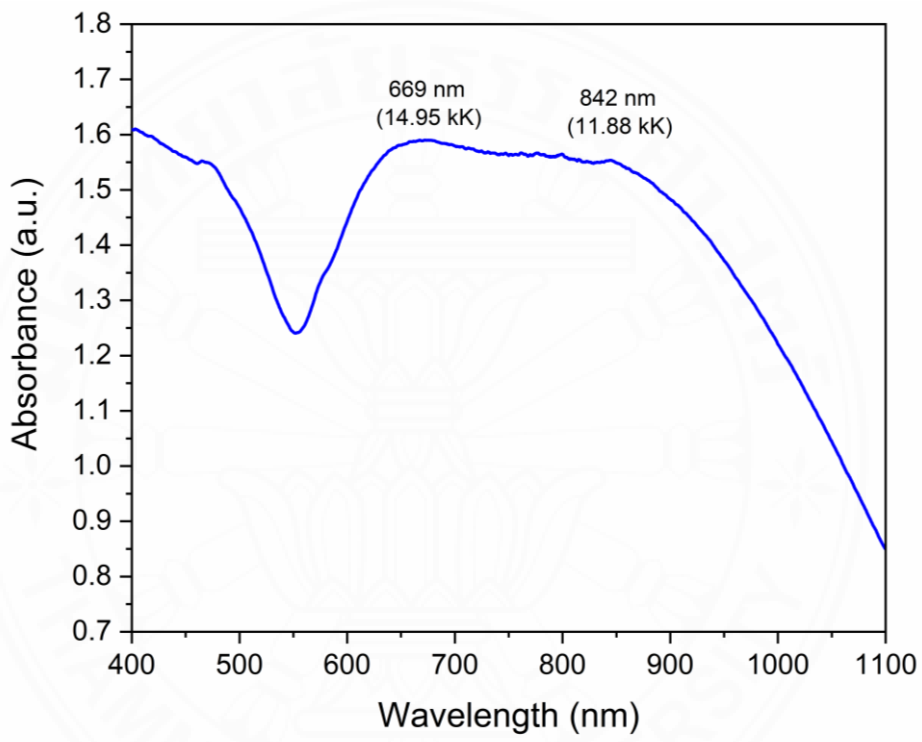

Figure 4.34 The solid-state diffuse reflectance spectrum of [Cu(dpyam)-(4-OHbenz)$_2$]·H_2O (**2**)

The solid-state diffuse reflectance spectra of complexes **1**, **3** and **4** show a single board band with λ_{max} at 645, 755 and 700 nm, respectively. These features could be assigned to the electronic *d-d* transition of d_{xy}, d_{xz}, d_{yz}, $d_{z}^{2} \rightarrow d_{x}^{2}$-$_{y}^{2}$ corresponding to the pentacoordinated square-based pyramidal geometry of Cu(II) complex [67, 68], as shown in Figure 4.35.

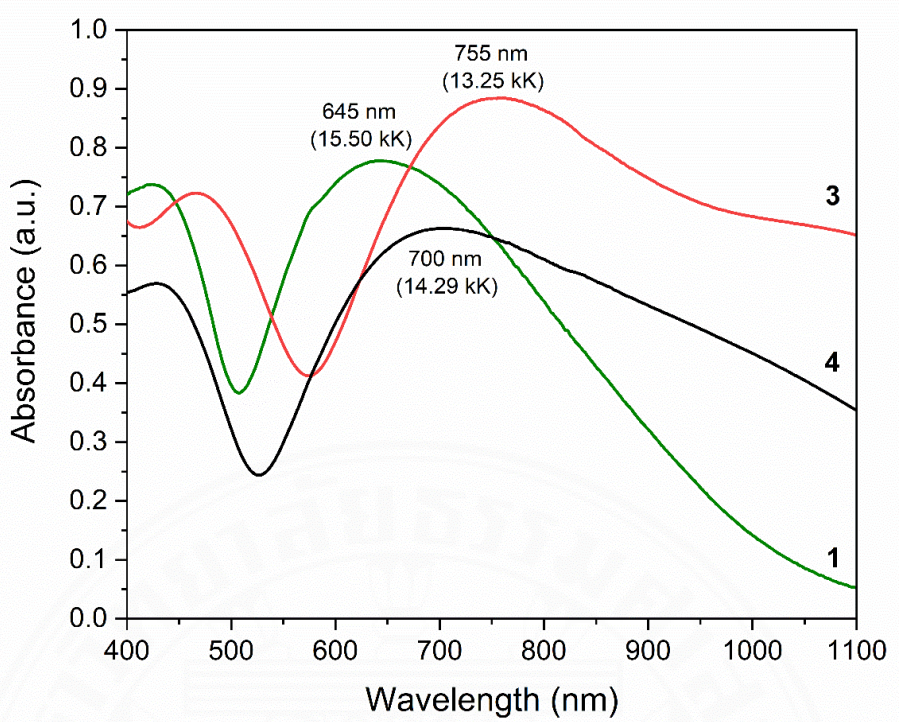

Figure 4.35 The solid-state diffuse reflectance spectra of) [Cu(dpyam)(3-OHbenz)-(HCO_2)] (**1**), [Cu(dpyam)(2-OHbenz)Cl] (**3**) and (d) [Cu(dpyam)(3-OH-benz)Cl] (**4**)

4.5.4 The solubility test

Cu(II) complexes are usually blue or green due to the presence of *d-d* absorption bands in the 200 to 900 nm region of the visible absorbance spectra [69]. Solubility testing can determine whether mononuclear Cu(II) complexes are stable in various solvents. For this research, the amount of complex **1** is insufficient for further studies of physical properties and catalytic activity. The solubility test of complexes **2**, **3** and **4** were measured by UV-vis spectrophotometer in various solvents at a concentration of 5 mM, the electronic spectra are shown in Figures 4.36-4.38. The solubility test of complexes **2**, **3** and **4** is summarized in Table 4.16. For catalytic studies, we focus on solubility in THF solvent. The results show that only the UV-vis spectrum of complex **2** exhibits λ_{max} at 672 nm due to the *d-d* transition of the Cu(II) complex (Figure 4.39). Due to complex **2** is partially soluble in THF solvent, while complexes **3** and **4** are insoluble in THF solution. So, complexes **3** and **4** were suitable for studying the catalytic properties.

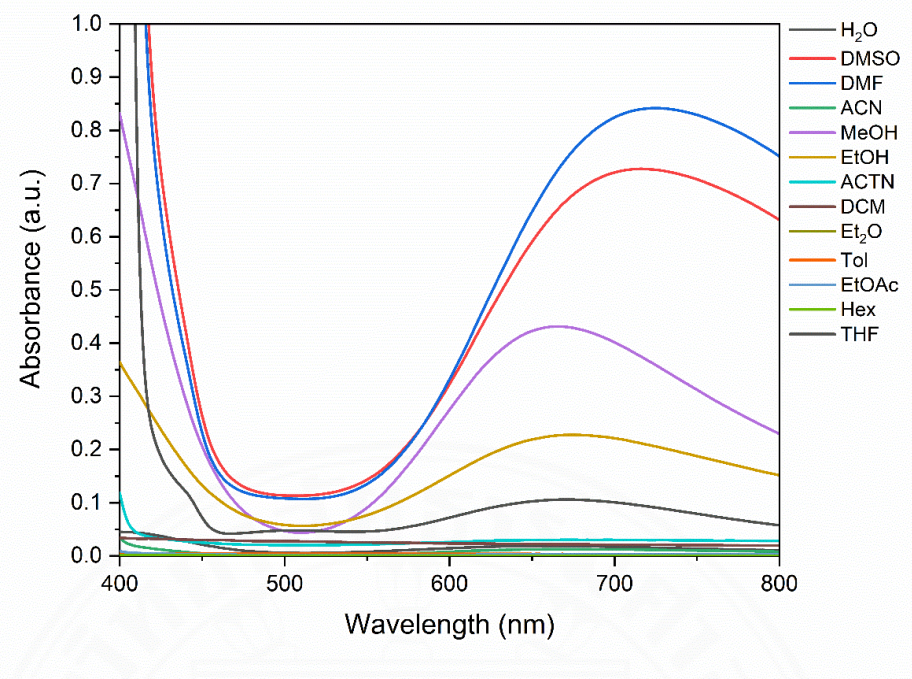

Figure 4.36 The UV-vis spectra of complex **2** (5 mM) in various solvents

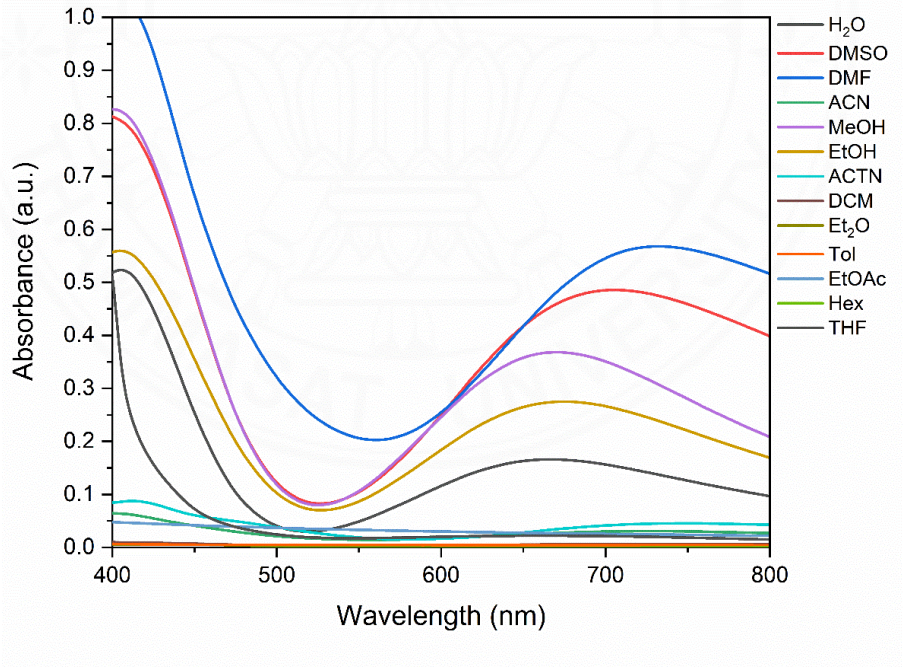

Figure 4.37 The UV-vis spectra of complex **3** (5 mM) in various solvents

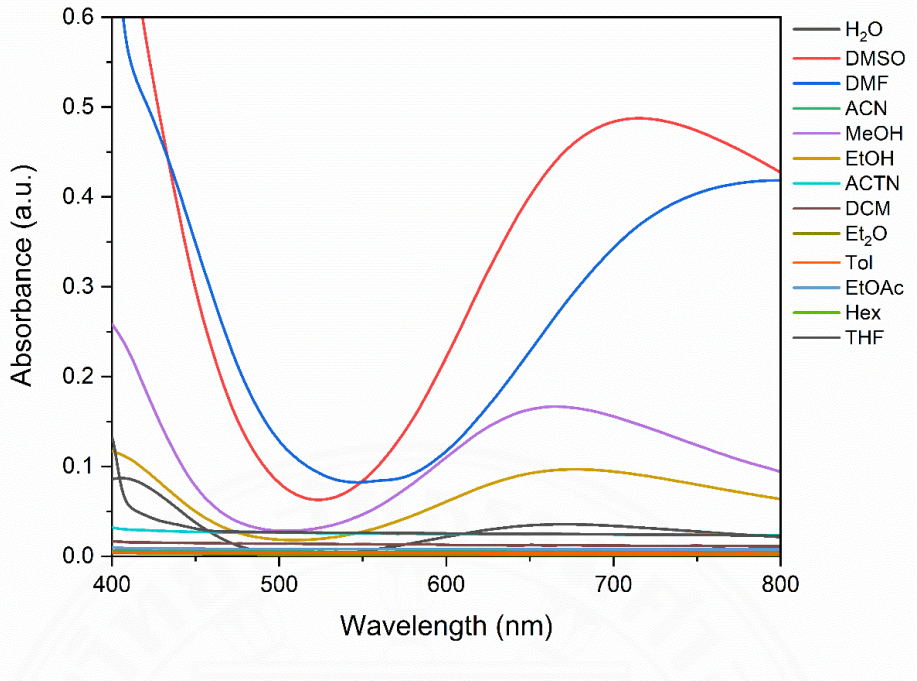

Figure 4.38 The UV-vis spectra of complex **4** (5 mM) in various solvents

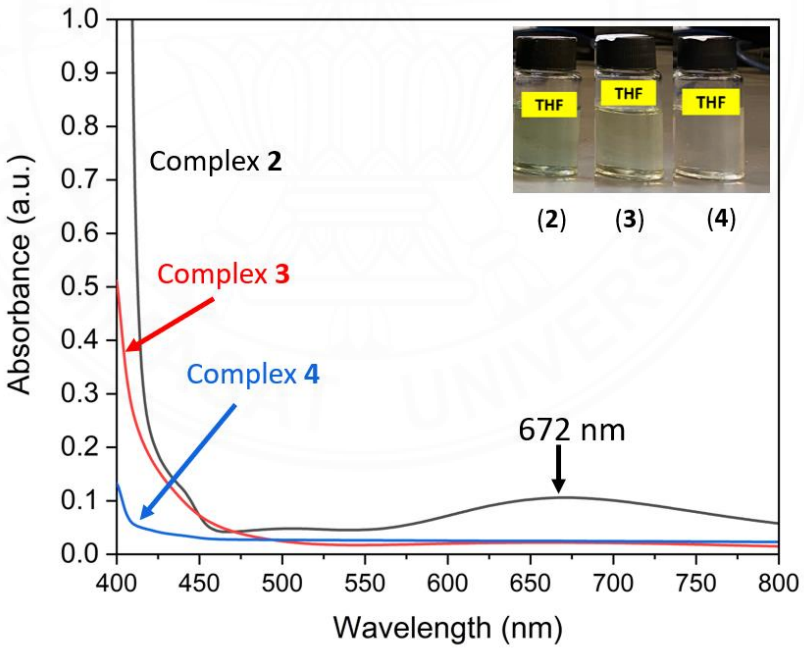

Figure 4.39 The UV-vis spectra of complexes **2**, **3** and **4** (5 mM) in THF solvent

Table 4.17 Solubility test of complexes **2**, **3** and **4** in various solvents

Solvents	Complexes		
	(**2**)	(**3**)	(**4**)
H_2O	I	P	P
DMSO	S	S	S
DMF	S	S	P
ACN	I	P	P
MeOH	S	S	P
EtOH	P	P	P
Ace	I	P	I
DCM	I	P	I
EtOAc	I	I	I
Tol	I	I	I
Hex	I	I	I
Et_2O	I	I	I
THF	P	I	I

Abbreviation. DMSO = Dimethyl sulfoxide, DMF = Dimethylformamide, ACN = Acetonitrile, MeOH = Methanol, EtOH = Ethanol, Ace = Acetone, DCM =, Dichloromethane, EtOAc = Ethyl acetate, Tol = Toluene, Hex = Hexane, Et_2O = Diethyl ether, S = Soluble, I = Insoluble, and P = Partially soluble

4.5.5 Powder X-ray diffraction patterns

Powder X-ray diffraction (PXRD) was used to verify the purity of complexes and to identify the phase in powder form. The Powder XRD patterns of each synthesized complex are compared with the simulated pattern from single-crystal X-ray diffraction data, which is generated by Mercury Program. The result showed that the Powder XRD patterns of complexes match well with the simulated pattern, as shown in Figure 4.41. Therefore, it confirmed that complexes are high purity and repeatable.

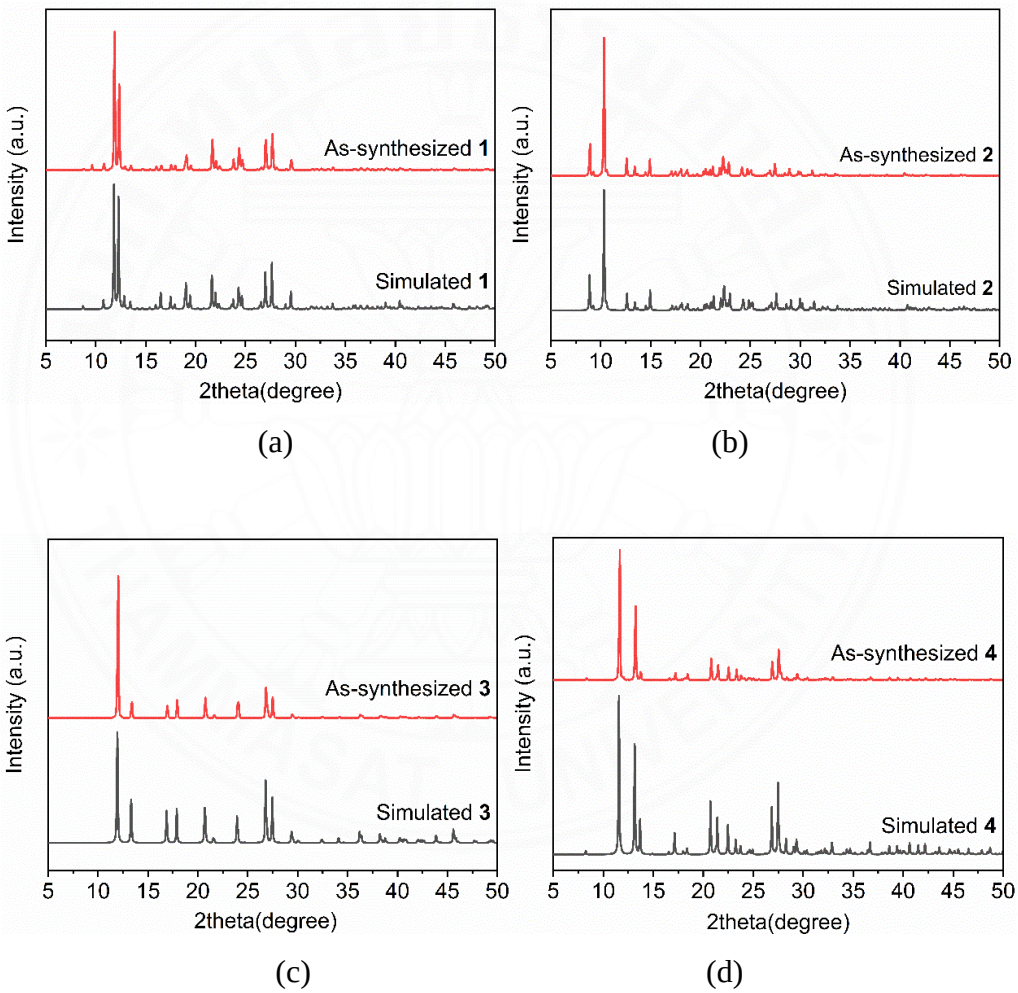

Figure 4.40 The powder X-ray diffraction patterns of (a) complex **1**, (b) complex **2**, (c) complex **3** and (d) complex **4**

4.5.6 Thermogravimetric analysis curves

The TGA was carried out to investigate thermal stability. For this research, the thermogravimetric curves were recorded at 35 to 800 °C under a nitrogen atmosphere. Complex **1** is insufficient for further studies of physical properties. For complex **2**, the first weight-loss step of 3.96% is observed from 30 to 148 °C and can be attributed to the loss of water molecules, while the weight loss of about 67.55% from 250 to 370 °C can be assigned to removing one dpyam molecule and one 4-OHbenz molecule ligand. So, it can be concluded that the thermal stability of complex **2** is up to 250 °C. The structure of complex **3** begins to collapse with a weight loss of 64.99% (calcd. 75.94%) in a temperature range from 240 to 485 °C that can be attributed to the removal of one dpyam molecule and one 2-OHbenz molecule, as shown in Figure 4.41b. Next, in the temperature range of 265 to 385 °C, the structure of complex **4** begins to collapse with a weight loss of 70.32% (calcd. 75.94%), which can be attributed to removing one dpyam molecule and one 3-OHbenz molecule, as shown in Figure 41c. Therefore, complexes **3** and **4** are stable up to 245 °C and 265 °C, respectively. It can be concluded that complexes have good thermal stability.

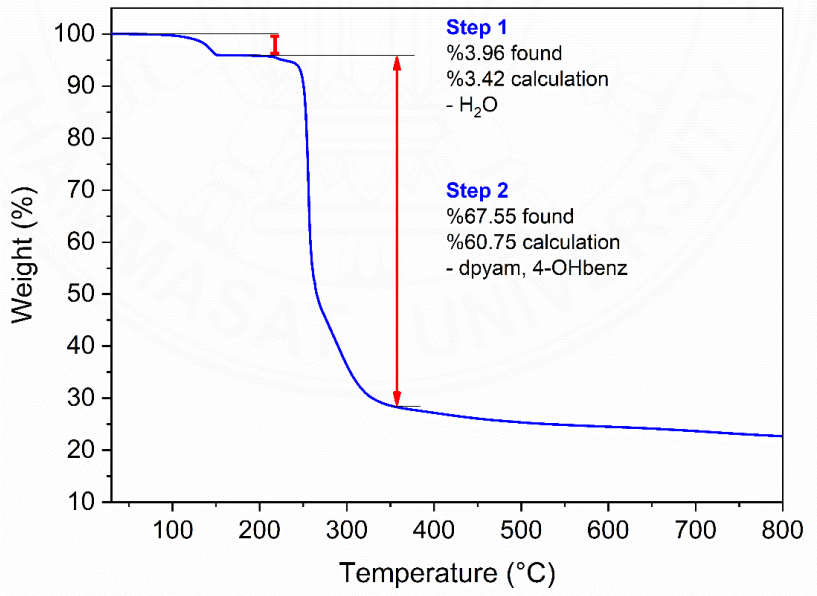

(a)

Figure 4.41 The TGA curves of (a) $[Cu(dpyam)(4\text{-}OHbenz)_2]\cdot H_2O$ (**2**), (b) [Cu(dpyam)(2-OHbenz)Cl] (**3**) and (c) [Cu(dpyam)(3-OHbenz)Cl] (**4**)

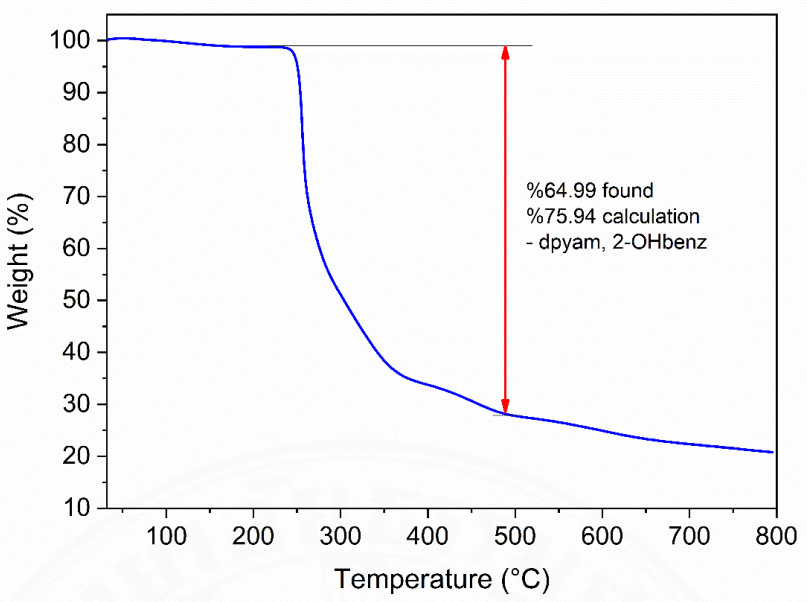

(b)

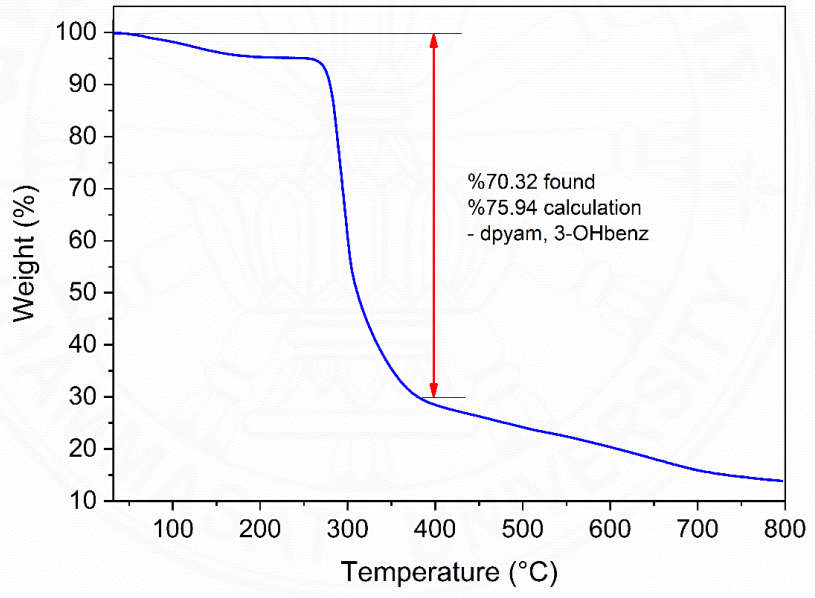

(c)

Figure 4.41 The TGA curves of (a) $[Cu(dpyam)(4\text{-}OHbenz)_2]\cdot H_2O$ (**2**), (b) [Cu(dpyam)(2-OHbenz)Cl] (**3**) and (c) [Cu(dpyam)(3-OHbenz)Cl] (**4**) (cont.)

4.5.7 CHN analysis

The CHN analysis presented the amounts of C, H, and N elements within complexes. The percent of C, H, and N elements of complexes **2**, **3**, and **4** are summarized in Table 4.18. The result showed that the calculated %CHN of new mononuclear Cu(II) complexes corresponds with the experimental results confirming the chemical formula of these complexes from the single-crystal X-ray diffraction technique.

Table 4.18 CHN elemental analysis of new mononuclear Cu(II) complexes

Chemical formula	Elements (%)					
	C		H		N	
	calcd.	found	calcd.	found	calcd.	found
[Cu(dpyam)(4-OHbenz)$_2$]·H_2O (**2**)	54.60	54.28	4.20	4.07	7.96	8.12
[Cu(dpyam)(2-OHbenz)Cl] (**3**)	50.01	50.26	3.70	3.58	10.29	10.34
[Cu(dpyam)(3-OHbenz)Cl] (**4**)	50.01	50.29	3.70	3.64	10.29	10.37

4.6 Catalytic properties of new mononuclear Cu(II) complexes

4.6.1 Optimization of the catalytic conditions

The conditions of the aerobic oxidation reaction of *N*-(benzyloxy-carbonyl)hydroxylamine (**1a**) reacted with 2-ethyl-2-oxazoline (**2a**), resulting in nitroso compound, (**3a**), which reacted with 2,3-dimethyl-1,3-butadiene (**4a**) *via* a Nitroso-Diels-Alder (HAD) and Nitroso-ene reaction giving cycloadduct (**5a**) and ene-product (**6a**), as shown in Scheme 4.1. For this work, the effect of solvent, amount of catalyst, and temperature were studied and investigated by using new mononuclear Cu(II) complexes as catalysts for the aerobic oxidation reaction.

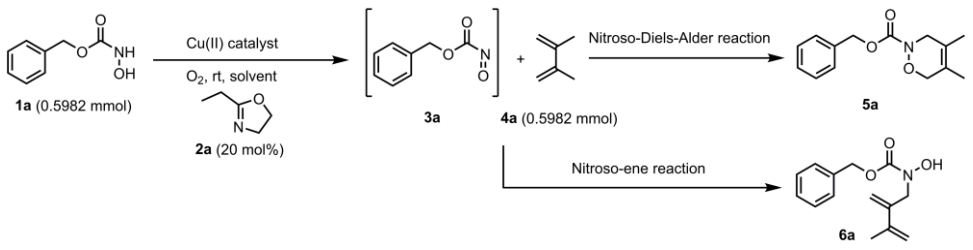

Scheme 4.1 The aerobic oxidation reaction in this work

4.6.1.1 The solvent screening studies

The types of solvents used in this reaction were nonpolar, polar protic, and aprotic solvents. For nonpolar solvents were toluene, dichloromethane, and hexane, and the polar protic solvent was MeOH, including aprotic solvents were acetonitrile and THF. The results are shown in Table 4.19. The reaction in acetonitrile solvent was completed in 7 hours, gaving cycloadduct (**5a**) and ene product (**6a**) a 67% overall yield with a 7:1 ratio (Entry 1). Meanwhile, the reactions in MeOH, dichloromethane, and toluene were completed in 19 hours with 72-77% yields, which was the same ratio (Entries 2-4). The reaction in hexane was completed within 48 hours with a 70% overall yield and a 35:1 ratio, which gave good chemoselectivities (Entry 5). Although the reaction in hexane gave good chemoselectivity, it takes a long time to react, so it is an unsuitable solvent. The reaction in THF solvent was completed within 6.5 hours, with the highest overall yield of 98% (Entry 6). The ratio of cycloadduct (**5a**) and ene product (**6a**) was 7:1 by the integration of the signals at δ 1.66 and 1.58 (CH_3 signals for **5a**) and 1.92 (CH_3 for **6a**) [43], as shown in Figure 4.42. Therefore, THF solvent is the optimum solvent for this reaction due to the shortest reaction time, the highest yield, and good chemoselectivities.

Table 4.19 The solvent screening studies for the aerobic oxidation reaction of *N*-(benzyloxy-carbonyl)hydroxylamine (**1a**)[a]

Entry	Solvent	Time (h)	Ratio of **5a**:**6a**	Yields %
1	MeCN	7	7:1	67
2	MeOH	19	7:1	77
3	DCM	19	7:1	74
4	Toluene	19	7:1	72
5	Hexane	48	35:1	70
6	THF	6.5	7:1	98

[a]Reaction condition: **1a** (100 mg, 0.5982 mmol), **2a** (12.07 μL, 0.1196 mmol), **4a** (68 μL, 0.5982 mmol) and heterogeneous catalyst (**3**) (10 mol%) in solvent (20 mL) at room temperature.

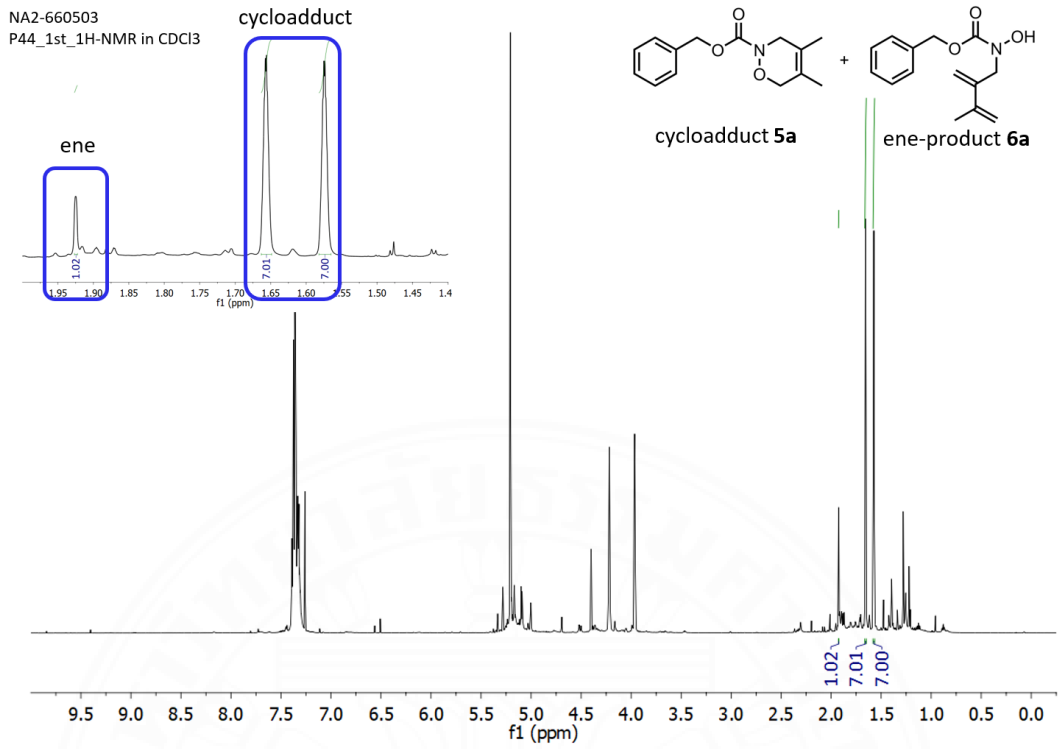

Figure 4.42 The ^{1}H NMR spectrum of the crude products of cycloadduct (**5a**) and ene product (**6a**)

4.6.1.2 The amount of catalyst screening studies

In the next step, the catalyst was screened by varying the amount of catalyst as follows: 0, 1, 5, 10, and 50 mol% of catalyst. The results are shown in Table 4.20. For entry 1, in the absence of the catalyst, the reaction did not occur, and there was no product. When the catalyst was increased to 1 mol%, the reaction was completed within 48 hours. The cycloadduct (**5a**) and ene product (**6a**) were obtained with an 83% yield and a 7:2 ratio (Entry 2). After that, the catalyst was increased to 5 mol%, and the reaction time was decreased to 10 hours from 48 hours with a 96% yield with the same ratio. Then, the catalyst was increased to 10 mol%, while the reaction time was decreased to 6.5 hours. The products obtained the highest yield of 98% with 7:1, which gave good chemoselectivities compared to 1 and 5 mol% catalysts (Entries 2-3). When the catalyst amount was increased to 50 mol%, the reaction time decreased from 6.5 hours to 5 hours, yield decreased to 87%, and chemoselectivities decreased compared with 10 mol% of catalyst. Because the amount of catalyst is too much, it causes many nitroso compounds. While the nitroso compound

has increased, the amount of dien remains the same, causing the nitroso compound to compete to react with diene, resulting in the reaction time decreasing and the selectivity of the cycloadduct also decreasing. For this reason, 10 mol% of the catalyst is the optimal amount for this reaction.

Table 4.20 The amount of catalyst screening studies for the oxidation reaction of *N*-(benzyloxy-carbonyl)hydroxylamine (**1a**)[a]

Entry	Amount of catalyst (mol%)	Time (h)	Ratio of **5a**: **6a**	Yield (%)
1	0	48	-	-
2	1	48	7:2	83
3	5	10	7:2	96
4	10	6.5	7:1	98
5	50	5	7:2	87

[a]Reaction condition: **1a** (100 mg, 0.5982 mmol), **2a** (12.07 μL, 0.1196 mmol), **4a** (68 μL, 0.5982 mmol) and heterogeneous catalyst (**3**) in THF solvent (20 mL) at room temperature.

4.6.1.3 The temperature screening studies

In the next step, the effect of temperature on the reaction was investigated. The reactions were done at room temperature, 77 °C heat under reflux, and 77 °C in a sealed tube. The results are shown in Table 4.21. The reaction at room temperature was completed in 6.5 hours with the highest yield of 98% with a 7:1 ratio, giving good chemoselectivities (Entry 1). The temperature was increased to 77 °C by heat under reflux and a sealed tube. For the reaction that was heated under reflux, the reaction time was increased from 6.5 to 24 hours, while the yield was decreased from 98 to 62 with a 7:1 ratio. Because diene was a volatile organic compound, the nitroso compound reacted less with diene, decreasing the products. The reaction was heated in a sealed tube at 77 °C. The result showed that the reaction was completed within 22 hours, and the yield decreased to 57% with a 7:2 ratio (Entry 3). The temperature and reaction time increased while yield decreased because the reaction was a closed system, resulting in insufficient oxygen in the air. Therefore, room temperature is the optimal temperature for this reaction.

Table 4.21 The temperature screening studies for the oxidation reaction of *N*-(benzyloxy-carbonyl)hydroxylamine (**1a**)[a]

Entry	Temperature	Time (h)	Ratio of **5a**: **6a**	Yield (%)
1	RT	6.5	7:1	98
2	77 (refluxed)	24	7:1	62
3	77 (sealed tube)	22	7:2	57

[a]Reaction condition: **1a** (100 mg, 0.5982 mmol), **2a** (12.07 μL, 0.1196 mmol), **4a** (68 μL, 0.5982 mmol) and heterogeneous catalyst (**3**) (10 mol%) in THF solvent (20 mL).

4.6.1.4 New mononuclear Cu(II) complexes screening as heterogeneous catalyst

The screening of new mononuclear Cu(II) complexes was $[Cu(dpyam)(4\text{-}OHbenz)_2]\cdot H_2O$ (**2**), [Cu(dpyam)(2-OHbenz)Cl] (**3**), and [Cu(dpyam)(3-OHbenz)Cl] (**4**). For [Cu(dpyam)(4-OHbenz)Cl] (**II**), it was already published in 2005 [40]. This mononuclear Cu(II) complex was studied in catalysis because it was isostructural with complexes **3** and **4**. Complex **1** could not be reproduced sufficiently for further studies of catalytic properties. The results are shown in Table 4.22. Complex **2** was presented as a homogeneous catalyst with a very long completed reaction time of 67 hours. The products were obtained with a 98% yield in a 7:2 ratio. The TOF value was 1.39 h^{-1} (Entry 1). So, complex **2** was not a suitable catalyst. Complexes **3**, **4,** and **II** present heterogeneous catalysts. Complex **3** exhibited the most catalytic efficiency with a reaction time of 6.5 hours and the highest yield of 98% with a 7:1 ratio, which gave good chemoselectivities, and the highest value was 15.29 h^{-1} (Entry 2), which is the good efficiency of a catalyst. Complex **4** was used in the reaction, the reaction time was increased from 6.5 to 25 hours, yield decreased from 98 to 82% with a 7:2 ratio, and TOF values decreased from 15.29 to 3.33 h^{-1} (Entry 3). Complex **4** as a catalyst was studied in the reaction, which was decreased to 19 hours with a 91% yield with a 7:1 ratio, and the TOF value was 4.86 h^{-1} (Entry 4). Therefore, complex **3** is suitable to be the optimal heterogeneous catalyst for this reaction, as shown in Scheme 4.2.

Table 4.22 The result of catalytic screening studies of new mononuclear Cu(II) complexes in the oxidation reaction of *N*-(benzyloxy-carbonyl)-hydroxylamine (**1a**)

Entry	Catalyst	Time (h)	Ratio of **5a**: **6a**	Yield (%)	TOF (h^{-1})
1	[Cu(dpyam)(4-OHbenz)$_2$]·H_2O (**2**)	67	7:2	93	1.39
2	[Cu(dpyam)(2-OHbenz)Cl] (**3**)	6.5	7:1	98	15.29
3	[Cu(dpyam)(3-OHbenz)Cl] (**4**)	25	7:2	82	3.33
4	[Cu(dpyam)(4-OHbenz)Cl] (**II**)	19	7:1	91	4.86

[a]Reaction condition: **1a** (100 mg, 0.5982 mmol), **2a** (12.07 µL, 0.1196 mmol), **4a** (68 µL, 0.5982 mmol) and Cu(II) catalyst (10 mol%) in THF solvent (20 mL) at room temperature

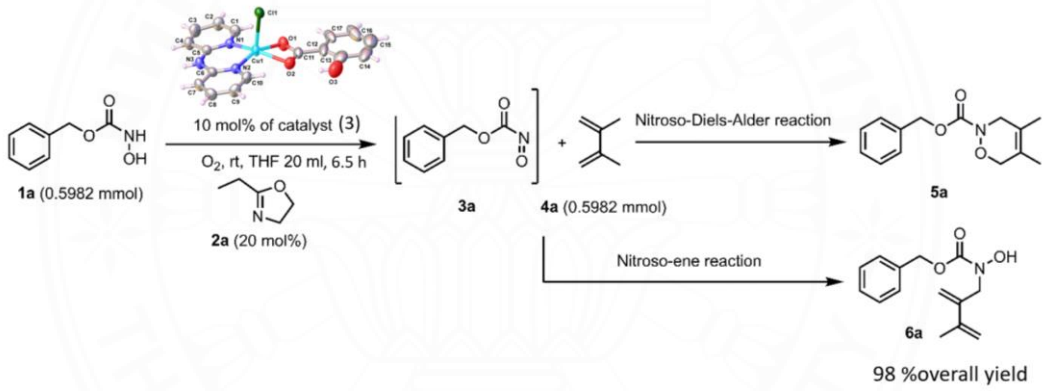

Scheme 4.2 The best condition of the aerobic oxidation reaction of **1a**

4.6.2 Recycling of the catalyst

The recycling test of the catalyst was investigated under optimized reaction conditions. When the reaction was completed, the catalyst was filtered by filter paper, washed with hexane and ethyl acetate (7:3 mL), and slowly evaporated in the air at room temperature to prepare the catalyst for the next cycle. Meanwhile, the products were washed with hexane and ethyl acetate ratio of 7:3 mL and evaporated at 40 °C. The results of this recycling study are shown in Table 4.23. The reaction of the 1st cycle to 5th cycle were completed within 6.5 hours and had a high yield range of 88 to 98% with a 7:1 ratio of cycloadduct (**5a**) and ene-product (**6a**), which gave chemoselectivity. The TOFs calculated for successive activity cycles were 15.29, 15.13, 14.66, 14.04, and

13.73, respectively. The TOF values are slightly different values, which is a good indication of catalyst recycling. After that, in the 6th and 7th cycles, the reaction time was increased from 6.5 to 9 hours, and yield decreased and chemoselectivities decreased compared to the 1st cycle to 5th cycle. The TOF values decreased significantly. So, complex **3** as heterogeneous catalysts could be recycled at least five cycles under the same conditions, as shown in Figure 4.43.

Table 4.23 The yield of cycloadduct (**5a**) and ene-product (**6a**) using the recovered heterogeneous catalyst (**3**)

Number of catalytic cycles	Time (h)	Ratio of **5a**:**5b**	Yield (%)	% Recovery of catalyst	TOF (h^{-1})[b]
1	6.5	7:1	98	100	15.29
2	6.5	7:1	97	95	15.13
3	6.5	7:1	94	94	14.66
4	6.5	7:1	90	91	14.04
5	6.5	7:1	88	86	13.73
6	9	7:2	81	78	9.13
7	9	7:2	76	99	8.56
8	6.5*	7:1	54	-	8.42

[a]Reaction condition: **1a** (100 mg, 0.5982 mmol), **2a** (12.07 μL, 0.1196 mmol), **4a** (68 μL, 0.5982 mmol) and heterogeneous catalyst (**3**) (10 mol%) in THF solvent (20 mL) at room temperature. * = stop reaction at 6.5 hours. [b]TOF calculation is shown in appendix D

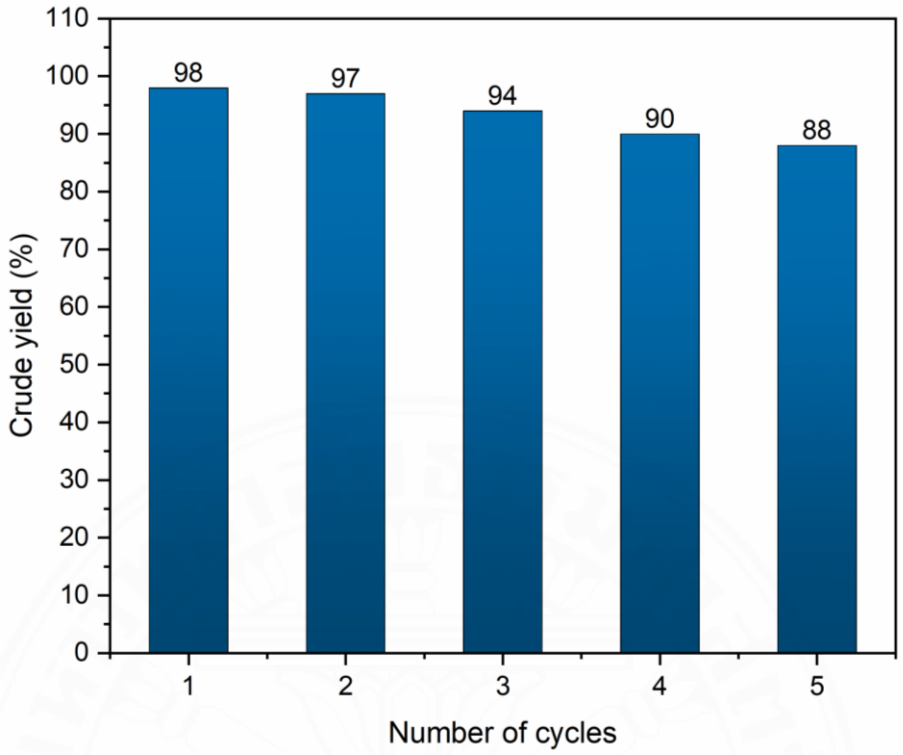

Figure 4.43 Overall yield of cycloadduct (**5a**) and ene-product (**6a**) using the recovered heterogeneous catalyst (**3**)[a]

4.6.3 The stability of the catalyst

The stability of the catalyst was analyzed by powder X-ray diffraction and IR spectroscopy (Appendices C). The PXRD patterns of the catalyst after the eighth cycle compared with as-synthesized and simulated, as shown in Figure 4.44. The PXRD pattern of the catalyst after the eighth cycle in the red line closely matches the as-synthesized catalyst in the blue line and the simulated pattern in the back line from single-crystal X-ray diffraction data, confirming the high stability and reuse ability of the catalyst.

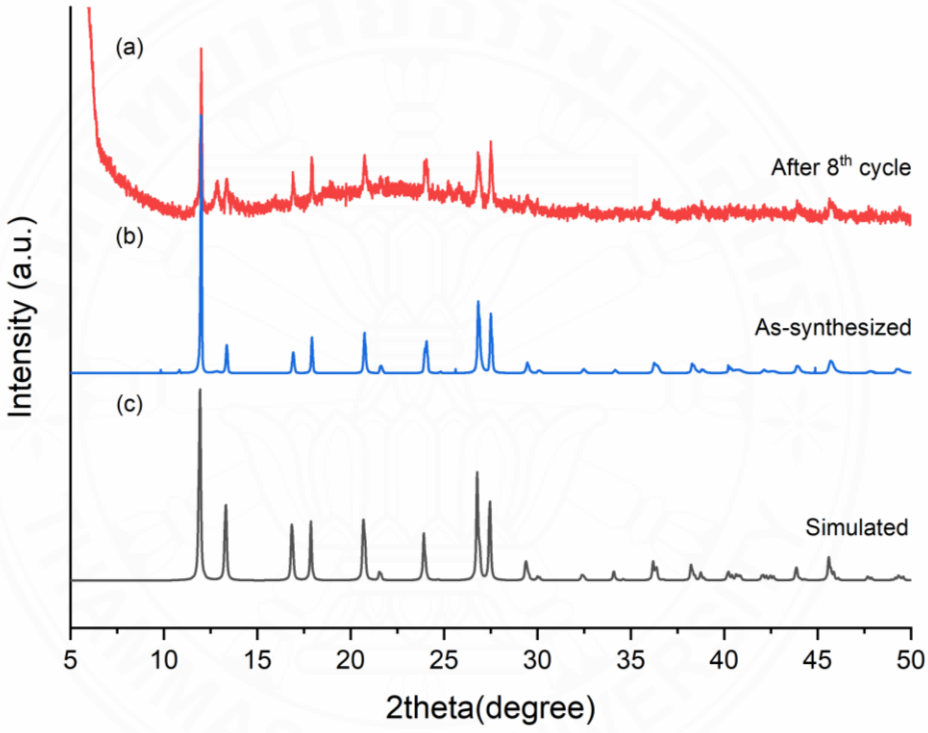

Figure 4.44 The powder X-ray diffraction patterns of (a) after 8th cycles, (b) as synthesized and (c) simulated of complex **3**

4.6.4 Proposed reaction mechanism

The possible aerobic oxidation reaction mechanism in this work was proposed and presented in Scheme 4.3. The ethyl oxazoline (**2a**) coordinates to the Cu(II) metal center of the complex **3** to stabilize the [Cu(dpyam)(2-OHbenz)(Cl)(EtOx)] intermediate, (**I**). Then, it was oxidized to the dioxo radical intermediate (**II**) under O_2 in the air. The hydroxamic acid (**1a**) was added to afford Cu(II)-hydroperoxo intermediate (**III**), giving nitroso compound (**3a**) and H_2O_2. Then, the intermediate (**III**) returned to be an intermediate (**I**) in the cycle again. Meanwhile, nitroso compound (**3a**) reacts with 2,3-dimethyl-1,3-butadiene (**4a**) through the Nitroso-Diels-Alder reaction and the Nitroso-ene reaction, resulting the mixed cycloadduct (**5a**) and ene-product (**6a**).

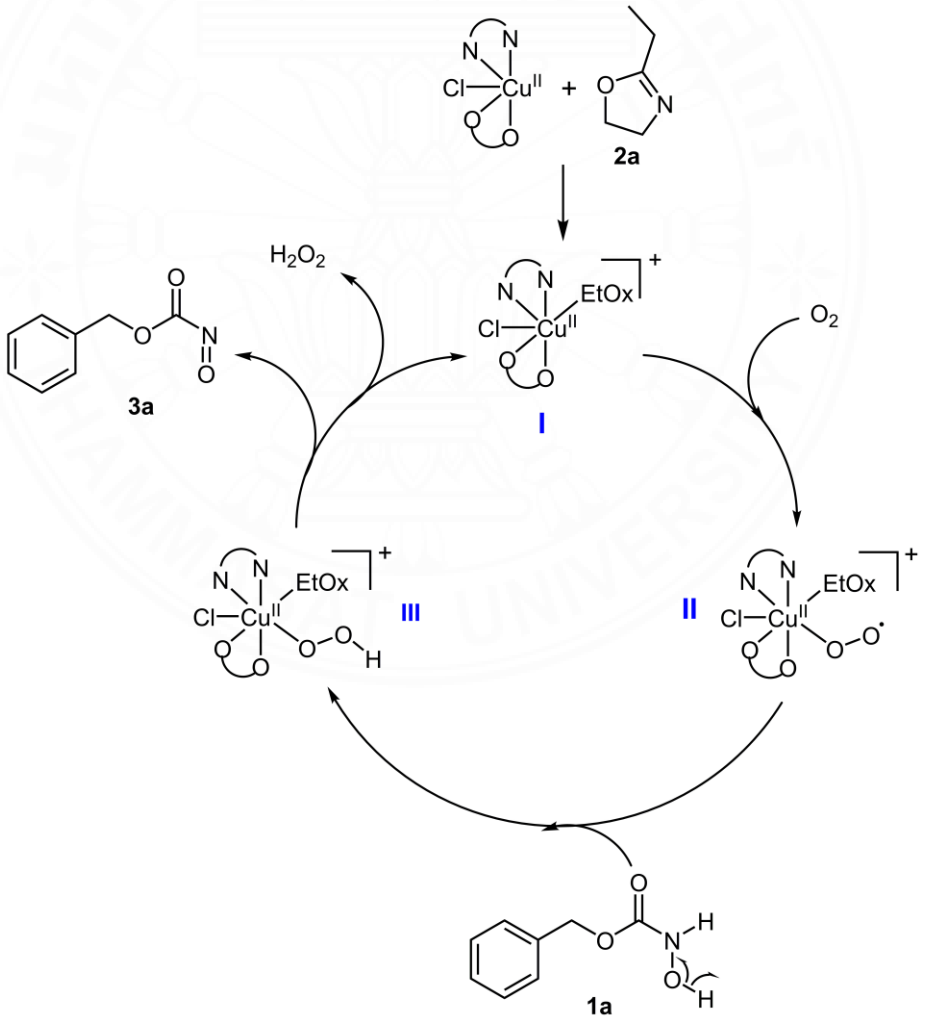

Scheme 4.3 Proposed mechanism for the aerobic oxidation in this work

4.6.5 Discussion of transition metal-catalyzed oxidation reactions of hydroxamic acids

In 2001 and 2002, the transition metal complexes were used as homogeneous catalysts in the aerobic oxidation reactions of hydroxamic acid [83-86] namely, $[RuCl_2(PPh)_4]$, [Ru(pybox-dh)(pydic)], $[Ir(cod)_2Cl]_2$, $[Ir(coe)_2Cl]_2$, $[Ru(salen)(PPh_3)_2]$, and $[RuCl_2(PPh_3)_4]$ (PPh = triphenylphosphine, pybox-dh = 2,6-bis(oxazolinyl)pyridine, pydic = pyridine-2,6-dicarboxylate, cod = cyclooctadiene, coe = cyclooctene, and salen = *N*,*N*′-bis-(salicylidene)ethylenediamine). These reactions were performed by using ^tBuOOH, 30% H_2O_2, and KOH as the oxidants in different solvents at low temperatures (0 °C) to room temperature. The results showed that the yields of cycloadducts were obtained ranging from 60 to 97%. In 2008 and 2011, there are the previous works reported the studies of oxidation reaction of hydroxamic acid by using Cu(I), Cu(II), and Fe(III) salts as the homogeneous catalyst with ^tBuOOH and 30% H_2O_2 in different solvents at room temperature. The results showed that yields of cycloadducts were obtained ranging from 75 to 95%.

For this research, we have designed and developed the molecular structure of new mononuclear Cu(II) complexes to be the heterogeneous catalyst for the aerobic oxidation reactions. The mononuclear Cu(II) complexes in a series **II** presented catalytic properties better than that of a series **I** because their structures contain the Cu(II) active site of the square pyramidal geometry. While the mononuclear Cu(II) complexes with the octahedral geometry in a series **I** present the steric effect from ligands. Regarding the previous works in Table 4.24, it is the first report that the heterogeneous catalysts have been used in this oxidation reaction of hydroxamic acids. In addition, this reaction could be taken place by using the air as an oxidant in THF solvent at room temperature, which reduced costs, energy, and environmentally friendly. Interestingly, the catalyst (**3**), [Cu(dpyam)(2-OHbenz)Cl] showed the best catalytic performance, and it can be reused at least five times.

Table 4.24. Summary of previously reported transition metal-catalyzed oxidation of a hydroxamic acid within *situ* Diels–Alder Trapping of the acyl nitroso derivative

Year	Catalyst	Type of complex	Geometry	Type of catalyst	Reaction					[Ref]
					Oxidant	Solvent	Temp.	Time (h)	Yield (%)	
2001	$[RuCl_2(PPh)_4]$	Mononuclear	Oct.	Homogeneous	^tBuOOH	DCM	rt	72	69	[85]
2001	[Ru(pybox-dh)(pydic)]	Mononuclear	Oct.	Homogeneous	30% H_2O_2	MeOH/H_2O	0°-rt	2	90	[86]
2002	$[Ir(cod)_2Cl]_2$	Dinuclear	Sq. Planar	Homogeneous	KOH	THF	0°-rt	-	74	[83]
	$[Ir(coe)_2Cl]_2$	Dinuclear	Sq. Planar	Homogeneous	air	THF	0°-rt	20	97	[83]
2002	$[Ru(salen)(PPh_3)_2]$	Mononuclear	Oct.	Homogeneous	^tBuOOH	DCM	rt	1	81	[84]
	$[RuCl_2(PPh_3)_4]$	Mononuclear	Oct.	Homogeneous	^tBuOOH	DCM	rt	0.5	60	[84]
2008	CuCl with ea	-	-	Homogeneous	30% H_2O_2	THF	rt	3	95	[88]
	$CuCl_2$ with ea	-	-	Homogeneous	30% H_2O_2	THF	rt	0.5	95	[88]
	$FeCl_3$ with en	-	-	Homogeneous	30% H_2O_2	DCM	rt	0.5	76	[88]
2011	CuCl with pyridine	-	-	Homogeneous	air	THF	rt	5-14	93	[42]
	$CuCl_2$ with EtOx	-	-	Homogeneous	air	MeOH	rt	2	85	[43]
	$CuCl_2$ with EtOx	-	-	Homogeneous	air	$CHCl_3$	rt	24	75	[43]
2023	$[Cu(dpyam)(4\text{-}OHbenz)_2]\cdot H_2O$ (**2**)	Mononuclear	Sq. Planar	Homogeneous	air	THF	rt	67	93	This work
	[Cu(dpyam)(2-OHbenz)Cl] (**3**)	Mononuclear	Sq. Py.	Heterogeneous	air	THF	rt	6.5	98	
	[Cu(dpyam)(3-OHbenz)Cl] (**4**)	Mononuclear	Sq. Py.	Heterogeneous	air	THF	rt	25	82	
	[Cu(dpyam)(4-OHbenz)Cl] (**II**)	Mononuclear	Sq. Py.	Heterogeneous	air	THF	rt	19	91	

Abbreviation: cod = cyclooctadiene, coe = cyclooctene, pydic = pyridine-2,6-dicarboxylate, pybox-dh = 2,6-bis(oxazolinyl)pyridine, EtOx = 2-ethyl-2-oxazoline, en = ethylenediamine, ea = ethanolamine**,** 2,2′-dipyridylamine, benz = benzoate, 2-OHbenz = 2-hydroxybenzoate, 3-OHbenz = 3-hydroxybenzoate, and 4-OHbenz = 4-hydroxybenzoate.

CHAPTER 5
CONCLUSIONS AND RECOMMENDATIONS

5.1 Conclusions

In summary, two series of new mononuclear copper(II) complexes containing 2,2′-dipyridylamine (dpyam) and hydroxybenzoate derivative (x-OHbenz, x = 2, 3 and 4) ligands were successfully synthesized by using a slow evaporation method with a ratio of Cu(II) salt: dpyam: OHbenzH is 1:1:2 in a mixed solution of DI water, MeOH and DMF solvents. The result shows that four new mononuclear copper(II) complexes were obtained, series **I**: [Cu(dpyam)(x-OHbenz)$_2$] namely [Cu(dpyam) (3-OHbenz)(HCO_2)] (**1**) and [Cu(dpyam)(4-OHbenz)$_2$]·H_2O (**2**) and series **II**: [Cu(dpyam)(x-OHbenz)Cl], when x = 2-OHbenz (**3**) and 3-OHbenz (**4**). All complexes were fully characterized by using FT-IR, UV-vis, solid-state diffuse reflectance spectroscopy, CHN elemental analysis, TGA and PXRD. All molecular structures of complexes were determined by using single-crystal X-ray diffraction. The molecular structure of complex **1** is distorted square-pyramidal with [CuN_2O_3] chromophore, corresponding to the τ_5 value of 0.19. While complex **2** shows a distorted square planar structure with [CuN_2O_2] chromophore, regarding τ_4 of 0.41. Complexes **3** and **4** are isostructural with a distorted square-pyramidal structure and [CuN_2O_2Cl] chromophore, the τ_5 values of 0.04 and 0.02, respectively. These new mononuclear copper(II) complexes are stabilized by various intermolecular interactions, such as hydrogen bonding, π–π and C–H···π intermolecular interactions. These supramolecular interactions were quantified by using Hirshfeld surface analysis (d_{norm}) and two-dimensional fingerprint plot to support the crystal structure data from single-crystal X-ray diffraction analysis.

As the results of the synthetic part, complex **1** could not be reproduced sufficiently for further physical properties and catalytic activity studies. Meanwhile, the physical properties of complexes **2**, **3** and **4** were investigated. It was found that complexes **3** and **4** are insoluble in the THF solution confirmed by UV-vis technique.

For TG analysis, the results showed that these complexes are thermally stable up to 245-265 °C, which are thermally stable enough for catalytic study.

The study of catalytic properties of complexes **2-4** for aerobic oxidation of hydroxamic acids were performed by using the following optimized conditions, *N*-(benzyloxy-carbonyl)hydroxylamine (**1a**) (0.5982 mmol) was reacted with 2-ethyl-2-oxazoline (**2a**) (0.12 mmol) and 2,3-dimethyl-1,3-butadiene (**4a**) in THF solution with 10 mol% of a heterogeneous catalyst at room temperature to produce cycloadduct (**5a**) and ene-product (**6a**), as shown in Scheme 5.1. The results showed that complex **2** is a homogeneous catalyst with a very long complete reaction time (67 h). So, complex **2** is not a suitable catalyst. To improve the catalytic properties, the new mononuclear ternary Cu(II) complexes in a series **II**, complexes **3** and **4** were designed with a square-pyramidal geometry to increase the active site and synthesized by using the same method as complexes in series **I**, except $CuCl_2 \cdot 2H_2O$ as the reactant. Both complexes could be presented as heterogeneous catalysts with efficient catalytic performance. Interestingly, complex **3** showed the most catalytic efficiency with the complete reaction time within 6.5 hours, and the overall yield of the cycloadduct (**5a**) and ene-product (**6a**) is up to 98%. Moreover, this catalyst can be reused for at least five cycles with the overall yield (%) range of 88 to 98 and the TOF value of 15.29 h^{-1}. The reaction mechanism was also proposed in this research.

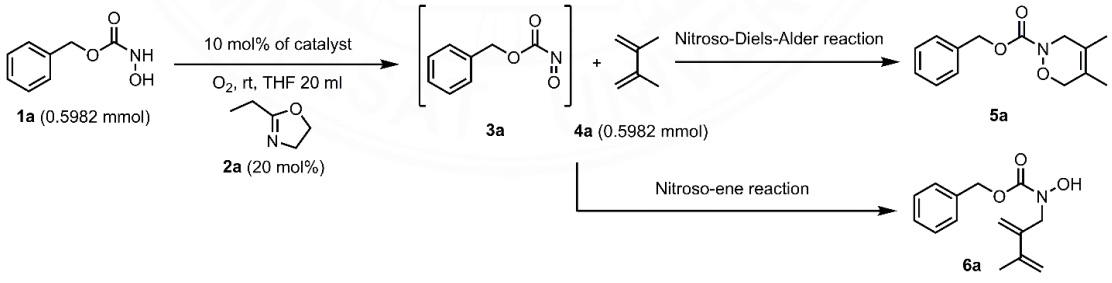

Scheme 5.1 The representation of the optimization conditions for the aerobic oxidation reaction of hydroxamic acid in this work

5.2 Recommendations

Regarding the catalytic study in this thesis, to improve the performance of new catalytic ternary mononuclear Cu(II) complexes in a series **II**, [Cu(dpyam)(x-OHbenz)Cl] by replacing the chloride ligand with bromide and iodide (Figure 5.1) has been recommended. Because these halides could be the good leaving group and enhance the *trans* effect series in the catalytic reaction, these halides are widely used as efficient catalysts for organic reactions.

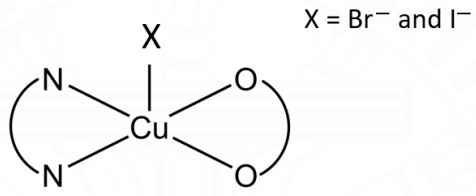

Figure 5.1 The proposed structures of the designed ternary mononuclear Cu(II) complexes

In addition, the proposed mechanism of the aerobic oxidation of hydroxamic acid in this work should be confirmed by using theoretical calculation such as the density functional theory (DFT) calculation [89].

REFERENCES

[1] Huang, K. B., Chen, Z. F., Liu, Y. C., Xie, X. L. & Liang, H. (2015). Dihydroisoquinoline copper (II) complexes: Crystal structures, cytotoxicity, and action mechanism. *RSC advances*, *5*(99), 81313-81323.

[2] Venkateswarlu, K., Anantha Lakshmi, P. V. & Shivaraj. (2022). Synthesis, spectroscopic and thermal studies of Cu^{+2}, Ni^{+2} and Co^{+3} complexes of Schiff base containing furan moiety. Antitumor, antioxidant, antibacterial and DNA interaction studies. *Applied Organometallic Chemistry*, *36*(2), e6530.

[3] Kacar, S., Unver, H. & Sahinturk, V. (2020). A mononuclear copper (II) complex containing benzimidazole and pyridyl ligands: Synthesis, characterization, and antiproliferative activity against human cancer cells. *Arabian Journal of Chemistry*, *13*(2), 4310-4323.

[4] Kumar, M., Mogha, N. K., Kumar, G., Hussain, F. & Masram, D. T. (2019). Biological evaluation of copper (II) complex with nalidixic acid and 2, 2′-bipyridine (bpy). *Inorganica Chimica Acta*, 490, 144-154.

[5] Silva, T. F. & Martins, L. M. (2020). Recent advances in copper catalyzed alcohol oxidation in homogeneous medium. *Molecules*, *25*(3), 748.

[6] Boča, R., Rajnák, C., Titiš, J. & Valigura, D. (2017). Field supported slow magnetic relaxation in a mononuclear Cu (II) complex. *Inorganic Chemistry*, *56*(3), 1478-1482.

[7] Santana, F. S., Briganti, M., Cassaro, R. A. A., Totti, F., Ribeiro, R. R., Hughes, D. L. & Reis, D. M. (2020). An oxalate-bridged copper (II) complex combining monodentate benzoate, 2,2′-bipyridine and aqua ligands: Synthesis, crystal structure and investigation of magnetic properties. *Molecules*, *25*(8), 1898.

[8] Fukuzumi, S., Kotani, H., Lucas, H. R., Doi, K., Suenobu, T., Peterson, R. L. & Karlin, K. D. (2010). Mononuclear copper complex-catalyzed four-electron reduction of oxygen. *Journal of the American Chemical Society*, *132*(20), 6874-6875.

[9] Santini, C., Pellei, M., Gandin, V., Porchia, M., Tisato, F. & Marzano, C. (2014). Advances in copper complexes as anticancer agents. *Chemical reviews*, *114*(1), 815-862.

[10] Phiokliang, P., Promwit, P., Chainok, K. & Wannarit, N. (2019). Crystal structure and Hirshfeld surface analysis of bis (benzoato-κ^2O, O')[bis (pyridin-2-yl-κN) amine] nickel (II). *Acta Crystallographica Section E: Crystallographic Communications*, *75*(9), 1301-1305.

[11] Ziyaev, M. A., Ashurov, J. M., Eshimbetov, A. G. & Ibragimov, B. T. (2021). Crystal structure, Hirshfeld surface analysis and DFT studies of tetrakis (μ-3-nitrobenzoato-κ^2O1:$O1'$)bis[(*N*,*N*-dimethylformamide-κO)copper(II)]dimethyl-formamide disolvate. *Acta Crystallographica Section E: Crystallographic Communications*, *77*(11), 1164-1169.

[12] Das, G., Shukla, R., Mandal, S., Singh, R., Bharadwaj, P. K., van Hall, J. & Whitmire, K. H. (1997). Syntheses and X-ray structures of mixed-ligand salicylaldehyde complexes of Mn (III), Fe (III), and Cu (II) ions: Reactivity of the Mn (III) complex toward primary monoamines and catalytic epoxidation of olefins by the Cu (II) complex. *Inorganic Chemistry*, *36*(3), 323-329.

[13] Nairn, A. K., Archibald, S. J., Bhalla, R., Gilbert, B. C., MacLean, E. J., Teat, S. J. & Walton, P. H. (2006). (N-Benzyl-bis-*N′, N″*-salicylidene)-cis-1, 3, 5-triaminocyclohexane copper (ii): a novel catalyst for the aerobic oxidation of benzyl alcohol. *Dalton Transactions*, (1), 172-176.

[14] Alaji, Z., Safaei, E., Chiang, L., Clarke, R. M., Mu, C. & Storr, T. (2014). A Copper Complex of a Noninnocent Iminophenol-Amidopyridine Hybrid Ligand: Synthesis, Characterization, and Aerobic Alcohol Oxidation. *European Journal of Inorganic Chemistry*, *2014*(35), 6066-6074.

[15] John, A., Katiyar, V., Pang, K., Shaikh, M. M., Nanavati, H. & Ghosh, P. (2007). Ni (II) and Cu (II) complexes of phenoxy-ketimine ligands: Synthesis, structures and their utility in bulk ring-opening polymerization (ROP) of L-lactide. *Polyhedron*, *26*(15), 4033-4044.

[16] Ranjan, R., Kundu, B. K., Kyarikwal, R., Ganguly, R. & Mukhopadhyay, S. (2022). Synthesis of Cu (II) complexes by N, O-donor ligand transformation and their catalytic role in visible-light-driven alcohol oxidation. *Applied Organometallic Chemistry*, *36*(1), e6450.

[17] Rajput, A. K. (2006). Coordination compounds. In Chemistry Part I Textbook for class XII (pp. 244-262). New Delhi: S.K. Offset (P.) Ltd.

[18] Subramanian, S., Rammaswamy, N. & Kartha, B. (2015). Synthesis of mononuclear Schiff base Cu (II), Ni (II), Co (II) and Mn (II) complexes and their application for DNA cleavage and antibacterial agent. *Chem. Sci. Rev. Lett*, *14*(13), 121-128.

[19] Louis, B., Detoni, C., Carvalho, N. M. F., Duarte, C. D. & Antunes, O. A. C. (2009). Cu (II) bipyridine and phenantroline complexes: Tailor-made catalysts for the selective oxidation of tetralin. *Applied Catalysis A: General*, *360*(2), 218-225.

[20] Kunishita, A., Kubo, M., Sugimoto, H., Ogura, T., Sato, K., Takui, T. & Itoh, S. (2009). Mononuclear copper (II)−superoxo complexes that mimic the structure and reactivity of the active centers of PHM and DβM. *Journal of the American Chemical Society*, *131*(8), 2788-2789.

[21] Samanta, S., Das, S., Samanta, P. K., Dutta, S. & Biswas, P. (2013). A mononuclear copper (II) complex immobilized in mesoporous silica: An efficient heterogeneous catalyst for the aerobic oxidation of benzylic alcohols. *RSC advances*, *3*(42), 19455-19466.

[22] Brogden, D. W. & Berry, J. F. (2016). Coordination chemistry of 2,2′-Dipyridylamine: the gift that keeps on giving. *Comments on Inorganic Chemistry*, *36*(1), 17-37.

[23] Vlachos, A., Psycharis, V., Raptopoulou, C. P., Lalioti, N., Sanakis, Y., Diamantopoulos, G. & Terzis, A. (2004). A nearly symmetric trinuclear chromium (III) oxo carboxylate assembly: preparation, molecular and crystal structure, and magnetic properties of $[Cr_3O(O_2CPh)_6(MeOH)_3](NO_3)\cdot 2MeOH$. *Inorganica chimica acta*, *357*(11), 3162-3172.

[24] Hökelek, T., Özkaya, S. & Necefoğlu, H. (2018). Crystal structure and Hirshfeld surface analysis of diaquabis (N, N-diethylnicotinamide-*κN1*) bis (2, 4, 6-trimethylbenzoato-*κO*) manganese (II). *Acta Crystallographica Section E: Crystallographic Communications*, *74*(4), 422-427.

[25] Paul, P., Roy, S., Sarkar, S., Chowdhury, S., Purkayastha, R. D., Raghavaiah, P. & Devi, S. I. (2015). Synthesis, structure and some properties of a manganese (II) benzoate containing diimine. *Journal of Molecular Structure*, 1102, 153-160.

[26] Hagadorn, J. R., Que, L. & Tolman, W. B. (2000). N-donor effects on carboxylate binding in mononuclear iron (II) complexes of a sterically hindered benzoate ligand. *Inorganic chemistry*, *39*(26), 6086-6090.

[27] Karmakar, A., Sarma, R. J. & Baruah, J. B. (2007). Synthesis and characterisation of dinuclear and mononuclear Cobalt (II) benzoate complexes. *Polyhedron*, *26*(6), 1347-1355.

[28] Kounavi, K. A., Manos, M. J., Tasiopoulos, A. J., Perlepes, S. P. & Nastopoulos, V. (2010). Zinc (II) and Nickel (II) Benzoate Complexes from the Use of 1-methyl-4,5-diphenylimidazole. *Bioinorganic Chemistry and Applications*, 2010.

[29] Solera-Rojas, J. A., Krause, L., Montero, M. L., Stalke, D. & Pineda, L. W. (2018). Synthesis and Crystal Structure of a Copper (II) Benzoate Complex Bearing a Bis-2, 2′-Tetrahydrofuryl Peroxide Moiety. *Journal of Chemical Crystallography*, 48, 138-144.

[30] Jiang, J., Li, J., Liu, C., Liu, R., Liang, X., Zhou, Y. & Ma, Z. (2020). Study on the substitution effects of zinc benzoate terpyridine complexes on photoluminescence, antiproliferative potential and DNA binding properties. *JBIC Journal of Biological Inorganic Chemistry*, 25, 311-324.

[31] Rao, C. N. R., Natarajan, S. & Vaidhyanathan, R. (2004). Metal carboxylates with open architectures. *Angewandte Chemie International Edition*, *43*(12), 1466-1496.

[32] Lin, H. H., Wei, H. H., Lee, G. H. & Wang, Y. (2001). Structure and magnetic properties of copper (II) carboxylate with pyridyl-substituted nitronyl nitroxides. *Polyhedron*, *20*(26-27), 3057-3063.

[33] Jagličić, Z., Šegedin, P., Zlatič, J., Zorko, A., Pirnat, J. & Trontelj, Z. (2007). Magetic interactions in a new copper (II) carboxylate complex. *Journal of magnetism and magnetic materials*, 310(2), 1444-1446.

[34] Sun, J., Sun, F., Tang, J., Tang, X., Wu, Q., Huo, R. & Shen, H. (2023). Carboxylate engineering for manipulating the optical and assembly properties of copper clusters. *Inorganic Chemistry Frontiers*, *10*(9), 2618-2625.

[35] Saxena, P. & Thirupathi, N. (2015). Reactions of $Cd(OAc)_2 \cdot 2H_2O$ with variously substituted pyridines. Efforts to unravel the factors that determine structure/nuclearity of the products. *Polyhedron*, 98, 238-250.

[36] Bodnar, B. S. & Miller, M. J. (2011). The Nitrosocarbonyl Hetero-Diels–Alder Reaction as a Useful Tool for Organic Syntheses. *Angewandte Chemie International Edition*, *50*(25), 5630-5647.

[37] Youngme, S., Chaichit, N. & Damnatara, K. (2002). The coordination chemistry of dinitrato-di-2-pyridylamine copper (II). Crystal structures of catena-poly[(di-2-pyridylamine)(nitrato-*O,O′*)copper(II)]-μ-nitrato-*O*:*O′*] and bis (nitrato-*O,O′*)(di-2-pyridylamine)copper(II) dihydrate. *Polyhedron*, *21* (9-10), 943-950.

[38] Okabe, N., Tsuji, A. & Yodoshi, M. (2007). (Benzoato-κ2O, O′) chlorido (di-2-pyridylamine-κ2N, N′) copper (II). *Acta Crystallographica Section E: Structure Reports Online*, *63*(6), m1756-m1757.

[39] Okabe, N., Tsuji, A. & Yodoshi, M. (2007). Chlorido (di-2-pyridylamine-κ^2*N, N′*)(4-nitrobenzoato-κ^2*O, O′*) copper (II). *Acta Crystallographica Section E: Structure Reports Online*, *63*(8), m2162-m2162.

[40] Wang, Y. & Okabe, N. (2005). Synthesis, structures, and DNA binding of ternary transition metal complexes M(II) L with the 2,2′-bipyridylamine (L = *p*-HB, M= Co, Ni, Cu and Zn). *Inorganica chimica acta*, *358*(12), 3407-3416.

[41] Wang, Y., Lin, G., Hong, J., Lu, T., Li, L., Okabe, N. & Odoko, M. (2009). Synthesis, structures, and DNA binding of ternary transition metal complexes M(II)L with the 2,2′-bipyridylamine (L= p-aminobenzenecarboxylic acid, M= Ni, Cu and Zn*). Inorganica Chimica Acta*, *362*(2), 377-384.

[42] Frazier, C. P., Engelking, J. R. & Read de Alaniz, J. (2011). Copper-catalyzed aerobic oxidation of hydroxamic acids leads to a mild and versatile acylnitroso ene reaction. *Journal of the American Chemical Society*, *133*(27), 10430-10433.

[43] Chaiyaveij, D., Cleary, L., Batsanov, A. S., Marder, T. B., Shea, K. J. & Whiting, A. (2011). Copper(II)-Catalyzed Room Temperature Aerobic Oxidation of Hydroxamic Acids and Hydrazides to Acyl-Nitroso and Azo Intermediates, and Their Diels–Alder Trapping. *Organic Letters*, *13*(13), 3442-3445.

[44] Flower, K. R., Lightfoot, A. P., Wan, H. & Whiting, A. (2002). The development and application of ruthenium catalysed oxidations of a hydroxamic acid and in situ Diels–Alder trapping of the acyl nitroso derivative. *Journal of the Chemical Society*, *Perkin Transactions 1*, (18), 2058-2064.

[45] Yao, X., Qiu, M., Lü, W., Chen, H. & Zheng, Z. (2001). Substituted salen–Ru (II) complexes as catalysts in the asymmetric cyclopropanation of styrene by ethyl diazoacetate: the influence of substituents and achiral additives on activity and enantioselectivity. *Tetrahedron: Asymmetry*, 12(2), 197-204.

[46] Iwasa, S., Tajima, K., Tsushima, S. & Nishiyama, H. (2001). A mild oxidation method of hydroxamic acids: efficient trapping of acyl nitroso intermediates. *Tetrahedron Letters*, 42(34), 5897-5899.

[47] Nishiyama, H. & Motoyama, Y. (1997). Novel ruthenium–pyridine-dicarboxylate complexes of terpyridine and chiral bis (oxazolinyl) pyridine: a new catalytic system for alkene epoxidation with [bis(acetoxy)iodo] benzene as an oxygen donor. *Chemical Communications*, (19), 1863-1864.

[48] Adamo, M. F. & Bruschi, S. (2007). Generation of acylnitroso dienophiles: a study of metal catalysis. *The Journal of Organic Chemistry*, 72(7), 2666-2669.

[49] Bruker (2016). APEX3 and SAINT. Bruker AXS Inc., Madison, Wisconsin, USA.

[50] Sheldrick, G. M. (2015a). Acta Cryst. A71, 3-8.

[51] Sheldrick, G. M. (2015b). Acta Cryst. C71, 3-8.

[52] Dolomanov, O. V., Bourhis, L. J., Gildea, R. J., Howard, J. A. K. & Puschmann, H. (2009). *J. Appl. Crystallogr*. 42(2), 339-341.

[53] Huang, G., Yang, P., Wang, N., Wu, J. Z. & Yu, Y. (2012). First lanthanide coordination polymers with *N, N*-dimethylformamide hydrolysis induced formate ligands. *Inorganica Chimica Acta*, 384, 333-339.

[54] Bovill, S. M., Dixey, R. J. & Saines, P. J. (2017). Three coordination frameworks with copper formate based low dimensional motifs: synthesis, structure and magnetic properties. *CrystEngComm*, 19(13), 1831-1838.

[55] Addison, A. W., Rao, T. N., Reedijk, J., van Rijn, J. & Verschoor, G. C. (1984). Synthesis, structure, and spectroscopic properties of copper (II) compounds containing nitrogen–sulphur donor ligands; the crystal and molecular structure of aqua [1,7-bis(N-methylbenzimidazol-2′-yl)-2,6-dithiaheptane]copper(II) perchlorate. Journal of the Chemical Society, *Dalton Transactions*, (7), 1349-1356.

[56] Brophy, M., Murphy, G., Osullivan, C., Hathaway, B. & Murphy, B. (1999). The range in static stereochemistry of the cation distortion isomers of the $[Cu\ (chelate)_2Cl]^+$ cation, where chelate = bipy, phen or bipyam. The low temperature crystal structure (150 K) of $[Cu(bipy)_2Cl][PF_6]\cdot H_2O$ and $[Cu(phen)_2Cl][BPh_4]$. *Polyhedron*, *18*(5), 611-615.

[57] Mao, H. Y., Shen, X. Q., Li, G., Zhang, H. Y., Xu, C., Liu, H. L. & Zhu, Y. (2004). Novel hydrogen-bonded and π–π interaction networks generated from the reaction of copper (II) chloride hydrates with heterocyclic diimines (2,2′-bipyridine, 1,10-phenanthroline) and bidentate diamine(ethylenediamine). *Polyhedron*, *23*(11), 1961-1967.

[58] Zhu, W. G., Lin, C. J., Zheng, Y. Q. & Zhu, H. L. (2016). Two dinuclear copper (II) coordination polymers constructed from *m*-hydroxybenzoic acid and *N*-donor ligands: synthesis, crystal structures, and magnetic properties. *Transition Metal Chemistry*, 41, 87-96.

[59] Chattopadhyay, P. & Sinha, C. (1997). Synthesis and Spectroscopic Studies of 2, 2-Dipyridylamine Complexes of La(III), Ce(III), Pr(III), Th(IV), UO_2(VI) and a Peroxo Derivative of UO_2(VI). *Synthesis and Reactivity in Inorganic and Metal-Organic Chemistry*, *27*(7), 997-1007.

[60] Gusrizal, G., Santosa, S. J., Kunarti, E. S. & Rusdiarso, B. A. M. B. A. N. G. (2017). Synthesis of silver nanoparticles by reduction of silver ion with *m*-hydroxybenzoic acid. *Asian Journal of Chemistry*, *29*(7), 1417-1422

[61] Darensbourg, D. J., Fischer, M. B., Schmidt Jr, R. E. & Baldwin, B. J. (1981). Formate ion as a monodentate ligand. Synthesis, structure, and decarboxylation of (eta. 5-cyclopentadienyl)dicarbonyl(formato) iron. *Journal of the American Chemical Society*, *103*(5), 1297-1298.

[62] Saini, A., Sharma, R. P., Kumar, S., Venugopalan, P., Gubanov, A. I. & Smolentsev, A. I. (2015). Two new isomeric copper (II) complexes: Syntheses, spectroscopic characterization, single-crystal X-ray structure determination and packing analyses of [Cu(L1/L2)$_2$(TEMED)], where L1= 4-chloro-2-nitrobenzoate, L2 = 5-chloro-2-nitrobenzoate and TEMED= *N,N,N′,N′*-tetra-methylethylenediamine. *Polyhedron*, 100, 155-163.

[63] Szymańska, I. B., Madajska, K., Butrymowicz, A. & Barwiołek, M. (2021). Copper(II) Perfluorinated Carboxylate Complexes with Small Aliphatic Amines as Universal Precursors for Nanomaterial Fabrication. *Materials*, *14*(23), 7451.

[64] Adams, D. M. & Lock, P. J. (1967). Copper-halogen stretching frequencies. *Journal of the Chemical Society A: Inorganic, Physical, Theoretical*, 620-623.

[65] Hathaway, B. & Billing, D. E. (1970). The electronic properties and stereochemistry of mono-nuclear complexes of the copper(II) ion. *Coordination Chemistry Reviews*, *5*(2), 143-207.

[66] Kasumov, V. T., Bulut, A., Köksal, F., Aslanogˇlu, M., Uçar, İ. & Kazak, C. (2006). Synthesis, structure, spectroscopic and redox properties of copper(II)-N-3,5-Bu2tphenylsalicylaldinine complexes: Crystal and molecular structure of bis (N-3, 5-Bu2t-phenylsalicylaldininato) copper (II). *Polyhedron*, *25*(5), 1133-1141.

[67] Emsley, J., Ernst, R. D., Hathaway, B. J., Warren, K. D. & Hathaway, B. J. (1984). A new look at the stereochemistry and electronic properties of complexes of the copper(II) ion. *In Complex Chemistry* (pp. 55-118). Springer Berlin Heidelberg.

[68] Cheansirisomboon, A., Youngme, S., Danvirutai, C., Chaichit, N. & Pakawatchai, C. (2008). Synthesis, X-ray Structures and Spectroscopic Characterization of Five New Polynuclear Paddle-wheel Cu(II) Complexes Containing Carboxylate as a bridging ligand. *KKU Research Journal (Graduate Studies)*, *8*(1), 25-35.

[69] Chandraleka, S. & Chandramohan, G. (2014). Synthesis, characterization and thermal analysis of the copper (II) complexes with 2,2'-bipyridyl and 1,10-phenanthroline. *African J Pure Appl Chem 2014*; 8: 162, 175.

[70] McKinnon, J. J., Jayatilaka, D. & Spackman, M. A. (2007). Towards quantitative analysis of intermolecular interactions with Hirshfeld surfaces. *Chemical Communications*, (37), 3814-3816.

[71] Spackman, M. A. & McKinnon, J. J. (2002). Fingerprinting intermolecular interactions in molecular crystals. *CrystEngComm*, *4*(66), 378-392.

[72] Turner, M. J., McKinnon, J. J., Wolff, S. K., Grimwood, D. J., Spackman, P. R., Jayatilaka, D. & Spackman, M. A. (2017). *CrystalExplorer17*. The University of Western Australia.

[73] Marais, L. & Swarts, A. J. (2019). *Catalysts*, 9(5), 395.

[74] Quadrelli, P., Mella, M. & Caramella, P. (1999). A photochemical generation of nitrosocarbonyl intermediates. *Tetrahedron letters*, *40*(4), 797-800.

[75] O'Bannon, P. E. & William, D. P. (1988). Rearrangement of nitrocarbenes to acyl nitroso compounds. *Tetrahedron letters*, *29*(45), 5719-5722.

[76] Corrie, J. E., Kirby, G. W. & Mackinnon, J. W. (1985). Reactions of transient C-nitrosocarbonyl compounds with dienes, mono-olefins, and nucleophiles. *Journal of the Chemical Society, Perkin Transactions 1*, 883-886.

[77] Quadrelli, P., Mella, M., Invernizzi, A. G. & Caramella, P. (1999). The mild oxidation of nitrile oxides affords a convenient entry to nitrosocarbonyl intermediates, versatile tools in organic syntheses. *Tetrahedron*, *55*(34), 10497-10510.

[78] Martin, S. F., Hartmann, M. & Josey, J. A. (1992). Diastereoselective [4+2] cycloadditions of acyl nitroso compounds. *Tetrahedron letters*, *33*(25), 3583-3586.

[79] Katritzky, A. R., Meth-Cohn, O. & Rees, C. W. (Eds.). (1995). *Comprehensive Organic Functional Group Transformations: Synthesis: carbon with one heteroatom attached by a single bond*. Elsevier.

[80] Dao, L. H., Dust, J. M., Mackay, D. & Watson, K. N. (1979). The formation and interconversion of oxazines and dioxazines from the reaction of nitrosocarbonyl compounds with cyclopentadienes. *Canadian Journal of Chemistry*, *57*(13), 1712-1719.

[81] Jenkins, N. E., Ware Jr, R. W., Atkinson, R. N. & King, S. B. (2000). Generation of acyl nitroso compounds by the oxidation of n-acyl hydroxylamines with the dessmartin periodinane. *Synthetic Communications*, *30*(5), 947-953.

[82] Howard, J. A., Ilyashenko, G., Sparkes, H. A. & Whiting, A. (2007). Development of new transition metal catalysts for the oxidation of a hydroxamic acid with in situ Diels–Alder trapping of the acyl nitroso derivative. *Dalton Transactions*, (21), 2108-2111.

[83] Iwasa, S., Fakhruddin, A., Tsukamoto, Y., Kameyama, M. & Nishiyama, H. (2002). Iridium(I)-catalyzed hydrogen peroxide oxidation of hydroxamic acids and hetero Diels–Alder reaction of the acyl nitroso intermediates with cyclopentadiene. *Tetrahedron letters*, 43(35), 6159-6161.

[84] Flower, K. R., Lightfoot, A. P., Wan, H. & Whiting, A. (2002). The development and application of ruthenium catalysed oxidations of a hydroxamic acid and in situ Diels–Alder trapping of the acyl nitroso derivative. *Journal of the Chemical Society, Perkin Transactions 1*, (18), 2058-2064.

[85] Flower, K. R., Lightfoot, A. P., Wan, H. & Whiting, A. (2001). Direct evidence for a ruthenium(iv) oxo complex-mediated oxidation of a hydroxamic acid in the presence of phosphine oxide donors. *Chemical Communications*, (18), 1812-1813.

[86] Iwasa, S., Tajima, K., Tsushima, S. & Nishiyama, H. (2001). A mild oxidation method of hydroxamic acids: efficient trapping of acyl nitroso intermediates. *Tetrahedron Letters*, 42(34), 5897-5899.

[87] Howard, J. A., Ilyashenko, G., Sparkes, H. A., Whiting, A. & Wright, A. R. (2008). Mechanistic Insights into Transition Metal-Catalysed Oxidation of a Hydroxamic Acid with in situ Diels–Alder Trapping of the Acyl Nitroso Derivative. *Advanced Synthesis & Catalysis*, *350*(6), 869-882.

[88] damo, M. F. & Bruschi, S. (2007). Generation of acylnitroso dienophiles: a study of metal catalysis. *The Journal of Organic Chemistry*, 72(7), 2666-2669.

[89] Cheng, L., Wang, J., Wang, M., & Wu, Z. (2010). Mechanistic insight into alcohol oxidation mediated by an efficient green Cu^{II}-bipy catalyst with and without TEMPO by density functional methods. *Dalton Transactions*, *39*(22), 5377-5387.

[90] Marais, L., & Swarts, A. J. (2019). Biomimetic Cu/Nitroxyl catalyst systems for selective alcohol oxidation. *Catalysts*, *9*(5), 395.

[91] Kacka-Zych, A., Mirosław, B., Wielgus, E., & Olszewska, A. (2022). Jasi nski, R. Green, one-pot synthesis of 1, 2-oxazine-type herbicides via non catalyzed Hetero Diels-Alder reactions comprising (2E)-3-aryl-2-nitroprop-2-ene nitriles. *J. Clean. Prod*, *356*, 131878.

APPENDICES

APPENDIX A
SYNTHESIS

Synthesis of mononuclear Cu(II) complex

Synthesis of [Cu(dpyam)(4-OHbenz)Cl] (II)

A blue solution of $Cu(Cl)_2 \cdot 2H_2O$ (0.1705 g, 1 mmol) in distilled water (10 mL) was heated at 65 ºC with continuous stirring. Next, a yellow solution of dpyam (0.1712 g, 1 mmol) in methanol (10 mL) was added, resulting in a clear green solution. After that, 4-OHbenzH (0.2762 g, 2 mmol) and sodium hydroxide (0.08 g, 2 mmol) in distilled water (10 mL) were added, resulting in the green precipitate. Then, DMF (9 mL), 1M HCl (3 ml), and DI water (5 ml) were added to dissolve the green precipitate, heated at 65°C, and continuously stirred for 30 minutes leading to a clear green solution. After that, the solution was filtrated. Finally, green block crystals were obtained after a stand at room temperature for 2 days and collected with a yield of 59.59% (286.10 mg based on Cu(II) salt).

Table A1. The appearance of the crystal of synthesized mononuclear Cu(II) complexes

Chemical formula	Crystals		%Yield (based on Cu(II) salt)	[Ref]
	Shape	Color		
[Cu(dpyam)(3-OHbenz)(HCO_2)] (**1**)	Plate	Green	10.09	This work
[Cu(dpyam)(4-OHbenz)$_2$]·H_2O (**2**)	Block	Dark Green	77.89	
[Cu(dpyam)(2-OHbenz)Cl] (**3**)	Block	Brown	73.77	
[Cu(dpyam)(3-OHbenz)Cl] (**4**)	Block	Green	59.59	
[Cu(dpyam)$_2$(NO_3)$_2$] (**I**)	Plate	Brown	36.21	[37]
[Cu(dpyam)(4-OHbenz)Cl] (**II**)	Block	Green	65.75	[40]

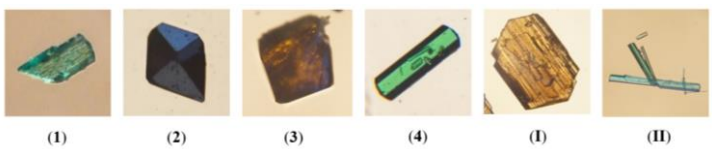

Figure A1. Single crystal of synthesized mononuclear Cu(II) complexes by Olympus BX50 microscope

APPENDIX B

SOLUBILITY TEST

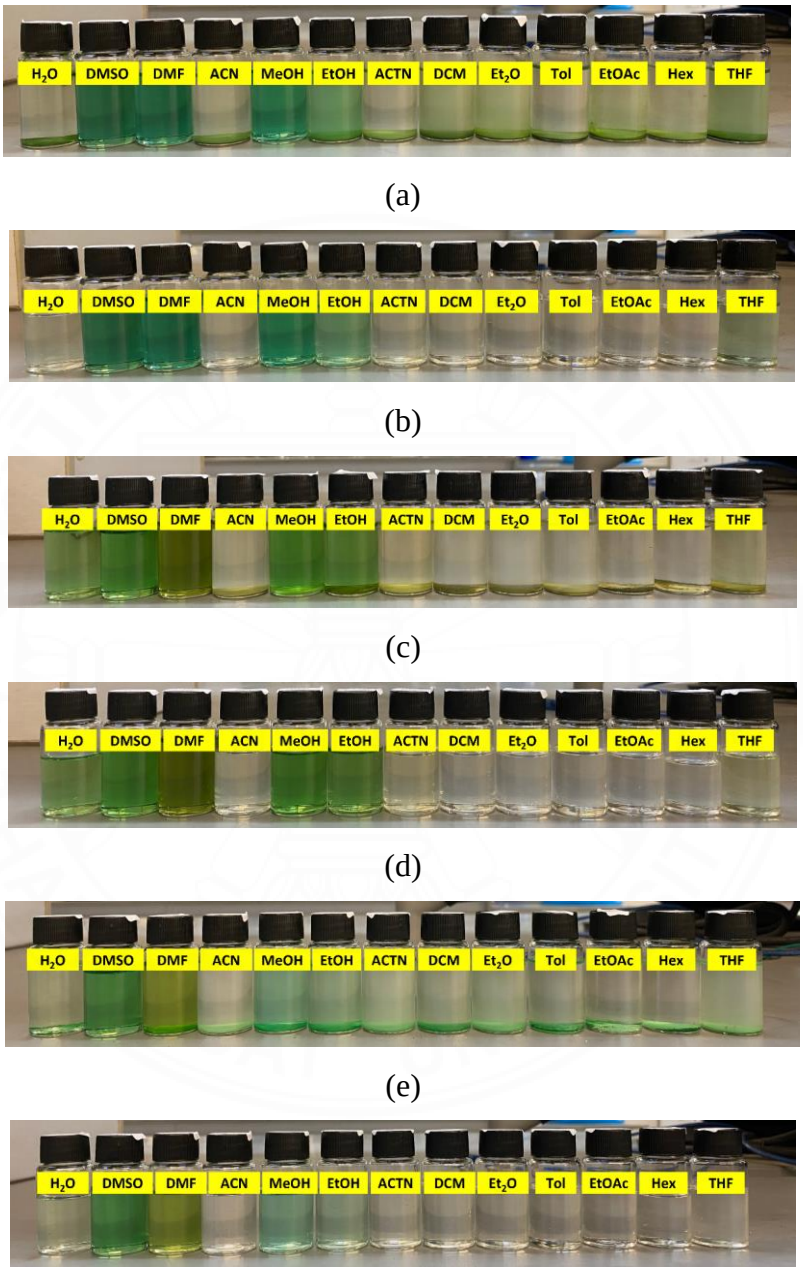

Figure B1. Solubility test in the various solvents (5×10^{-3} M) of complex **2**, (a) before and (b) after filtration at room temperature, (c) before and (d) after filtration at room temperature of complex **3**, (e) before and (f) after filtration at room temperature of complex **4**

Electron paramagnetic resonance spectroscopy

Generally, a Cu(II) ion has the [Ar] $3d^9$ electron configuration with an unpaired electron, which is paramagnetic and can induce magnetic properties. Cu(II) ions have g-values between 2.0 and 2.4, corresponding to the g-values of complexes in Figure 4.39. it is confirmed that the complex has Cu(II) ion.

The next issue to study, the physical properties of complexes **2**, **3**, and **4**, was investigated using the EPR technique. Only one peak was found in the EPR spectra of complexes **2**, **3**, and **4**, indicating no interference or interaction by another nucleus. Therefore, it confirmed that the complexes were insoluble in the THF solution.

(a)

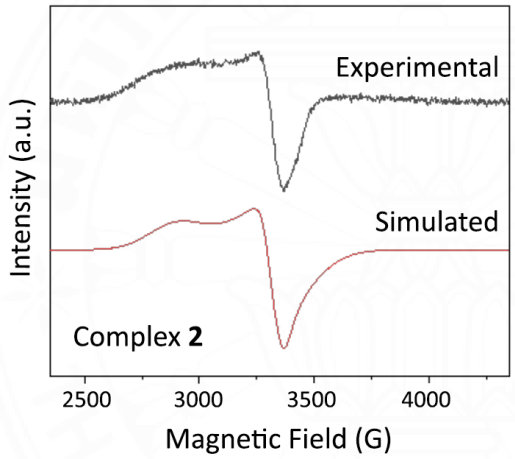

g-values
$g_x = 2.07$
$g_y = 2.03$
$g_z = 2.38$

(b)

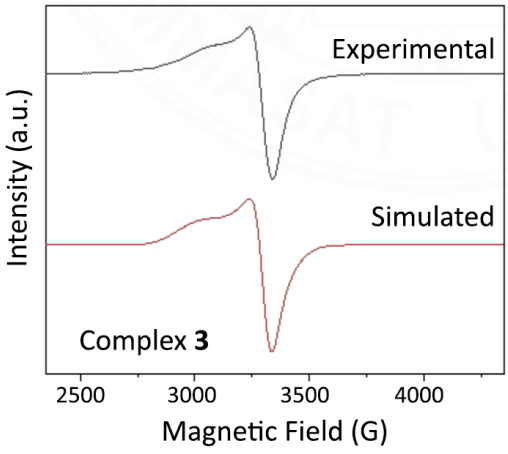

g-values
$g_x = 2.06$
$g_y = 2.08$
$g_z = 2.28$

Figure B2. The EPR spectra of (a) complex **2**, (b) complex **3** and (c) complex **4** in THF solution

(c)

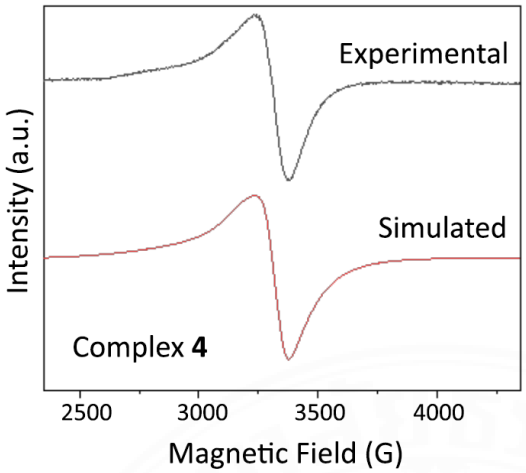

g-values

$g_x = 2.07$

$g_y = 2.09$

$g_z = 2.23$

Figure B2. The EPR spectra of (a) complex **2**, (b) complex **3** and (c) complex **4** in THF solution (cont.)

APPENDIX C
IR SPECTRA

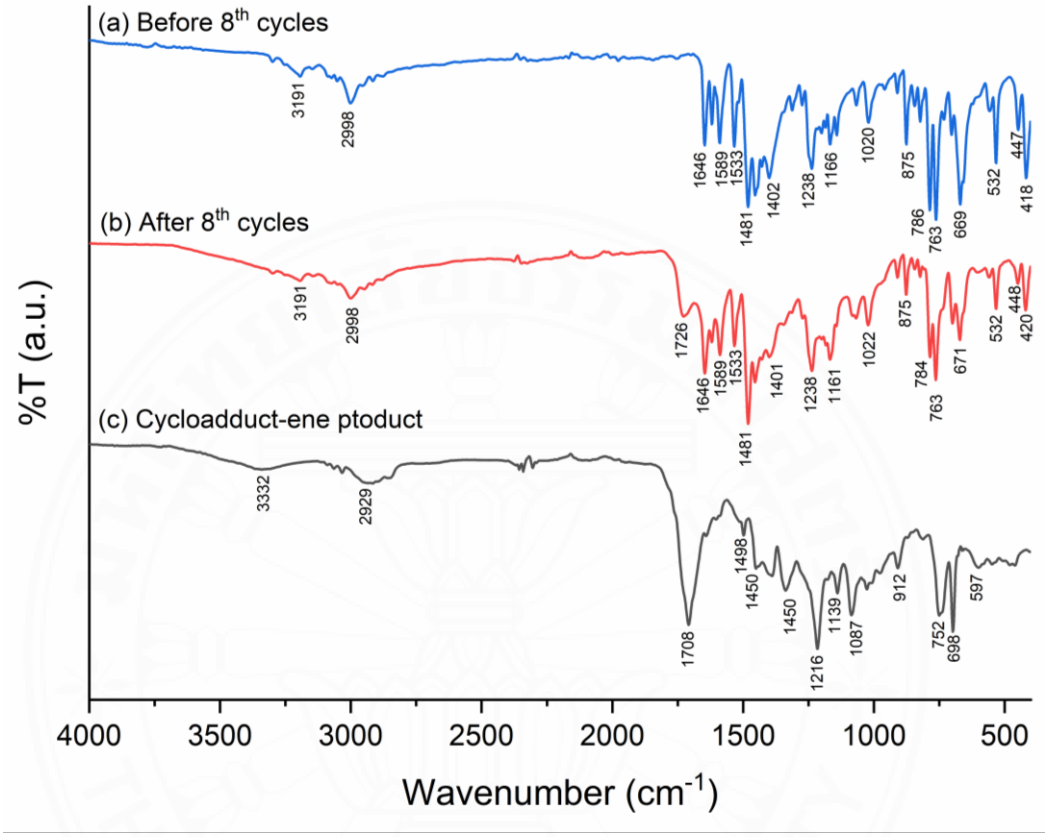

Figure C1. IR spectra of (a) before 8th cycles, (b) after 8th cycles and (c) cycloadduct-ene-product

APPENDIX D

CATALYTIC PROPERTIES

Table 4.23 The yield of **5a** and **6a** using the recovered heterogeneous catalyst (**3**)

Number of catalytic cycles	Time (h)	Ratio of **5a**:**5b**	Yield %	TOF (h^{-1})
1	6.5	7:1	98	15.29
2	6.5	7:1	97	15.13
3	6.5	7:1	94	14.66
4	6.5	7:1	90	14.04
5	6.5	7:1	88	13.73
6	9	7:2	81	9.13
7	9	7:2	76	8.56
8	6.5*	7:1	54	8.42

[a]Reaction condition: **1a** (100 mg, 0.5982 mmol), **2a** (12.07 µL, 0.1196 mmol), **4a** (68 µL, 0.5982 mmol) and 10 mol% [Cu(dpyam)(2-OHbenz)Cl] (**3**) catalyst in THF solvent (20 mL) at room temperature. * = stop reaction at 6.5 hours.

Mole of catalyst of complex **3** $= \frac{\text{g}}{\text{Mw}}$

$= \frac{2.4031 \times 10^{-3}\ g}{407.30\ g \cdot mol^{-1}}$

$= 5.90 \times 10^{-6}$ mol

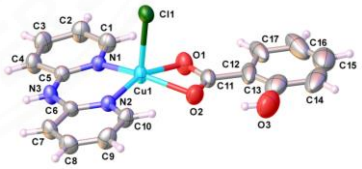

Formula weight: 407.30 g·mol^{-1}

Turnover number (TON) $= \frac{\text{number of moles of reactant consumed}}{\text{mole of catalyst}}$

$= \frac{0.5982 \times 10^{-3}\ mol}{5.90 \times 10^{-6}\ mol}$

$= 101.39$

Turnover frequency (TOF_1) $= \frac{\text{TON}}{\text{time of reaction}} \times \text{Yield (\%)}$

$= \frac{101.39}{6.5\ h} \times 0.98 = 15.29\ h^{-1}$

$$\text{Turnover frequency } (TOF_2) = \frac{\text{TON}}{\text{time of reaction}} \times \text{Yield (\%)}$$

$$= \frac{101.39}{6.5\ h} \times 0.97$$

$$= 15.13\ h^{-1}$$

$$\text{Turnover frequency } (TOF_3) = \frac{\text{TON}}{\text{time of reaction}} \times \text{Yield (\%)}$$

$$= \frac{101.39}{6.5\ h} \times 0.94$$

$$= 14.66\ h^{-1}$$

$$\text{Turnover frequency } (TOF_4) = \frac{\text{TON}}{\text{time of reaction}} \times \text{Yield (\%)}$$

$$= \frac{101.39}{6.5\ h} \times 0.90$$

$$= 14.04\ h^{-1}$$

$$\text{Turnover frequency } (TOF_5) = \frac{\text{TON}}{\text{time of reaction}} \times \text{Yield (\%)}$$

$$= \frac{101.39}{6.5\ h} \times 0.88$$

$$= 13.73\ h^{-1}$$

$$\text{Turnover frequency } (TOF_6) = \frac{\text{TON}}{\text{time of reaction}} \times \text{Yield (\%)}$$

$$= \frac{101.39}{6.5\ h} \times 0.81$$

$$= 9.13\ h^{-1}$$

$$\text{Turnover frequency } (TOF_7) = \frac{\text{TON}}{\text{time of reaction}} \times \text{Yield (\%)}$$

$$= \frac{101.39}{6.5\ h} \times 0.76$$

$$= 8.56\ h^{-1}$$

$$\text{Turnover frequency } (TOF_8) = \frac{\text{TON}}{\text{time of reaction}} \times \text{Yield (\%)}$$

$$= \frac{101.39}{6.5\ h} \times 0.54$$

$$= 8.42\ h^{-1}$$

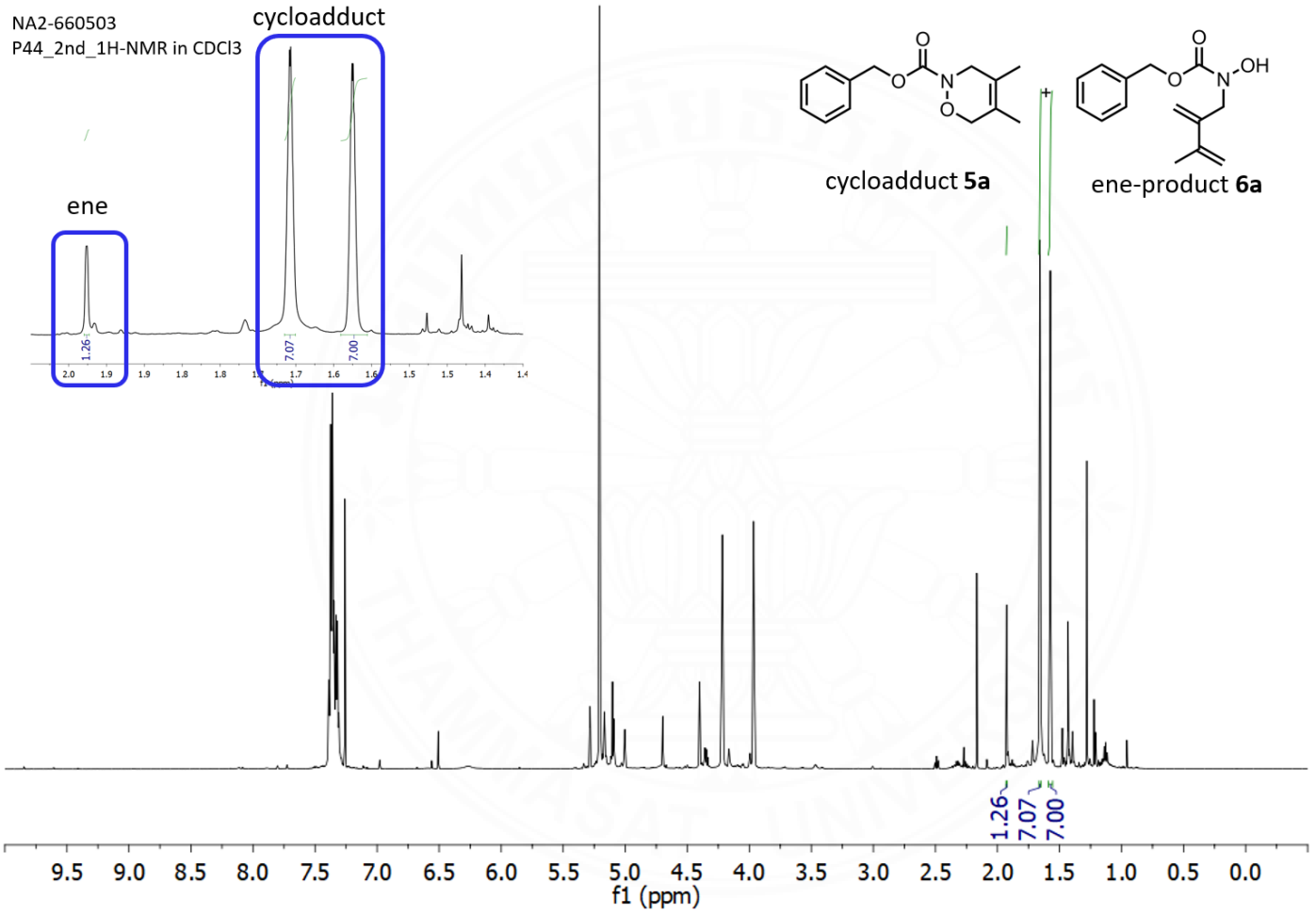

Figure D1 The ^{1}H NMR spectrum of the crude products of cycloadduct (**5a**) and ene product (**6a**) by using the recovered complex **3** cycle 2nd

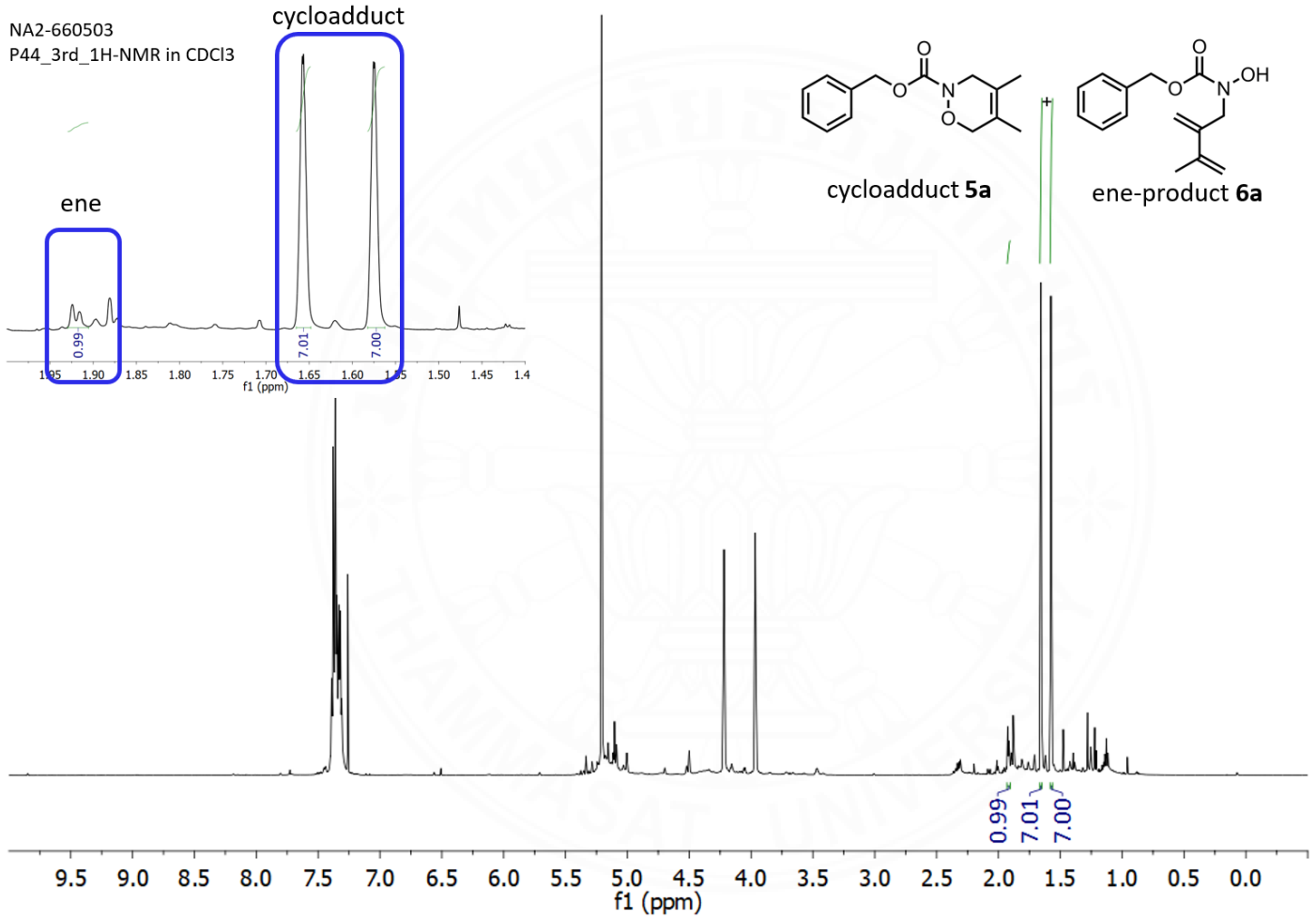

Figure D2 The ^{1}H NMR spectrum of the crude products of cycloadduct (**5a**) and ene-product (**6a**) by using the recovered complex **3** cycle 3rd

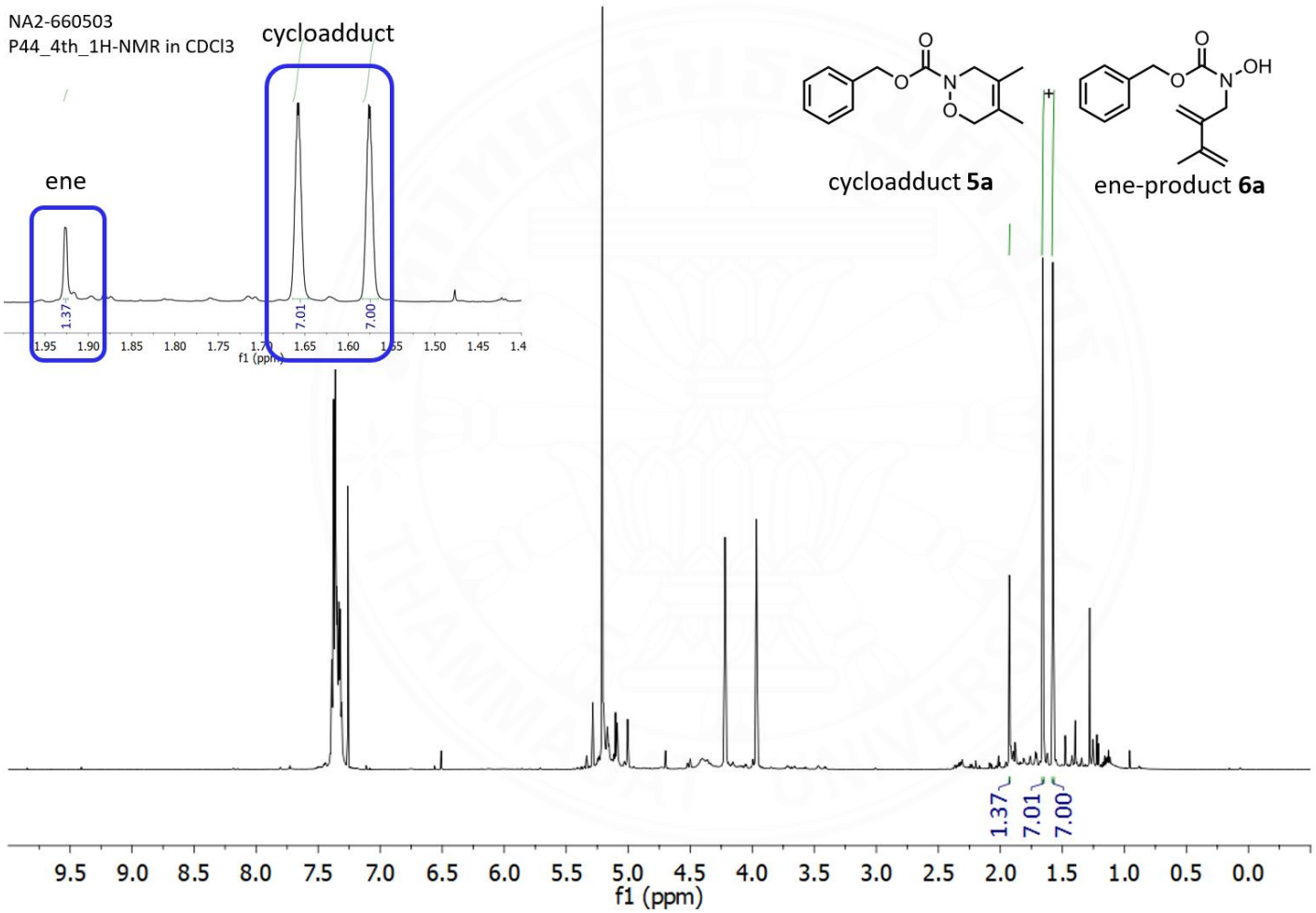

Figure D3 The ^{1}H NMR spectrum of the crude products of cycloadduct (**5a**) and ene-product (**6a**) by using the recovered complex **3** cycle 4th

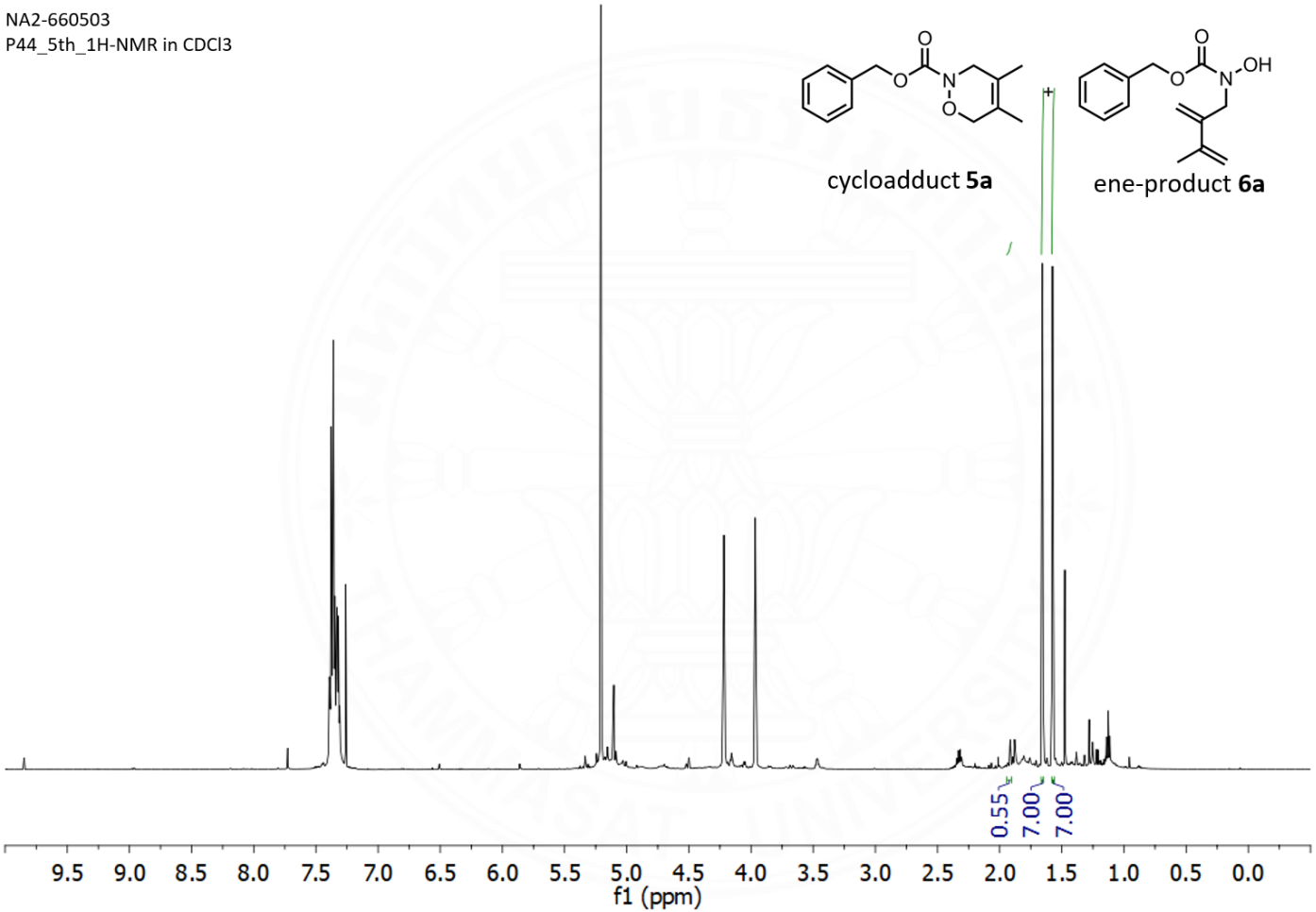

Figure D4 The ^{1}H NMR spectrum of the crude products of cycloadduct (**5a**) and ene-product (**6a**) by using the recovered complex **3** cycle 5th

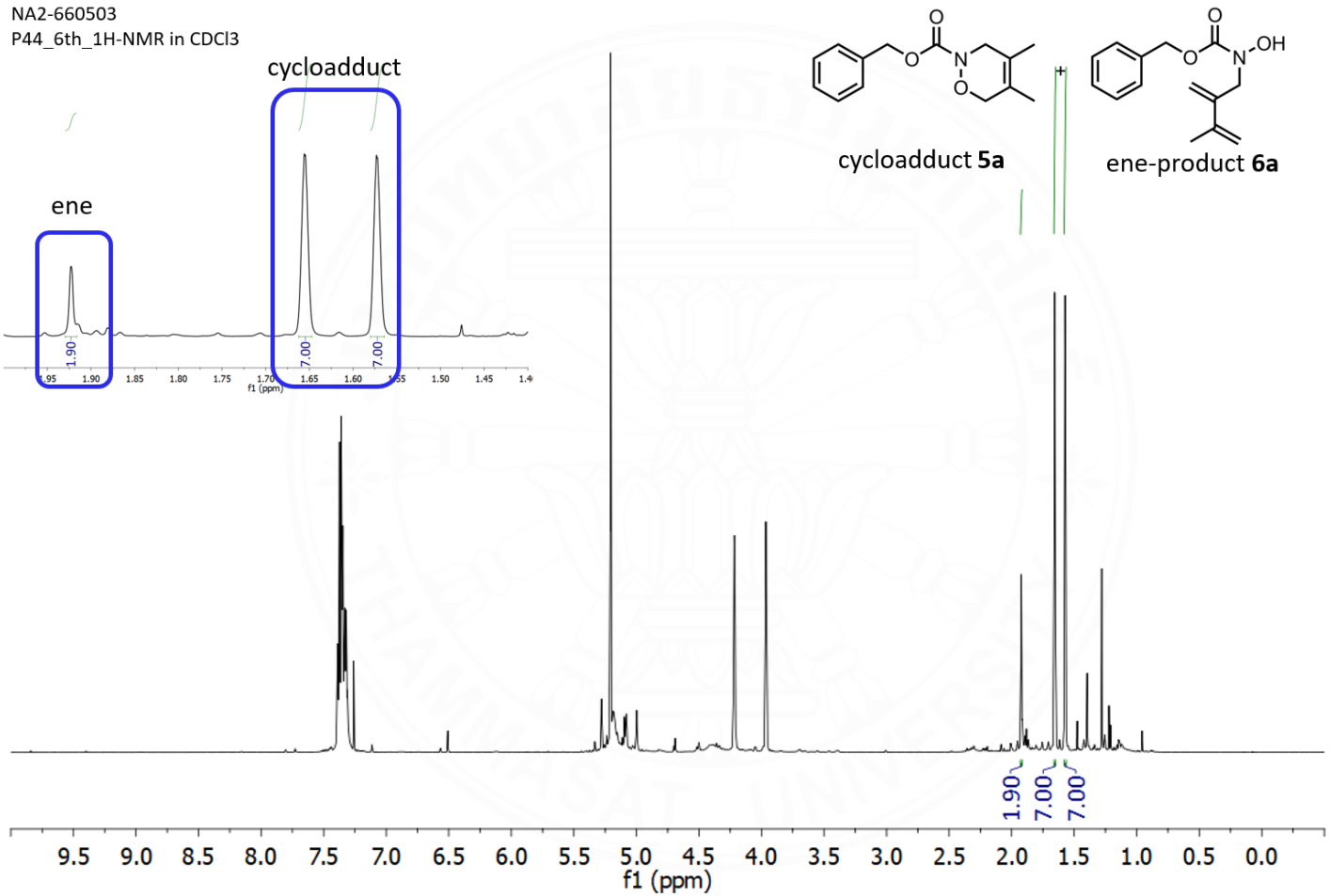

Figure D5 The ^{1}H NMR spectrum of the crude products of cycloadduct (**5a**) and ene-product (**6a**) by using the recovered complex **3** cycle 6th

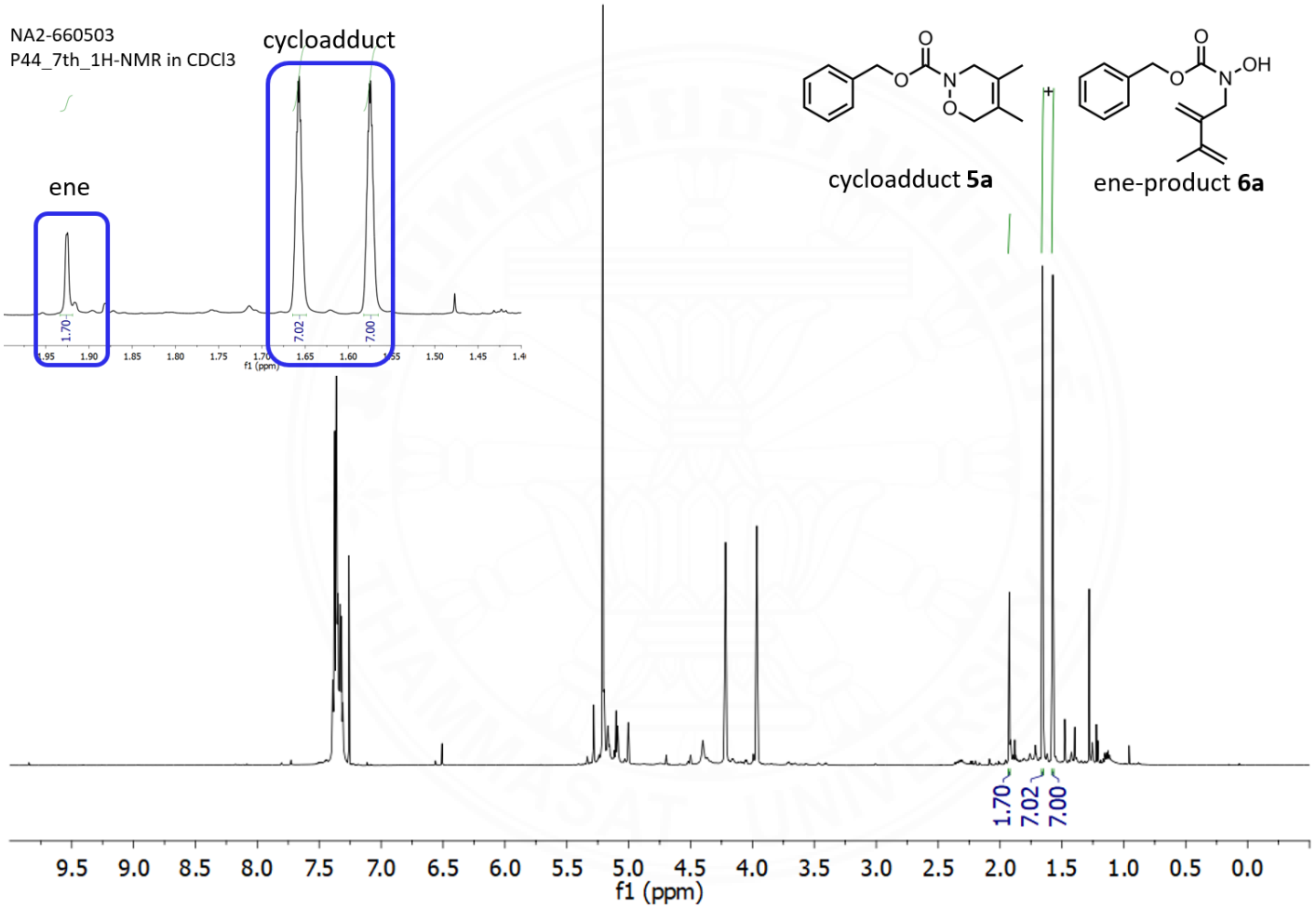

Figure D6 The ^{1}H NMR spectrum of the crude products of cycloadduct (**5a**) and ene-product (**6a**) by using the recovered complex **3** cycle 7th

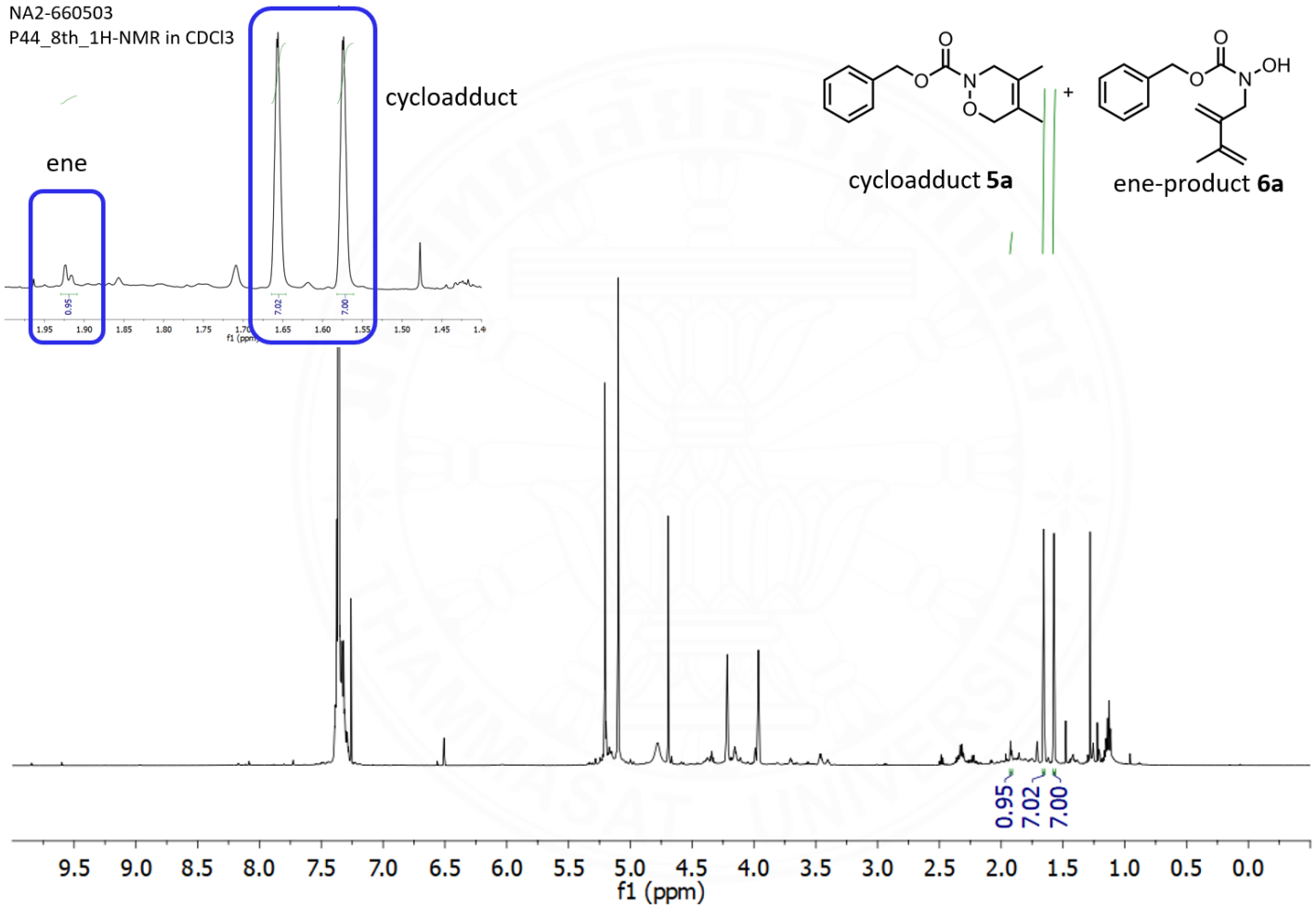

Figure D7 The ^{1}H NMR spectrum of the crude products of cycloadduct (**5a**) and ene-product (**6a**) by using the recovered complex **3** cycle 8th

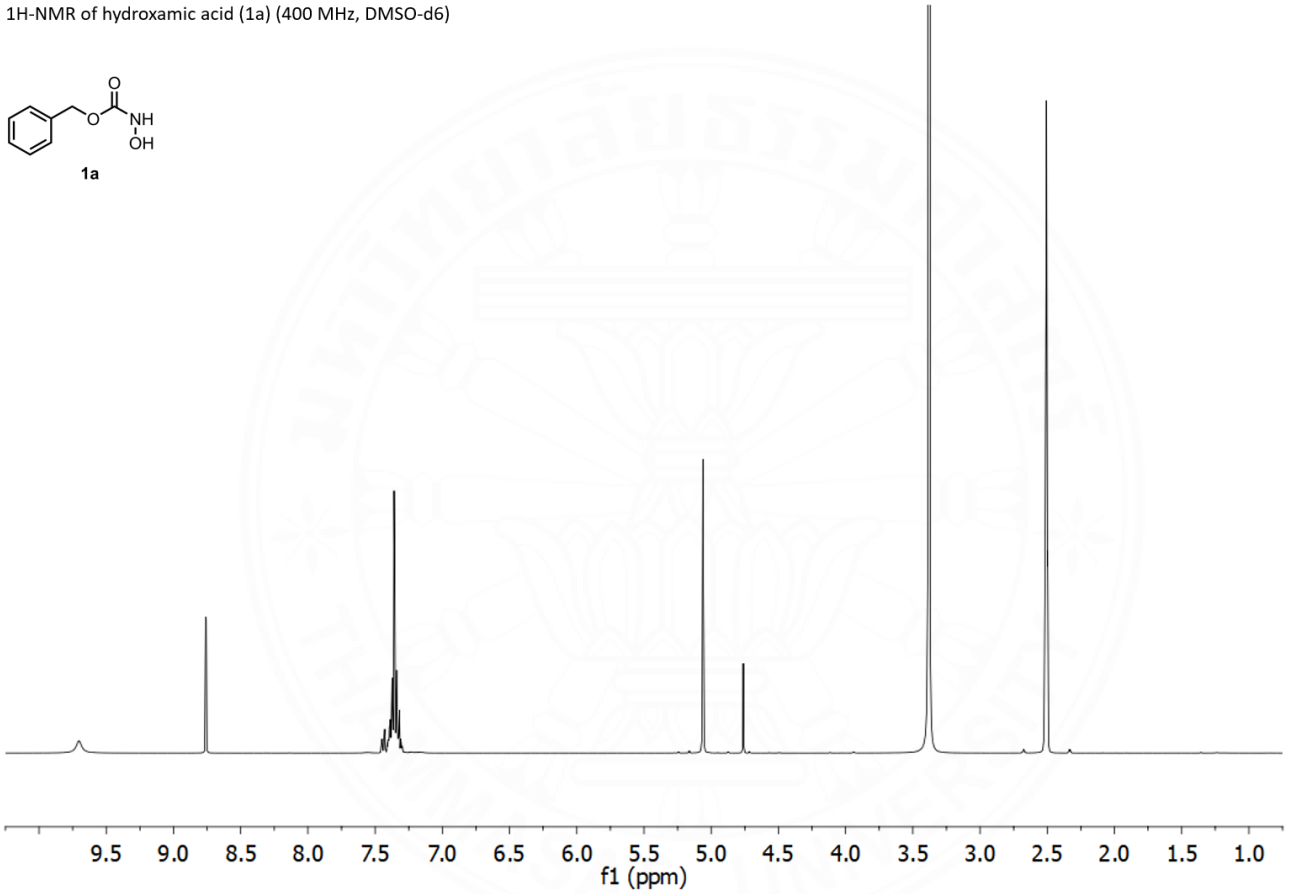

Figure D8 The ^{1}H NMR spectrum of the crude of *N*-(benzyloxy-carbonyl)hydroxylamine (**1a**)

BIOGRAPHY

Name	Wanassanan Chaisuriya
Educational Attainment	2019: B. Sc. in Chemistry, Thammasat University, Thailand
Present status	M. Sc. student, Chemistry (Inorganic Chemistry), Thammasat University, Thailand

Publication

1. Chaisuriya, W., Chainok, K., & Wannarit, N. (2023). Crystal structure and Hirshfeld surface analysis of a new mononuclear copper (II) complex: [bis (pyridin-2-yl-*κN*)amine](formato-κ*O*)(m-hydroxybenzoato-κ^2*O,O′*)copper (II). *Acta Cryst*. E**79**, 1115-11120.

Presentations

1. W. Chaisuriya, K. Chainok and N. Wannarit "Synthesis, characterization, and crystal structure of new mononuclear copper(II) complexes containing 2,2´-dipyridylamine and hydroxybenzoate derivatives" ***Poster*** presentation on the 12th International Symposium on Nano & Supramolecular Chemistry & the 3rd Thailand Biorefinery Symposium, July 23-25, 2023, Chiang Mai, Thailand.
2. W. Chaisuriya, K. Chainok and N. Wannarit "Crystal structures and Hirshfeld surface analysis of two new copper(II) complexes with 2,2´-dipyridylamine and hydroxybenzoate derivatives" ***Poster*** presentation on The 48th International Congress on Science, Technology and Technology-Based Innovation (STT48), 29 November-1 December 2022, School of Science Walailak University, Thailand.

3. W. Chaisuriya, K. Chainok and N. Wannarit "Synthesis, characterization, and crystal structure of new mononuclear copper(II) complexes containing 2,2´-dipyridylamine and hydroxybenzoate derivatives" ***Poster*** presentation on the 17th Conference of the Asian Crystallographic Association (AsCA2022), 30 October-2 November 2022, Ramada plaza hotel, Jeju-si, Jeju-do, South Korea.
4. W. Chaisuriya, K. Chainok and N. Wannarit "Synthesis, crystal structures and Hirshfeld surface analysis of three new mononuclear 3-chlorobenzoate copper(II) complexes with 2,2′-bipyridine and 1,10-phenanthroline chelating ligands" ***Poster*** presentation on the Pure and Applied Chemistry International Conference 2020 (PACCON2020), 13-14 February 2020, IMPACT Forum, Muang Thong Thani, Nonthaburi, Thailand.
5. W. Chaisuriya, K. Chainok and N. Wannarit "Synthesis, crystal structures and Hirshfeld surface analysis of three new mononuclear 3-chlorobenzoate copper(II) complexes with 2,2′-bipyridine and 1,10-phenanthroline chelating ligands" ***Poster and flash talk*** presentations on the 45th Congress on Science and Technology of Thailand (STT45), 7-9 October 2019, Mae Fha Luang University, Chiang Rai, Thailand.

Award

1. **Best poster presentation award: Session SP3 : Crystallography.** "Crystal structures and Hirshfeld surface analysis of two new copper(II) complexes with 2,2´-dipyridylamine and hydroxybenzoate derivatives" ***Poster*** presentation at The 48th International Congress on Science, Technology and Technology-Based Innovation (STT48), 29 November-1 December 2022, Thailand.

Work Experiences:

1. Teaching assistant in the chemistry courses at Department of Chemistry, Faculty of Science and Technology, Thammasat University, Thailand. Course SC171 Chemistry Laboratory (Semesters 1/2563 and 1/2565), SC173 Fundamental Chemistry Laboratory (Semesters 2/2563 and 1/2564) and SC174 Fundamental Chemistry Laboratory for Medical Students.
2. Research Assistant of Thammasat University Research Unit in Multifunctional Crystalline Materials and Applications (TU-MCMA) under the research topic of "Development of Porous Metal-Organic Frameworks for Gas Adsorption" Contract number: 65-B602000-11-IO.SS03B3008617. Cooperation between Thammasat University Research Unit in Multifunctional Crystalline Materials and Applications (TU-MCMA), Faculty of Science and Technology, Thammasat University, Thailand, and the Electricity Generating Authority of Thailand (EGAT).

Qualification

2020-present	M. Sc. student (Chemistry), Thammasat University, Thailand
Thesis title:	Mononuclear copper(II) complexes containing 2,2′dipyridyl-amine and hydroxybenzoate derivatives as catalyst for aerobic oxidation of hydroxamic acids
2016–2019	B. Sc. student (Chemistry), Thammasat University, Thailand
Senior project:	Synthesis, characterization and crystal structure of new mononuclear copper(II) complexes with 3-chlorobenzoate, 2,2′-dipyridylamine and 1,10-phenanthroline chelating ligands

Instrument skills:

Fourier Transform Infrared Spectrometer (FT-IR),
Ultraviolet-visible spectrophotometers (UV-Vis),
Electronic diffuse reflectance spectrophotometer,
Powder X-ray Diffractometer (PXRD)

Computational skills:

Office programs:	Microsoft office and Origin
Crystallographic programs:	PLATON, Mercury and *OLEX2*
Computational Chemistry:	ChemDraw, ChemSketch, CrystalExplorer, MestreNova and TopSpin
Graphic programs:	Adobe Photoshop and Adobe llustrator

Language:

English:	Listening: Fair	Reading: Good
	Writing: Fair	Speaking: Fair

Reference:

1. Assistant Professor Nanthawat Wannarit, Ph.D.
   Department of Chemistry, Faculty of Science and Technology,
   Thammasat University, Khlong Luang, Pathum Thani 12121, Thailand
   Email address: nanthawat0110@gmail.com, nwan0110@tu.ac.th
2. Assistant Professor Duangduan Chaiyaveij, Ph.D.
   Department of Chemistry, Faculty of Science and Technology,
   Thammasat University, Khlong Luang, Pathum Thani 12121, Thailand
   Email address: dchaiyav@tu.ac.th